Imperial College
London

Modified Poly-γ-Glutamic Acid Scaffolds for Tissue Engineering

by

Jessica Rose May

A Thesis Submitted to Imperial College

for the Award of PhD and the

Diploma of Imperial College

The Department of Materials

Imperial College London

April 2011

London, England

"*Make the most of yourself... for that is all there is of you.*" - *Ralph Waldo Emerson*

Abstract

The PhD thesis concerns the development of scaffolds inspired by biology for musculoskeletal tissue engineering. This was accomplished by chemical modification of poly-DLγ-glutamic acid (γ-PGA) to reduce its water solubility for use in regenerative medicine applications.

A series of water-insoluble modified γ-PGA polymers were synthesised, yielding materials with varying hydrophilicity and dissolution rates. All polymers were fully characterised using techniques such as differential scanning calorimetry, size-exclusion chromatography, wide-angle x-ray scattering, thermogravimetric analysis, Fourier transform infrared spectroscopy, and contact angle determination.

Following characterisation, esterified γ-PGA polymers were oriented to different degrees above their glass transition temperatures using tensile deformation. This drawing induced crystallisation, and thus orientation, on a molecular scale, leading to increased mechanical properties that were calculated from tensile tests.

Synthesised polymers were found to be non-cytotoxic using the pre-clinical ISO 10993:5 test, and supported human fibroblast cell growth, as determined by LIVE/DEAD® staining. Oriented, modified γ-PGA polymers were produced with a wide range of mechanical properties, displaying tailorability for specific tissue engineering applications.

Author's declaration

This thesis is a record of the work performed by me in either at Imperial College London in the Department of Materials and the Institute of Biomedical Engineering or on an IDEA League exchange at ETH Zurich in the Polymer Technology lab headed by Prof. Paul Smith, unless otherwise noted.

The work described herein is my own with the exception of some work having been performed by:
- Mr. Ryan Bayliss, for running the wide-angle x-ray scattering measurements at Imperial College, reported in Section 2.3.3
- Mr. Yaroslav Odarchenko and Dr. Dimitri Ivanov, who performed the wide-angle x-ray scattering (WAXS) measurements and polarised Raman (both in Section 5.4.5), as well as writing the methods for both sections and calculating the WAXS analysis for presentation
- Dr. Thomas Schweizer who performing all size exclusion chromatography measurements throughout this thesis at ETH Zurich, other than that of γ-PGA-H, which was performed by Smithers Rapra (UK) under EPSRC.
- Dr. Cristina Gentilini, who previously optimised the esterification reactions for the synthesis performed in this thesis.
- All nuclear magnetic resonance measurements were performed by the technicians in the Chemistry department at Imperial College.

Acknowledgements

I would like to begin my many acknowledgements with a disclaimer: I have an extensive list of people who have helped me get to where I am and it would be inappropriate not to thank them all, therefore, if acknowledgements aren't your cup of tea, you may want to turn to page 13 now.

First and foremost, I would like to thank Professor Ton Peijs from Queen Mary University of London and Dr. Natalie Stingelin from Imperial College London for agreeing to be examiners for both myself and the work presented in this thesis.

I'd like to acknowledge a few people that inspired me from a young age to follow my dreams, no matter what challenges life threw at me along the way: Dr. J., Mr. Nesbitt, Mrs. Murphy, and Mr. Davis. Their academic support and encouragement to venture afar following high school to follow my aspirations to study biomedical engineering is still influencing me to this day. Dr. Wilmont Kreis, thank you for an experience of a lifetime, shadowing surgeries, to understand the immense need for orthopaedic tissue engineering.

I owe a huge thanks to Johns Hopkins University for accepting me from the thousands applying to their BME program as this opened numerous opportunities for me. It's not easy to leave a small town and start university several states away without knowing a soul, therefore I must also thank those at Johns Hopkins who enriched my life and continue to support me though I am thousands of miles away. Furthermore, I am grateful to the Vredenburg Scholarship committee at Johns Hopkins who awarded me funding to travel to London for the summer of 2005 to perform research at Imperial College.

Next, I wish to thank Professor Molly M. Stevens for taking a chance on a placement student she had never met, who had to ask if a resume was the same thing as a CV. If it weren't for this opportunity, my life would be drastically different and I wouldn't be here today. In 2005, Molly welcomed me into her lab group here at Imperial for a summer research placement, joint with Dr. Julian Jones. I also wish to thank Julian for mentoring me at several stages, including the summer of 2005, as an examiner of my first-year transfer, and always having an open door to discuss experimental work.

Through my initial research experience, I met several people that influenced my decision to return and do a PhD within the Stevens group, both academically and socially. In January of 2006, Molly offered me a coveted PhD position when I finished at JHU. Since my arrival in September 2006, many have come and gone that have helped me along the

way in the lab, including these three alumnae: Dr. Mike Ball, as his patience and training in cell culture and microbiology techniques were unparalleled; Dr. Olga Tsigkou, for her many conversations offering advice about various techniques and for being a great friend; and Dr. Nicholas Evans, for his jovial spirit whenever my experiments weren't behaving.

During my time here, Molly has always inspired me towards achieving academic excellence. Her support and guidance with projects provided me with unique opportunities within my PhD that have truly enlightened the entire experience. Her encouragement to strive for the very best is contagious, motivating me to win two poster prizes and to always produce top quality presentations. Furthermore, she has helped me gain several sources of funding: a scholarship from the Overseas Research Scheme to cover the difference between home and overseas tuition fees; two IDEA League grants to fund living costs in Switzerland while on exchange at ETH Zurich; funding from the Rosetrees Trust to cover some of my research consumables while here at Imperial; and numerous travel grants to support my participation in conferences including funding from the Institute of Materials, Minerals and Mining (IOM3), Imperial College Trust, the Royal Academy of Engineering, Armourers and Brasiers Gauntlet Trust and the Tissue and Cell Engineering Society (TCES). Molly also helped greatly in securing a Knowledge Transfer Secondment fellowship which will allow me to continue the work performed here for another year. Her experience with grant writing is notorious, and she has always presented an excellent example from which to learn this skill. Always in *Vogue* with science (or the July 2011 issue), Molly's research focuses have provided me with a breadth of knowledge during my time here.

Her group of carefully-picked researchers who serve not only as colleagues, but as friends and even family, have supported me and gotten me through both the good and bad times. Some of my fellow students have always been there for me in one way or another: Air, Ben, Benji, Elsie, Erh-hsuin, Farina, Ian, Kristy, John, Julian, Liling, Maria, Mathew, Nasrin, Nia, Oli, Pelin, Pinyuan, Piotr, Reza, Robin, Sam, Stu, Thomas, and Vanessa. Of course, the extensive advice from amazing postdocs also cannot be forgotten: Anna, Anthony, Caterina, Gavin, Helene, Heiko, Lesley, Lijun, Lise, Luis, Mark, Morgan, Nicolas, Seth, Rekha, Roberto, Sangwon, Sergio, and Shalini. Also, both Nick and Sabrina, thank you for putting up with my many orders, my thesis would not have happened without you. One Stevens' group alumnae has been invaluable in preparing this thesis - Mr. Richard Keller, thank you for all your support, help, guidance with LaTeX programming, and friendship through this stressful time, I really appreciate it. Pelin, your help with the immunostaining was amazing, thank you for all your time you sacrificed to help ensure I got the images needed for this thesis. I must also thank the γ-PGA crew - Dr. Cristina, Dave, Tommy, Yixiang, and Silvia, for persevering to achieve the impossible. Thank you also to Dr. Cristina, Eileen, and Luis for taking time to assess parts of this work.

Finally, a massive thanks to the three fellow students I spent a large amount of time

with, Yann (”Frenchie”) Fredholm for helping make this group into friends rather than just colleagues, to Tais for always keeping a smile on my face and nose to the ground, and to James for making me happy I didn't work with nanoparticles. These people really have been some of the best friends one could ask for.

There are two postdocs whom I must acknowledge a little more in depth. First, Dr. Eileen Gentleman, thank you for being my fellow American from the start. You have helped me through both the up and down times, always been there for advice on cell-related questions, and you really are one of the best. Thank you for both pushing me and always stopping to share a cupcake or two. Dr. Cristina (Gentilini), I would not have achieved this thesis without your amazing guidance. Your (lab) cooking is impeccable (without your expertise I'd probably still be in the lab!) and anyone who works with you really gains a fantastic experience. Dr. Cristina, you are an inspiration, and it has truly been a privilege to work so closely with you.

This thesis would not have been possible without two incredibly amazing people from ETH Zurich - Professor Paul Smith and Dr. Kirill Feldman. I wish to thank Paul for allowing me into not only his laboratories, but also into his Polytech ”family” and including me on his annual group ski trip in 2010. The guidance from Paul and Kirill enabled me to accomplish what seemed like the impossible. They have both provided unlimited support, patience, advice and mentoring which has enabled me to complete this work, in particular the tensile deformation studies. Their polymer expertise has proved invaluable and it is truly impossible to put how incredibly grateful I am to them in words. I look forward to our next game of pool at Geordie's, whose inspiration and stimulating academic discussions are one of a kind.

Similarly, I owe an immense thank you to the entire Polymer Technology group at ETH, namely Jan, Karin, Markus, Joanna, and particularly Felix and Pascal who selflessly sacrificed their own research time to teach experimental techniques and assist me with any problems that arose. The group's kind acceptance as a surrogate member of the Polytech clan, great times spent together, and immense help in the lab will never be forgotten.

Thank you also to Werner Schmidheiny for designing and building the ”Rolls Royce” of tiny sample punches, without which the work in Chapter 5 would have never happened. I wish to acknowledge Vappu Hammerli for all of her assistance with paperwork, accommodation during my visits, and generally with anything and everything else at ETH. Finally, I wish to thank Dr. Theo Tervoort for his assistance with the Irvine-Smith model in Chapter 5 and any questions I had along the way.

Eleanor Roosevelt once famously said, “You gain strength, courage and confidence by every experience in which you really stop to look fear in the face. You are able to say to yourself, ‘I have lived through this horror. I can take the next thing that comes along.’ You must do the thing you think you cannot do.” In light of this, two medical doctors must be mentioned who have enabled me to lead a mostly normal life and fulfil my dream of

achieving this PhD: Dr. Howard Rossman, who is truly a daily inspiration in himself, and Dr. Kevin Johnson who has helped me see the light where there is none.

Of course, those I must finally thank are my family - through *everything*, you have been my rocks that keep me grounded, the light that shines, and the gas that keeps me going. I am eternally grateful to each and every one of you, including my parents Ken and Bonnie for supporting me, both emotionally and financially throughout my time here. Jeanne and Bam, your positive attitude through tough times has always kept a smile on my face. To my siblings, Ken and Amey, your protection and encouragement has helped shape me into who I am today. I only hope I have made you all as proud of me as I am to be related to you. Finally, Steve - thank you, for everything, and being there through it *all*, Y.N.W.A.

Contents

Abstract **5**

Author's declaration **7**

Acknowledgements **9**

Abbreviations **24**

1 Introduction **27**

1.1 Damaged and degenerated tissues 27

1.2 Tissue engineering 28

1.2.1 Musculoskeletal tissues 30

1.2.2 Tissue mechanical properties 33

1.2.3 Cell sources 35

1.2.4 Extracellular matrix and cellular interactions 36

1.3 Polymers and their role in tissue engineering 38

1.3.1 Scaffolds 38

1.3.2 Polymers to use for scaffolds 38

1.3.3 Scaffold fabrication methods 42

1.4 Summary 42

2 Reduction of poly-γ-glutamic acid water solubility via side chain esterification **45**

2.1 Introduction 45

2.2 Experimental 46

2.2.1 Chemical synthesis 46

2.2.2 Chemical analysis 47

2.3 Results and discussion 49

2.3.1 Nuclear magnetic resonance 49

2.3.2 Fourier transform infrared spectroscopy 55

2.3.3 Wide-angle x-ray scattering 60

2.3.4 Size exclusion chromatography 65

2.3.5 Thermogravimetric analysis 65
2.3.6 Differential scanning calorimetry 66
2.3.7 Contact angle 72
2.4 Conclusions 72

3 Modification of γ-PGA with Phenylalanine 75
3.1 Introduction 75
3.2 Experimental 76
3.2.1 Chemical synthesis 76
3.2.2 Chemical analysis 77
3.2.3 Thermal analysis 78
3.3 Results and discussion 78
3.3.1 One-step γ-PGA-Phe coupling 78
3.3.2 Two-step γ-PGA-Phe coupling 79
3.3.3 Nuclear magnetic resonance 80
3.3.4 ^{13}C- DEPT NMR 82
3.3.5 ^{1}H-^{13}C- COSY NMR 82
3.3.6 Thermal analysis 82
3.4 Conclusions 85

4 Cytotoxicity and culture stability of esterified γ-PGA 87
4.1 Introduction 87
4.2 Experimental 87
4.2.1 ISO 10993:5 pre-clinical cytotoxicity test 88
4.2.2 LIVE/DEAD® assay 88
4.2.3 Immunofluorescence staining 89
4.2.4 Dissolution soaking study 90
4.3 Results and Discussion 91
4.3.1 ISO 10993:5 pre-clinical cytotoxicity test 91
4.3.2 LIVE/DEAD® assay for cell viability 93
4.3.3 Immunostaining of cells 95
4.3.4 Dissolution soaking study 97
4.4 Conclusions 105

5 Enhancing mechanical properties of esterified γ-PGA polymers using tensile deformation 107
5.1 Introduction 107
5.2 Experimental 108
5.2.1 Materials 108

5.2.2 Sample preparation . . . 108
5.2.3 Room temperature tensile testing and tensile deformation . . . 109
5.3 Analysis . . . 110
5.3.1 Mechanical testing . . . 110
5.3.2 Optical microscopy . . . 110
5.3.3 Wide-angle x-ray scattering (WAXS) . . . 110
5.3.4 Polarised Raman spectroscopy . . . 110
5.3.5 Thermal analysis . . . 111
5.4 Results and discussion . . . 112
5.4.1 Room temperature tensile properties of as-cast films . . . 112
5.4.2 Tensile deformation . . . 113
5.4.3 Mechanical properties of drawn films . . . 114
5.4.4 Estimated theoretical chain stiffness . . . 118
5.4.5 Structural characteristics . . . 119
5.5 Conclusions . . . 130

6 Scaling up γ-PGA-Bn synthesis 131
6.1 Introduction . . . 131
6.2 Experimental . . . 132
6.2.1 Chemical synthesis . . . 132
6.2.2 Characterisation . . . 133
6.3 Results . . . 133
6.3.1 Synthesis . . . 133
6.3.2 ^{1}H-NMR . . . 133
6.3.3 Size exclusion chromatography . . . 135
6.3.4 Thermal characterisation . . . 135
6.3.5 Density measurements . . . 138
6.4 Conclusions . . . 138

7 Conclusions and outlook 139

Bibliography 143

Publications 159

List of Figures

1.1 The typical tissue engineering approach: 1) Remove cells; 2) Expand number in culture; 3) Seed onto an appropriate scaffold with suitable growth factors and cytokines; 4) Place into culture; 5) Re-implant engineered tissue repair damaged site. Figure used with permission from author.[1] 28

1.2 Hierarchical organisation of cartilage. A) Articular cartilage covers the ends of long bones B) with distinct zonal organisation of C) collagen structure. Resident D) Chondrocytes are surrounded by a matrix of E) aggrecan/hyaluronic acid super-aggregates and macrofibrillar collagen networks. Adapted from[2] with permission. Copyright 2004, AAAS. 31

1.3 Diagram adapted from[3] detailing tendon/ligament-bone and muscle/tendon interface compositions including aggrecan (orange), collagen fibres (light blue), mineralised tissue (dark blue) and muscle fibres (red). 32

1.4 Ashby-style plot of stiffness versus tensile strength of human tissues tested in tension using data taken from[4–24] 34

1.5 Ashby-style plot of stiffness versus tensile strength of biomaterials commonly as tissue replacements, using data taken from[4–24] 34

1.6 Synthesis of FDA approved polyesters. A) PLA, B) PLGA, C) PEG, D) PCL. 40

1.7 γ-PGA, protonated at pH < 4.2, and anionic at higher pH values. 41

2.1 Esterification of γ-PGA using ethyl, propyl, or benzyl bromide to produce γ-PGA-Et, γ-PGA-Pr, and γ-PGA-Bn, respectively. 50

2.2 A)^{1}H-NMR and B) ^{13}C-NMR spectra for unmodified γ-PGA-H polymer (DMSO-d6, 25°C). 51

2.3 A)^{1}H-NMR and B) ^{13}C-NMR spectra for γ-PGA-Et series polymers (DMSO-d6, 25°C). 52

2.4 A)^{1}H-NMR and B) ^{13}C-NMR spectra for γ-PGA-Pr series polymers (DMSO-d6, 25°C). 53

2.5 A)^{1}H-NMR and B) ^{13}C-NMR spectra for γ-PGA-Bn series polymers (DMSO-d6, 25°C). 54

2.6 Fourier transform infrared spectra of native γ-PGA-H. 55
2.7 Fourier transform infrared spectra of the synthesised γ-PGA-Et series. . . 56
2.8 Fourier transform infrared spectra of the synthesised γ-PGA-Pr series. . . 57
2.9 Fourier transform infrared spectra of the synthesised γ-PGA-Bn series. . 58
2.10 Wide-angle x-ray scattering pattern of the synthesised γ-PGA-Et series. . 61
2.11 Wide-angle x-ray scattering pattern of the synthesised γ-PGA-Pr series. . 62
2.12 Wide-angle x-ray scattering pattern of the synthesised γ-PGA-Bn series. 63
2.13 Wide-angle x-ray scattering pattern of the all γ-PGA-polymers plotted together. 64
2.14 DSC heating traces of synthesised γ-PGA-Et series, where black indicates first heating and red is the second. 68
2.15 DSC heating traces of synthesised γ-PGA-Pr series, where black indicates first heating and red is the second. 69
2.16 DSC heating traces of synthesised γ-PGA-Bn series, where black indicates first heating and red is the second. 70
2.17 Plot of T_m as a function of T_g for γ-PGA-Na^+ and modified γ-PGA polymers. 71
2.18 Contact angle analysis for for as-cast, dried γ-PGA films compared to PLLA(* $p < 0.001$, n.s. = not significant). 72

3.1 ^{1}H-NMR for retrieved γ-PGA-Phe polymer coupled using DCC and 5 molar equivalents of phenylalanine. 79
3.2 ^{1}H-NMR for fully coupled γ-PGA-Phe polymer, where impurities (DCU) indicated in red diminish with repeated wash steps. 80
3.3 A) ^{1}H-NMR and B) ^{13}C-NMR for fully coupled γ-PGA-Phe polymer. Side group peaks are labeled in red lettering while peaks from impurities are indicated with black ”x” symbols. 81
3.4 ^{13}C- DEPT 135 NMR for fully coupled γ-PGA-Phe polymer. 82
3.5 ^{1}H-^{13}C-COSY NMR for fully coupled γ-PGA-Phe polymer. 82
3.6 First and second heating DSC traces for fully coupled γ-PGA-Phe polymer, with excess solvent visible in the first heating, thus a separate, preheat run was performed to 120°C for the second heating trace to remove excess solvent for accurate T_g calculation. 83

4.1 UV-Vis calibration curve for benzyl alcohol absorbance at λ = 257 nm. . 90
4.2 MC3T3-E1 cells exposed to conditioned media for 24 h. A) Tissue culture plastic (blank control), B) γ-PGA-Et, C) Negative control, D) γ-PGA-Pr, E) Positive control, F) γ-PGA-Bn. 92

4.3 ISO 10993:5 pre-clinical test of esterified γ-PGA films, normalised to negative control. All polymers passed and metabolic activities were not significantly different to the negative control, but were significantly different from the positive cytotoxic sample (* $p < 0.001$). 93
4.4 LIVE/DEAD® assay of human foreskin fibroblasts (P2) cultured for 1 and 7 days on esterified γ-PGA films at 10x and 4x magnification, respectively. 94
4.5 Immunostained images of HFF-1 (P2) cells cultured on γ-PGA-Bn films for 4 days at 37°C, 5%CO_2. Confocal images taken at 20x (A), 40x (B), and 63x (C-D) magnification. Blue represents cell nuclei, green shows F-actin filaments and red displays vinculin-positive focal adhesions. . . . 96
4.6 Areas of interest from immunostained images shown in Figure 4.5 of HFF-1 (P2) cells cultured on γ-PGA-Bn films for 4 days (37°C, 5%CO_2), displaying F-actin stress fibres associated with focal adhesions at both ends of the fibres highlighed in yellow boxes (A) or radially arranged focal adhesions highlighted in purple boxes (B). Blue represents cell nuclei, green shows F-actin filaments and red displays focal adhesions. 97
4.7 Mass retained for films soaked in a) H_2O, B) PBS, or C) SBF for 7, 14, 21, and 28 days at 37°C. Significance determined by One-way ANOVA (Tukey post-hoc) and as indicated in figure. 98
4.8 Optical photographs of films as cast or soaked in H_2O for 7, 14, 21, and 28 days at 37°C. 99
4.9 Optical photographs of films soaked for 7, 14, 21, and 28 days in PBS or SBF at 37°C. 100
4.10 Scanning electron microscope photographs of films as cast. Scale bars = 1 μm. 101
4.11 Scanning electron microscope photographs of films soaked for 7, 14, 21, and 28 days in H_2O at 37°C. Scale bars = 1 μm. 102
4.12 Scanning electron microscope photographs of films soaked for 7, 14, 21, and 28 days in PBS at 37°C. Scale bars = 1 μm. 103
4.13 Scanning electron microscope photographs of films soaked for 7, 14, 21, and 28 days in SBF at 37°C. Scale bars = 1 μm. 104

5.1 Coordinate system used for recording of the polarised Raman spectra of the glutamate films. The incident beam is polarised in the X-direction or Y-direction. 111
5.2 Typical nominal stress/strain curve recorded at room temperature for the native γ-PGA-H films. 112

5.3 Nominal stress/strain curves recorded at room temperature for esterified γ-PGA films. 113
5.4 Nominal stress/strain curves recorded at RT of drawn γ-PGA-Et films drawn at 125°C. Draw ratios are indicated in the figure. 114
5.5 Nominal stress/strain curves recorded at RT of drawn γ-PGA-Pr films drawn at 125°C. Draw ratios are indicated in the figure. 115
5.6 Nominal stress/strain curves recorded at RT of drawn γ-PGA-Bn films drawn at 115°C. Draw ratios are indicated in the figure. 115
5.7 Influence of tensile deformation on Young's modulus, E, tensile strength, σ, and strain at break, ϵ, at RT for all polymers studied. 116
5.8 Tensile strength vs. stiffness of the present polymer series compared with human tissues in the Ashby style plot presented earlier (Section 1.2.2). . 117
5.9 Polarised optical microscopy images of overlayed, 10 times drawn polymer films γ-PGA-Et (A,B) γ-PGA-Pr (C,D), and γ-PGA-Bn (E,F). Orientation is seen using both normal polarized light (A,C,E) and with the use of a quarter wavelength retardation plate (B,D,F). 120
5.10 Wide-angle x-ray scattering of γ-PGA-Et film, λ = 9, drawn at 115°C and annealed at 145°C for 5 min, drawing direction vertical. 121
5.11 Wide-angle x-ray scattering of γ-PGA-Pr film, λ = 13, drawn at 120°C and annealed at 145°C for 5 min, drawing direction vertical. 123
5.12 Wide-angle x-ray scattering of γ-PGA-Bn film, λ = 13.5, drawn at 115°C . 125
5.13 Raman spectra recorded in X|X (red) and Y|Y(blue) orientations for oriented A) γ-PGA-Et, B) γ-PGA-Pr, and C) γ-PGA-Bn polymer films. . . . 127
5.14 First-heating DSC thermograms of γ-PGA-Et films drawn to λ = 10. . . . 128
5.15 First-heating DSC thermograms of γ-PGA-Pr films drawn to λ = 10. . . . 129
5.16 First-heating DSC thermograms of γ-PGA-Bn films drawn to λ = 10. . . 129

6.1 ^{1}H-NMR for γ-PGA-Bn scaled up batches (DMSO-d6, 25°C). 134
6.2 DSC heating traces for γ-PGA-Bn scaled up batches where black indicates first heating and red is the second. 137

List of Tables

1.1 Examples of advantages and disadvantages of graft or tissue engineering construct origin. 29
1.2 Basic characteristics of a perfect tissue engineering scaffold. 38

2.1 Degree of esterification as synthesised and calculated from NH peak in ^{1}H-NMR. 49
2.2 Fourier transform infrared spectra absorptions and chemical groups of interest for native γ-PGA and esterified polymers. Table generated from values listed in[25,26] 59
2.3 Distances between similar atomic planes for batches of γ-PGA polymers. 63
2.4 SEC results for differing batches of γ-PGA esterifications. 65
2.5 Thermogravimetric analysis of esterified γ-PGA polymers. 66
2.6 Thermal results for all γ-PGA polymers obtained via DSC, where T_{rc} is measured during heating and T_c from cooling. 70
2.7 Thermal results for all γ-PGA polymers obtained via DSC in K. 71

3.1 Thermal characterisation of coupled γ-PGA-Phe. 83
3.2 Thermal and mechanical properties of γ-PGA polymers as presented in Chapter 5. 84
3.3 Thermal and mechanical properties of nylon polymers as presented in[27]. 84

5.1 Structure and properties of polymers used in this work as produced in Chapter 2. Glass transition temperature, $\mathbf{T_g}$, and melting temperature, $\mathbf{T_m}$, of native powder were determined by differential scanning calorimetry; average molecular weight, $\mathbf{M_w}$, calculated from size-exclusion chromatography. 109
5.2 Mechanical characteristics at room temperature of differently esterified γ-PGA films tested at room temperature. 113
5.3 Mechanical properties of esterified γ-PGA films as-cast and maximum properties achieved by drawing to $\lambda = 10$. 117
5.4 Calculated theoretical moduli for esterified γ-PGA films using Equation 5.1. 118

5.5 Calculated WAXS lattice parameters from Figure 5.10 for γ-PGA-Et, oriented to λ = 9. 122
5.6 Calculated WAXS lattice parameters from Figure 5.11 for γ-PGA-Pr, oriented to λ = 13. 124
5.7 Calculated WAXS lattice parameters from Figure 5.12 for γ-PGA-Bn, oriented to λ = 13.5. 125
5.8 Common Raman shift values for secondary protein structures, as reproduced from[28]. 126
5.9 Normalised endotherm/exotherm ratios for γ-PGA films drawn to λ = 10. 130

6.1 SEC results for scaled up γ-PGA-Bn series polymers. 135
6.2 Thermal characterisation of all γ-PGA-Bn batches, where T_c represents crystallisation upon cooling. 136
6.3 Density of all γ-PGA-Bn scaled-up batches. 138

Abbreviations

Name	Abbreviation
1,1,1,3,3,3-hexafluoroisopropanol	HFIP
Alpha minimum essential medium	α-MEM
Arginine-glycine-aspartic acid	RGD
Attenuated total reflectance	ATR
Benzyl-esterified poly(γ-glutamic) acid	γ-PGA-Bn
Boc-protected poly(γ-glutamic) acid	Boc-γ-PGA
Bovine serum albumin	BSA
Crystallisation temperature	T_c
De-ionised water	diH_2O
Deoxyribonucleic acid	DNA
Deuterated dimethyl sulfoxide	DMSO-d6
Dicyclohexylurea	DCU
Diethyl ether	Et_2O
Differential scanning calorimetry	DSC
Dimethyl sulfoxide	DMSO
Dimethylformamide	DMF
Dulbecco's modified eagles medium	DMEM
Dulbecco's phosphate buffered saline	DPBS
Embryonic stem cell	ESC
Ethidium homodimer-1	EthD-1
Ethyl-esterified poly(γ-glutamic) acid	γ-PGA-Et
Extracellular matrix	ECM
Foetal bovine serum	FBS
Food and drug administration	FDA
Fourier transform infrared spectroscopy	FTIR
Glass transition temperature	T_g
Glycosaminoglycan	GAG
Haematopoetic stem cell	HSC
Human foreskin fibroblast cell-1	HFF-1
International Organization for Standardization	ISO
L-Phenylalanine amide hydrochloride	Phe-$CONH_2$

Name	**Abbreviation**
Melting temperature	T_m
Mesenchymal stem cell	MSC
N,N'-dicyclohexylcarbodiimide	DCC
N,N'-diisopropylcarbodiimide	DIC
N,N-diisopropylethylamine	DIPEA
N-methyl pyrrolidone	NMP
Nuclear magnetic resonance	NMR
Number-average molecular weight	M_n
Phenylalanine-conjugated poly(γ-glutamic) acid	γ-PGA-Phe
Polarised optical microscopy	POM
Poly(γ-glutamic) acid	γ-PGA
Poly(epsilon-caprolactone)	PCL
Poly(ethylene glycol)	PEG
Poly(lactide-co-glycolide)	PLGA
Poly(L-lactide)	PLLA
Poly(methyl methacrylate)	PMMA
Polydispersity index	PDI
Polytetrafluoroethylene	PTFE
Propyl-esterified poly(γ-glutamic) acid	γ-PGA-Pr
Recrystallisation temperature	T_{rc}
Room temperature	RT
Scanning electron microscopy	SEM
Size exclusion chromatography	SEC
Thermogravimetric analysis	TGA
UV-visible spectroscopy	UV-Vis
Water contact angle	CA
Water soluble carbodiimide	WSC
Weight-average molecular weight	M_w
Wide-angle x-ray scattering	WAXS
Poly(γ-glutamic) acid (acid form)	γ-PGA-H
Poly(γ-glutamic) acid (salt form)	γ-PGA Na^+

Chapter 1

Introduction

1.1 Damaged and degenerated tissues

Musculoskeletal diseases and disorders are of growing concern for both tissue engineers and orthopaedic surgeons. In 2004, the total estimated cost (both direct and indirect) of musculoskeletal related diseases in America was $849 billion, which comprised 7.7% of the gross domestic product.[29] These burdens are excepted to increase as the medical community faces an increasing demand of treating an ageing population.

Injuries to soft tissues, such as tendons, ligaments, or cartilage, lead over 800,000 people to seek medical care annually worldwide.[30,31] These afflictions most commonly involve the shoulder, ankle, or knee joints, causing pain and debilitation of the patient.[30] The most common causes of shoulder pain are disease, degeneration, and impingement of the rotator cuff, a group of four muscles in the shoulder complete with corresponding tendons which interdigitate to form one common insertion into the humerus of the arm.[32] Damage to these tendons occurs either through traumatic injury or gradual wear and tear, often caused by the bony acromion process of the scapula. These tissues have a limited regeneration capacity and usually require surgical repair to regain arm function.[33]

While some ligaments can heal fairly well, such as the collateral ligaments on the side of the knee, others require surgical intervention, namely the cruciate ligaments inside the knee joint. Cruciate ligaments are often repaired or replaced to maintain stability of the knee joint, which is vital to protection of cartilage tissue. Joint instability is known to cause premature osteoarthritis, a degenerative disease affecting the articular cartilage (lining ends of the long bones).

The leading causes of disability afflicting the elderly are osteoarthritis and other rheumatic conditions. In the United States alone, over 47.8 million people live with doctor-diagnosed arthritis.[34] This number is projected to increase to nearly 67 million people (25% of the adult population), with 25 million experiencing arthritis-related activity limitations (9.8% of the adult population).[34]

More specifically, osteoarthritis results in many changes[35], which cause mobility loss,

debilitation, and a lessened quality of life.[36] Cartilage has poor regenerative capability, and current clinical therapies focus solely on symptomatic treatment with only one "cure" of joint replacement surgery.[37] Those afflicted in America account for nearly 50% of joint replacement surgeries each year.[38] Unfortunately, implants have a finite lifespan owing to loosening of the prosthesis, requiring further surgery and increasing morbidity of the patient.[36,37]

The future of medical treatment for osteoarthritis and other disorders requires a focus on regeneration of diseased and damaged tissues, which has the potential to improve patients' conditions, disability, and thus quality of life.

1.2 Tissue engineering

Tissue Engineering is an exciting, relatively new field of research with the ultimate aim to make a three-dimensional cell-containing "scaffold" that can be implanted into the body to cure a disease or repair a defect.[39] This discipline also has the potential to change the face of medicine: reducing the need for organ transplantations, speeding up development of drugs and medical devices, or eventually even replacing organ transplant altogether.[40]

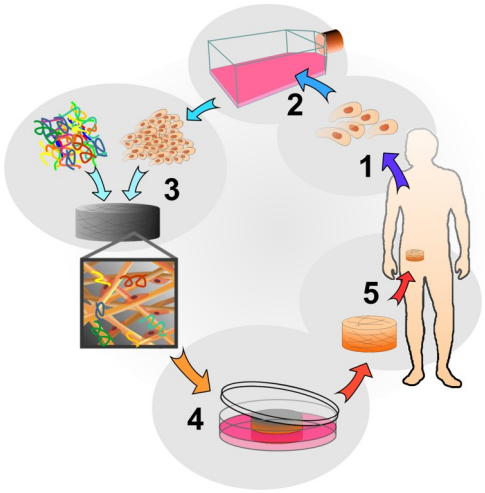


Figure 1.1: The typical tissue engineering approach: 1) Remove cells; 2) Expand number in culture; 3) Seed onto an appropriate scaffold with suitable growth factors and cytokines; 4) Place into culture; 5) Re-implant engineered tissue repair damaged site. Figure used with permission from author.[1]

A general example of tissue engineering using autologous cells is shown in Figure 1.1 Cells are removed from the patient, grown up in culture, seeded and cultured on a type of bioactive scaffold, and then surgically re-implanted in the body. While these steps are considered key factors, some research is focused on creating a bioactive, biomimetic, and cell-free scaffold to implant directly into the body. This eliminates both the need for harvesting cells from the body and cell culture. Scaffolds can be modified with biological signals to incorporate better with the implant site.

One goal of researchers is to use a scaffold that will slowly degrade at the same rate of native host tissue regeneration. Different tissues in the body have diverse compositions of the surrounding extracellular matrix (ECM). This poses another challenge for tissue engineers to make tissues, whereby a scaffold intended for bone would not suit liver, cartilage, or nerve regrowth.

Defects of tissue resulting in loss or failure have been treated with surgical manipulations of tissues or organs. Often referred to as grafts, the obtained tissue is named for its location of origin. If acquired and implanted in the same patient, it is called an autograft; if implanted in an individual of the same species, it is an allograft; if placed in a different species, a xenograft.[41]

While each source has their advantages and disadvantages (Table 1.1), there is a distinct need for tissue engineering to improve upon these choices. Surgery to obtain tissue for implants is expensive and carries risks for the patient. The Food and Drug Administration (FDA) in the United States has already granted approval for some polymers to be used in the body, with which scaffolds are produced easily and at low cost. Unfortunately, proteins adsorb non-specifically to the polymers in their native state, and cell-binding motifs do not exist on the polymers, so there is a need to functionalise these polymers for enhanced tissue incorporation.

Table 1.1: Examples of advantages and disadvantages of graft or tissue engineering construct origin.

Scaffold Source	**Advantages**	**Disadvantages**
Autograft (Same patient)	Little to no immunorejection Considered ”gold-standard” for tissue choice[41]	Limited donor sites Extra surgery to obtain tissue Increased donor-site morbidity Expensive
Allograft (Same species)	Same species, likely to incorporate Tissue can be obtained from donors not afflicted by the disease of the recipient	Possibility of pathogen transfer More likely to experience immunorejection than autograft Procurement of tissue is complex and expensive
Xenograft (Different species)	Large amount of tissue availability	Possibility of xenozoonosis (pathogen transfer from another species)[42] Highly likely to elicit immune response Issues of incorporation into host tissue
Artificial (Polymer origin)	Cells can be seeded and cultured on the scaffold Naturally degraded by the body Easy to produce in bulk FDA approved polymers Cheap to produce	May be recognized as a foreign body and elicit an immune response Unfunctionalised, often hydrophobic No blood vessel formation within artificial polymer network

1.2.1 Musculoskeletal tissues

Bone

There are two types of bone in the body, distinguished by their density: cortical (often called compact) and trabecular bone (spongy, or cancellous). Cortical bone consists of concentric rings of matrix circumventing both central and perforating canals, while trabecular bone has bone marrow filled amongst the irregular, porous lattice structure.[43] A natural composite of inorganic hydroxyapatite and organic matrix, bone can withstand both tensile and compressive forces. The organic extracellular matrix is mostly collagen (90% total ECM, with 97% type I and 3% type III collagen) while 10% is composed of other non-collagenous proteins, namely osteocalcin, osteonectin, proteoglycans, fibronectin, growth factors and more.[44] The collagens contribute to tensile properties, while the mineral crystals increase the hardness and toughness of the tissue.[43]

Bone is a dynamic tissue, constantly remodelling itself in response to mechanical stimulation. Three types of cells exist in bone, osteoblasts (form bone), osteoclasts (resorb bone), and osteocytes (highest population of cells in bone; translate mechanical stimulation into chemical signals that affect bone renovation[45–47]). The cells control the balance of storing and releasing calcium for use in the body, however this is disproportional in osteoporotic patients and more bone is resorbed. This results in less dense bone which is more brittle and thus prone to fracture.

If a patient experiences a loss of bone from cancer or trauma, the defect may be too large to regenerate, requiring an implant in the damaged site. One option is transplantation from another area in the body, but this is limited due to limited availability of non-weight bearing bone, donor site morbidity, increased pain and recovery time for the patient, and risk of additional surgical complications.[48] Tissue engineering could provide an alternative option to replace the damaged or missing tissue, assisting the bone in its regeneration.

Cartilage

Prone to damage, articular cartilage (hyaline cartilage) also has a poor ability to repair itself and injuries often lead to an earlier onset of osteoarthritis.[37,49–51]. A commonly used treatment, called microfracturing, involves cracking the underlying bone surface to induce repair. Unfortunately, the cartilage formed is often fibrocartilage, which has poor mechanical properties and integration with the native hyaline tissue. Autologous cell transplantation also appears to fail long-term in repairing articular cartilage defects. Better techniques for cartilage repair are needed to prevent or treat premature osteoarthritis.

Articular cartilage is mainly acellular, with chondrocytes only comprising about 2% of the total cartilage volume in adults.[52] It also is organized into three zones, differing in composition, organisation, and cell concentration (Figure 1.2).[2] Cartilage is avascular

and chondrocytes are dependent on successful nutrient and oxygen diffusion through its extracellular matrix (ECM).

Chondrocyte metabolism operates at low oxygen tension within the cartilage matrix, ranging from 10% at the surface to less than 1% in the deep zones. During physiological hypoxia, the hypoxia inducible factor-1α acts as a survival factor for the chondrocyte in the avascular cartilage matrix, permitting maintenance of homeostasis and the capacity to respond to environmental change.[53] These properties of cartilage are key challenges that researchers must address with scaffolds and tissue engineering.

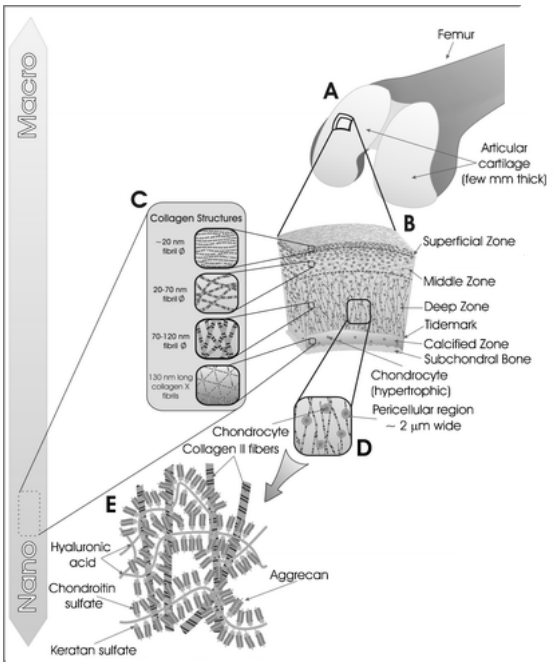


Figure 1.2: Hierarchical organisation of cartilage. A) Articular cartilage covers the ends of long bones B) with distinct zonal organisation of C) collagen structure. Resident D) Chondrocytes are surrounded by a matrix of E) aggrecan/hyaluronic acid super-aggregates and macrofibrillar collagen networks. Adapted from[2] with permission. Copyright 2004, AAAS.

Connective tissues

Two types of connective tissue are of interest in musculoskeletal tissue engineering: ligament, connecting bone to bone, and tendon, which connects muscle to bone.[3,54] Ligaments determine the range of motion which the joint can endure before rupture.[54] In contrast, tendons transmit forces generated by muscles to bone, resulting in skeletal motion and stability of the joint.[54,55] Ligaments are key passive joint stabilisers, while tendons can actively store and return elastic energy.[54,56]

Collagen type I is the predominant solid constituent of ligaments and tendons (typically greater than 75%), and may compromise up to 99% of the dry weight in some tendons.[55] While ligaments and tendons appear similar, there are differences which greatly affect their function. In 1984, Amiel *et al.* performed a histological and biochemical comparison

between rabbit tissues,[57] which helped to distinguish that these tissues are not as similar as previously thought. They found that tendons contained more collagen type I, less glycosaminoglycans (GAG), less DNA, and a different collagen cross-linking pattern than ligaments.[57] On the other hand, ligaments contained more type III collagen (attributed to be less mature), more GAGs, larger and more cells, and a collagen cross-linking pattern similar to granulation tissue (involved in wound healing).[57]

Due to the nature of their purpose of transmitting forces to and from bone, both tissues must endure an interfacial gradient change to integrate well into bone. The mechanical properties of the tissues are drastically different, seeing as bone responds to compression while ligaments and tendons are very strong in tension.[3,54,58] Thus tissues have developed gradual changes (Figure 1.3) to prevent stress concentrations, namely using fibrocartilage as a transition. Moffat *et al.* reported that the mineralised transition in fibrocartilage transfers compressive load.[59] Young's modulus was been shown to increase across the juncture, with the mineralised fibrocartilage withstanding significantly higher compression.[3,59] This demonstrates a common challenge for tissue engineering applications, as improper fixation, integration, or distribution of mechanical properties would cause an imbalance in force transfer and ultimately lead to failure.

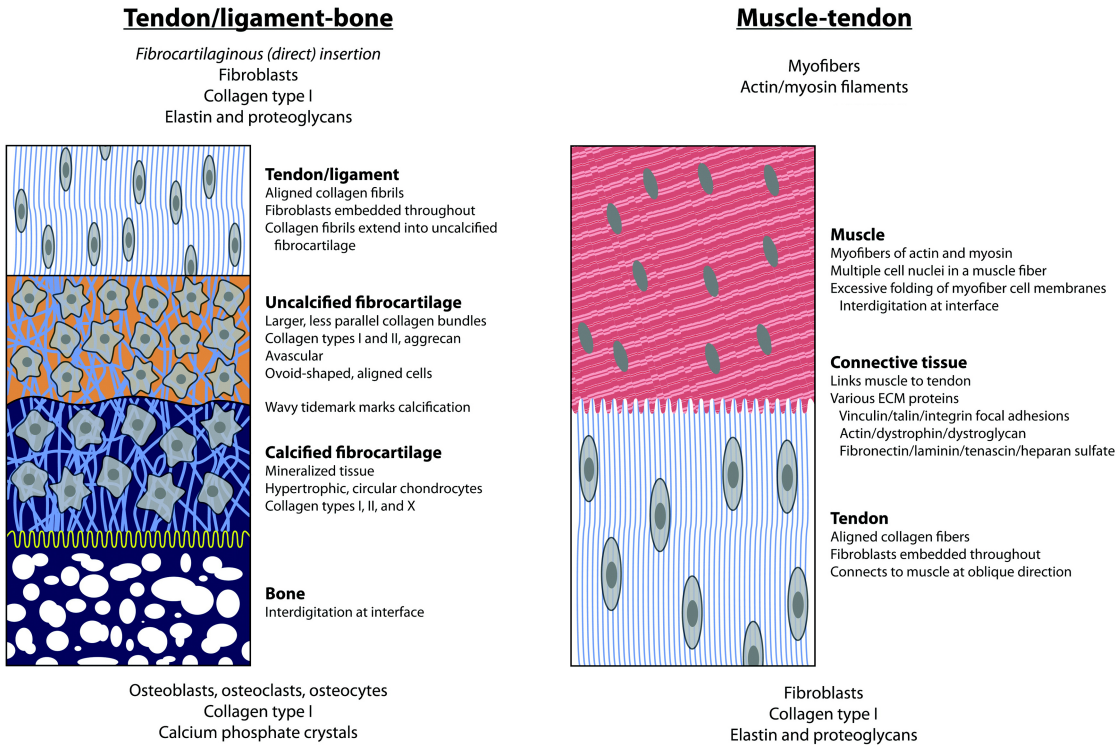


Figure 1.3: Diagram adapted from[3] detailing tendon/ligament-bone and muscle/tendon interface compositions including aggrecan (orange), collagen fibres (light blue), mineralised tissue (dark blue) and muscle fibres (red).

1.2.2 Tissue mechanical properties

In order to target specific tissues, engineered constructs should also take into account the native mechanical properties. For example, titanium alloy implants, the current gold standard bone replacement, are orders of magnitude stiffer than the tissue itself. As a result, the implant bears the majority of mechanical loading, leading to stress shielding within the bone.[60] As mechanical stimulation is necessary to maintain healthy bone tissue, this discrepancy can result in loss of bone around the implant, causing loosening and, ultimately, failure of the implant. Therefore, researchers must also be aware of the native tissue properties to appropriately tailor the replacement product.

Figure 1.4 compares bulk mechanical properties of hard (mineralised) and soft (unmineralised) human tissues subjected to tensile testing in a plot modelled after Ashby *et al.*,[61] while Figure 1.5 presents materials commonly used as tissue replacements.

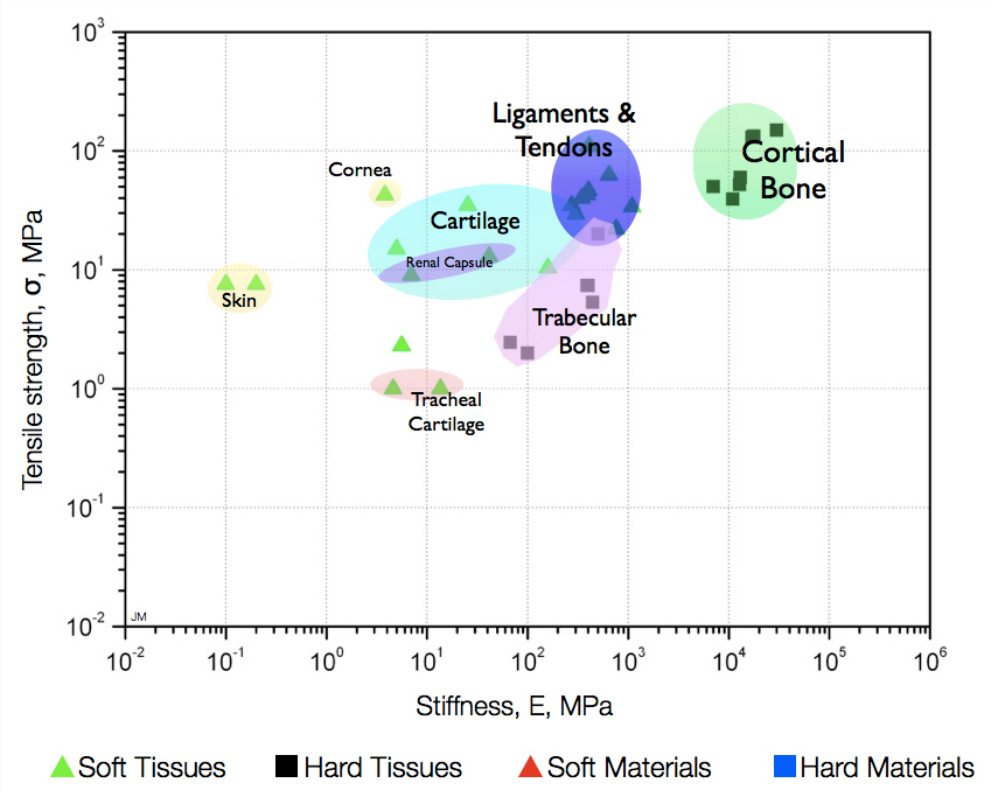


Figure 1.4: Ashby-style plot of stiffness versus tensile strength of human tissues tested in tension using data taken from[4–24]

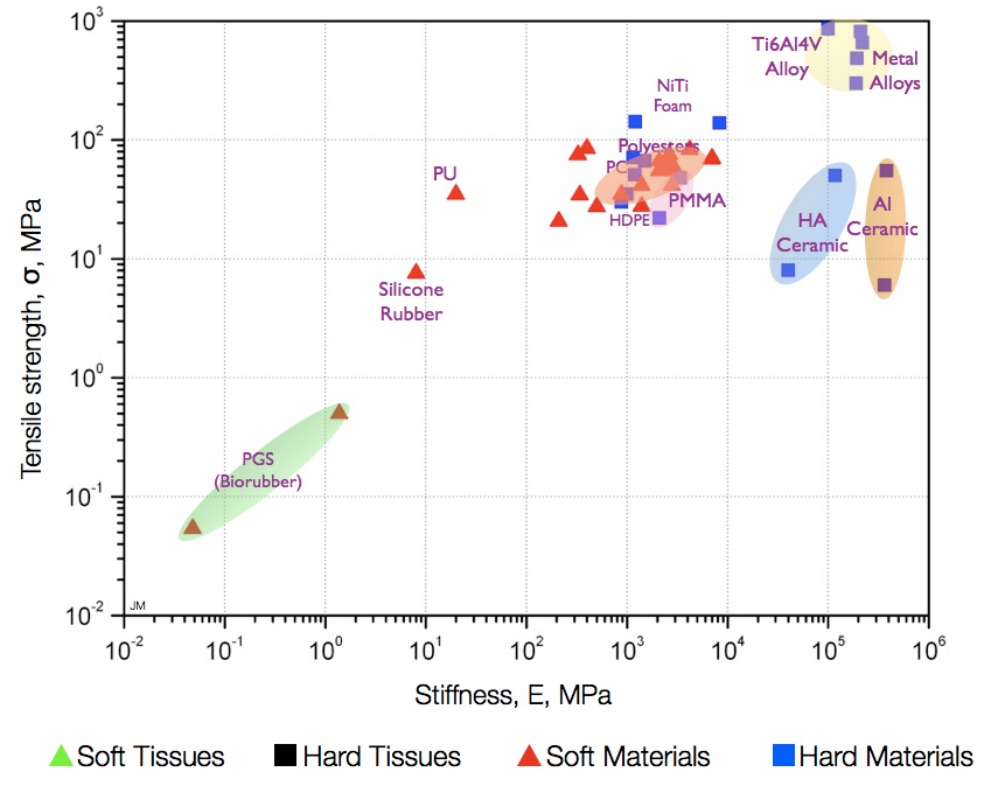


Figure 1.5: Ashby-style plot of stiffness versus tensile strength of biomaterials commonly as tissue replacements, using data taken from[4–24]

1.2.3 Cell sources

Stem cells

Several cell types can be used in tissue engineering, depending on the desired outcome of the engineered construct. In recent years, researchers have been investigating the potential of stem cells. The two most common classifications of stem cells are adult stem cells and embryonic stem cells. Haematologists treating leukaemia with bone marrow transplants first discovered adult stem cells, and today the two most common adult stem cells are haematopoetic stem cells (HSCs) and mesenchymal stem cells (MSCs or marrow stromal cells).[39,62,63]

On the other hand, embryonic stem cells (ESCs) are derived from a blastocyst, a ball of cells formed after fertilisation. These cells have generated lots of ethical debate surrounding their origin, and as such the first human ESCs were developed in 1998 while murine ESCs were developed in 1981.[39,64] Termed 'pluripotent', ESCs have the ability upon dividing to become any cell in the body, based on the culturing environment, while also retaining their ability to divide indefinitely in an undifferentiated state.[39] For tissue engineers this is exciting because ESCs have the potential to provide an unlimited source of cells, whereas adult stem cells have a limited dividing capacity.[39]

Lately, the periosteum has been gaining attention in tissue engineering. The periosteum is a multi-layer tissue that serves as the boundary between the long bones and the surrounding soft tissues and contains multiple cell types.[65] Within the cambium layer of the periosteum, researchers have found cells that appear to be stem-cell like, with the ability to generate into other tissues such as bone and cartilage.[66–72] This is also another potential source of cells for regenerative medicine.

Primary cells

Osteoblasts might be an attractive source for bone tissue engineering as they synthesise, secrete, and mineralise matrix to form bone. Derived from bone marrow, osteoblasts mainly synthesise collagen type I, but also produce growth factors and other proteins necessary for healthy bone formation.[73] Unfortunately, once they are embedded in their formed matrix, they either experience apoptosis or differentiate to form osteocytes, which resemble nerve cells and are also known as inactive osteoblasts.[73,74]

Chondrocytes are a potential source of cells for cartilage tissue engineering. Native to articular cartilage, these cells seem an ideal source, and autologous cartilage transplantation has recently been used as a clinical therapy for osteochondral defects.[51,75] Unfortunately, due to chondrocytes' limited regenerative capacity, this treatment is unsuitable, and the surgery required to obtain cartilage is associated with donor-site morbidity.[75] Furthermore, osteoarthritic patients will typically have limited amounts of viable articular cartilage available for harvesting.

Hui et al.[75] have investigated several therapies for repairing chondral lesions, including using chondrocytes and MSCs transplants, periosteal grafts, and mosaicplasty (osteochondral autograft) in rabbits. This group found that while osteochondral autografts did well initially, the periosteal grafts did "less than favourably", and the chondrocytes and MSCs, encapsulated in a fibrin glue, had comparable enhancing effects of hyaline cartilage.[75] While chondrocytes and MSCs had comparable effects, chondrocytes have little to no regenerative capacity, making MSCs a more ideal cell choice.

Ligament and tendons are sparsely populated, yet the main cell type found in these tissues is the fibroblast. Responsible for collagen production, these cells are elongated and well known to align in the direction of collagen fibre orientation. Fibroblasts upregulate genes responsible for matrix proteins in response to injury, generating randomly organised, fibrous scar tissue.[76] Fibroblasts also respond to mechanical stimulation, producing more matrix as a result of mechanotransduction.[77] In addition, these cells are responsible for reorganisation of the extracellular matrix, so in advanced healing they degrade and replace the scar tissue with newly synthesised, organised matrix.[76] Despite their ability to generate large amounts of extracellular matrix, fibroblasts have a low mitotic rate,[31] thus are not ideal for tissue engineering applications.

1.2.4 Extracellular matrix and cellular interactions

Central to tissue engineering, researchers are coming to realize that the ECM plays a vital role in cell and tissue growth. The nanoscale ECM structure in the body provides a natural web of intricate fibre-like nanostructured proteins to support cells and present an instructive background to guide their behaviour.[38] The ECM is composed of mainly three classes of biomolecules: (1) structural proteins, collagens and elastin; (2) specialized proteins, such as laminin and fibronectin; and (3) proteoglycans, which have a protein core with many disaccharide chains attached called glycosaminoglycans.[78] Researchers must produce a three-dimensional scaffold that encourages cells-ECM interaction, allows sufficient nutrient diffusion, and supports tissue ingrowth.

The outer membrane of an animal cell is usually covered with specific signalling proteins and carbohydrate structures. It also has at least six different receptor systems that can be activated in several ways, such as interactions with ligands in the ECM, neighbouring cells, or soluble signalling molecules.[38] Integrins are an important example of a transmembrane protein receptor, consisting of a combination of one α-subunit and one β-subunit. There are 18 known α- and 8 β-subunits, from which 24 pairs are characterised. The specific combinations of subunits determine the ligand specificity, though some are less specific than others.[79,80]

Upon binding to the ECM, integrins undergo activation via conformational change, triggering numerous signal transduction pathways that serve to regulate many aspects of cell behaviour: cell proliferation, differentiation, gene expression, shape, polarity, motility,

and survival/apoptosis.[81] The cytoplasmic tails of integrin subunits are generally short and adapter proteins associate with the tails to connect the integrins to the cytoskeleton. Once attached, the cell spreads, and integrins begin to cluster together, successfully anchoring the cell to the ECM. The actin filaments inside the cell reorganise into larger stress fibres, and acting as a positive feedback system, the number of clustering integrins increases until proteins on either side of the integrins form well-developed aggregates known as focal adhesions.[82]

One well-studied ECM protein motif that nearly half of the 24 integrins bind is Arginine-Glycine-Aspartic Acid (RGD). RGD exists in many ECM components, such as collagen, laminin, osteopontin, vitronectin, and fibronectin.[79] RGD peptides were first found to promote cell adhesion in 1984[83], and since then many materials have been functionalised with RGD. Stable linking of RGD peptides to a surface is necessary to promote focal adhesions as their formation only occurs if the ligands can withstand the cells' contractile forces.[79,84–87]

Other short peptide sequences which mimic ECM components have been studied as candidates for functionalising surfaces for biomaterials and tissue engineering.[88] In 1991, Staatz *et al.* identified the sequence DGEA as a collagen type I binding peptide.[89] This sequence has gained popularity in recent years for bone[90] related applications, and some groups have even looked to DGEA to direct stem cell differentiation.[88,91,92]

Other peptide sequences pertaining to collagen type I and bone have been identified, such as P15[93] and GFOGER[94]. The sequence of P15 comes from a biologically active region of a type I collagen alpha-1 chain, namely amino acids 766-780, and is involved in bone formation.[93,95] Similarly, GFOGER also has a positive effect on bone cells, and even promotes improved osseointegration of functionalised implants *in vivo*[96,97].

Identification of matrix mimicking protein sequences and their effect both *in vitro* and *in vivo* is advantageous for making tissue engineered constructs more like the native ECM. While synthetic polymers can be produced with the same morphology as the ECM, they lack the necessary cellular signals. Therefore, there is a prominent need for biofunctionalisation of these polymers in tissue engineering. Relevant fragments that have been identified to have a positive effect, much like the whole biological protein, provide an option to functionalise synthetic polymers for better cellular and tissue integration.

1.3 Polymers and their role in tissue engineering

1.3.1 Scaffolds

Scaffold requirements

The scaffold is a temporary supporting structure for growing cells and tissues.[41] Just like the ECM, the artificial scaffold must play a vital role in tissue growth and cell proliferation. An ideal scaffold would possess all the characteristics and functions of the ECM under physiological conditions. Tissue-specific structure and properties are exhibited in the native ECM's complex and dynamic environment, filled with nano-sized features of pores and fibers.[38,41,98] Some basic characteristics are listed below in Table 1.2.

Table 1.2: Basic characteristics of a perfect tissue engineering scaffold.

Characteristics	General remarks
Biodegradable	Degradation rate must equal the rate of tissue regeneration
Biocompatible (non-toxic)	Material should not cause any inflammatory or toxic response and any byproduct of degradation should not harm native tissue
Porous 3-D structure	Assist cellular ingrowth & allow adequate oxygen/nutrient supply
Chemically modifiable	Functionalise chemical or peptide sequences to improve cell adhesion or direct cell growth & differentiation
Mechanical properties	Provide support for regenerating tissue while generating appropriate mechanical stimulation
Sterilisable	Using common medical techniques for medical implants

1.3.2 Polymers to use for scaffolds

Material selection is one of the most important factors for tailoring a scaffold to a specific tissue. Currently, there is an immense array of biocompatible materials that can be used to construct a scaffold. Several factors of these materials, such as degradation rate, mechanical properties, hydrophilicity, cell adhesion and cell proliferation are necessary considerations when choosing one for engineering a specific tissue.[99]

Synthetic polyesters

Poly(lactide) (PLA) is the polymer produced from the cyclic diamer of lactic acid. Two isomers exist, D (dexorotary form, PDLA) and L (levorotoary, PLLA, naturally occurring form), and the polymer is formed by ring-opening polymerisation.[100] A synthetic blend of D,L-lactide can also be formed, though it makes an amorphous polymer. PLLA is a very hydrophobic, semicrystalline polymer, and has a degradation time of one to two years in the body.[100] All isomers degrade by hydrolysis into lactic acid, which can be removed from the body by regular metabolic processes.

Poly(lactide-co-glycolide) (PLGA) is a copolymer formed from the cyclic diamers of lactic acid and glycolic acid by ring-opening polymerisation. For a PLGA copolymer, it

is important to note that a linear relationship between composition and degradation time does not exist[100,101]. PLGA also degrades by hydrolysis into lactic acid and glycolic acid that are removed by metabolic processes in the body.

Poly(ethylene glycol) (PEG) is a very hydrophilic polymer of ethylene glycol, produced by polycondensation step polymerisation.[102] PEG is commonly used in drug delivery, tissue engineering, and can be used to increase the hydrophilicity of a polymer blend. PEG is non-toxic, non-immunogenic, and non-antigenic.[103] PEG also has a prolonged residence in the human body, decreased degradation by metabolic enzymes and a reduction or elimination of protein immunogenicity.[103]

Poly(ϵ-caprolactone) (PCL) is a semicrystalline polymer, produced by ring-opening polymerisation. PCL has a lower melting temperature than PLA, but has a degradation time of around two years.[100] PCL also degrades by hydrolysis, and could be a promising polymer for tissue engineering, but it is unfunctionalised and hydrophobic. The formation of PCL and other polymers is shown in Figure 1.6.

Some feature all hydrophobic, FDA-approved polyesters have in common is their degradation mechanism, acidic byproducts, and unfunctionalised polymer backbone. Furthermore, their degradation products may build up in tissues, causing a drop in pH, which can catalyse the hydrolysis, resulting in bulk degradation of the scaffold and a drastic loss of mechanical properties. Polyesters are also well known to cause cysts from the acidic buildup in bone tissue.[104] Thus, alternative polymers that may be functionalised, degrade in a more-controlled manner, and release byproducts which are more tolerable than those from polyesters are of interest in tissue engineering.

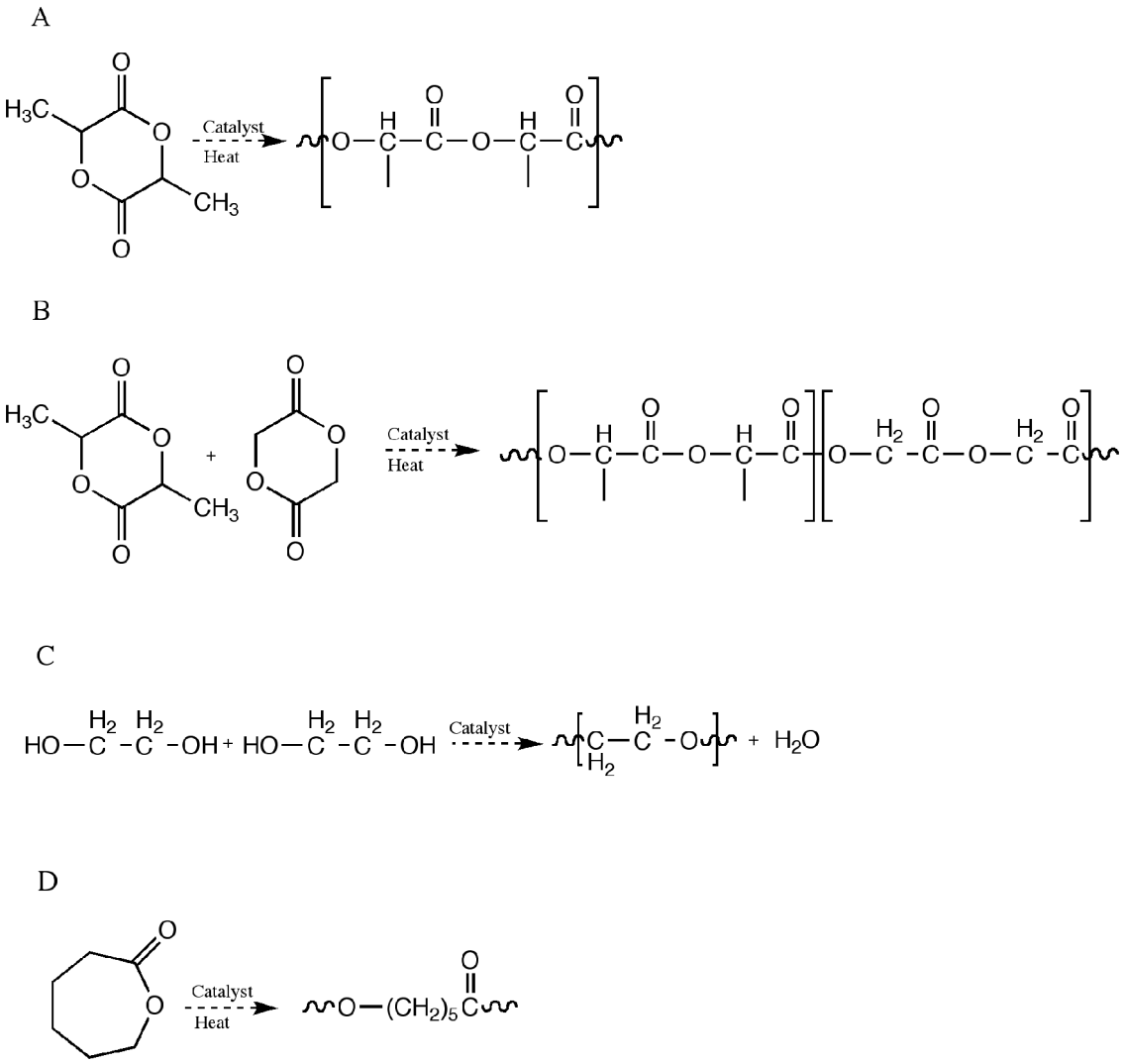


Figure 1.6: Synthesis of FDA approved polyesters. A) PLA, B) PLGA, C) PEG, D) PCL.

Naturally produced polymers

Many researchers have concluded that further functionalisation is necessary to mimic the ECM as well as producing scaffolds with features of the same size. Natural polymers have been used as tissue scaffolds as they may retain the necessary cues for cells from the ECM. For example, groups have successfully fabricated scaffolds from fibrinogen,[105,106] hyaluronic acid,[107,108] chitosan,[109] collagen types I[110–113] and II[114,115] chondroitin sulfate,[112] DNA,[116] gelatin,[117,118] and silk.[119–122] Unfortunately, these natural polymers are very expensive to purchase and often, their mechanical properties are decreased from those in the native ECM. Some components fundamental to cartilage, such as collagen type II or hyaluronic acid, are not practical to make scaffolds solely of the single polymer and usually need to be strengthened after fabrication.

Poly-γ-glutamic acid

Poly(γ-glutamic acid) (γ-PGA) is a non-toxic,[123,124] natural polymer synthesised by several *Bacillus* species, two archea, and few eukaryotes.[125] In fact, γ-PGA has even been discovered to be linked to α-tubulin in murine neurons as a post-translational modification of a glutamic acid polymer consisting of 455 subunits.[125,126] Janke *et al.* identified several polyglutamase enzymes involved in this modification and found they were necessary for neurite outgrowth[127]. Furthermore, Rogowski *et al.* discovered this is a reversible process which must be balanced,[128] between polyglutamylases and deglutamylases, as hyperglutamation results in neurodegeneration.[129]

Poly(γ-glutamic acid) is a polyamino acid where the glutamic acid residues are linked via a peptide bond through the γ-carboxyl group (Figure 1.7). One attractive feature is the free α-carboxyl group which both renders the γ-PGA very water soluble and opens numerous possibilities for chemical functionalisation of the polymer. At neutral pH, the polymer is anionic and highly soluble as an ionic salt, such as the readily available Na^+ salt form produced by *Bacillus subtilis*. Other highly water soluble forms Ca^{2+}, K^+, Mg^{2+}, and NH_4^+ have also been discovered.[130]

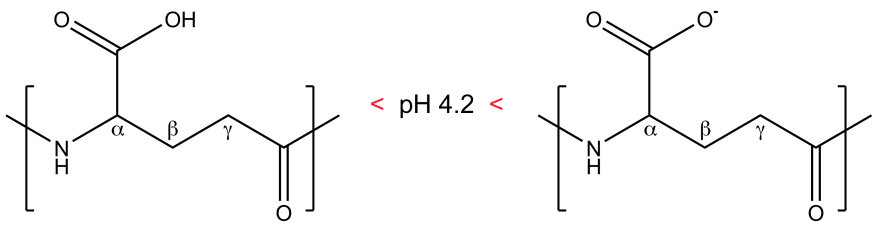


Figure 1.7: γ-PGA, protonated at pH < 4.2, and anionic at higher pH values.

Several industries have extensive uses for γ-PGA, including cosmetics, food, water treatment, drug delivery, heavy metal chelation, agriculture, biodegradable plastics, medical adhesives, vaccines, and tissue engineering. Popular foods in Japan (natto) and Korea (chungkookjang), fermented soybeans using strains of *Bacillus subtilis* utilise the γ-D,L-PGA which is produced as gooey, extracellular mucilage.[130,131]

Since the initial discovery in 1937 by Ivanovics and Bruchner[132] in the capsule of *Bacillus anthracis*,[125] researchers have cultivated γ-PGA production in *Bacillus subtilis*. This bacteria yields a semicrystalline polymer with a racemic mixture of D- and L-subunits, whereas that from *Bacillus anthracis* is only formed from D-subunits and completely crystalline.[125,133] Depending on the culture conditions, the ratio of enatiomers may be optimised for the desired application. In the same way, the weight-average molecular weight (M_w) of the resultant polymer depends on which strain is cultured and salt content in the media. For example, Sung *et al.* discovered that at high concentrations of NaCl, *Bacillus subtilis* produced very low M_w γ-PGA (10-200 kDa with more than 10% NaCl).[124] Today companies sell γ-PGA produced by *Bacillus subtilis* with a M_w of over

to 2 million Da.

With tissue engineering applications in mind, one attractive feature of γ-PGA is that it degrades by enzymes rather than hydrolysis.[134–136] This offers an advantage over FDA approved polyesters, which degrade by random hydrolysis of the polymer chain as discussed in the previous section. The enzymatic degradation of γ-PGA has the potential to be tailored, allowing for a more gradual decrease in mechanical properties as the tissue regenerates.

In 1954, Kream *et al.* studied the enzymatic hydrolysis of γ-PGA produced by *Bacillus subtilis*. As γ-PGA was used either for a sedimenting agent of red blood cells from plasma or an extender of blood plasma volume, they incubated various human tissues with γ-PGA and evaluated their digestion of the polypeptide by testing for free glutamic acid molecules.[134] They found that whole human blood, brain, kidney, spleen, and liver tissue all digested the γ-PGA , while plasma and muscle did not, therefore they concluded that red blood cells are likely to contain enzymes which degrade the polypeptide.[134] There is an apparent lack of *in vivo* studies identifying the specific mammalian enzymes which act upon γ-PGA produced by *Bacillus subtilis* in the literature. Thus, the specific mechanism of degradation in large mammals and humans is unclear and should be further investigated.

1.3.3 Scaffold fabrication methods

There are numerous methods to fabricate polymer scaffolds for use in tissue engineering. Some techniques commonly used[137,138] include gas foaming,[139], fiber bonding,[140], thermally induced phase separation,[141] porogen leaching (salt leaching),[142] rapid prototyping (computer-assisted deposition),[143] freeze drying,[144] and electrospinning.[145] Each technique has advantages and drawbacks when cross-compared, however as each tissue has specific requirements, choosing a method of fabrication should be approached with an ideal, appropriate application in mind.

1.4 Summary

Tissue engineering has the potential to change modern medicine by encouraging the human body to repair itself. With many aspects to consider including tissue-specific requirements, this interdisciplinary field requires a breadth of knowledge from materials, mechanics, chemistry, biology, medicine, and engineering. Whether using a scaffold that is cell-free, cell-containing, or only cells, many approaches are being researched. Biodegradable scaffolds provide a framework upon which cells secrete matrix to regenerate damaged or diseased tissues. Tailorability of materials to target multiple applications also offers flexibility to address patient-to-patient variations often seen in medicine. It is the purpose of this thesis to address chemical and mechanical tailorability of a biopolymer for use in various tissue engineering applications.

Scope of thesis

The ultimate goal of this research is to develop a novel material for the repair of tissues in regenerative medicine. The use of biomaterials to act as a framework upon which cells grow and deposit extracellular matrix (ECM) while the biomaterial degrades, allows tailoring of many properties for specific biomedical applications.

In all the studies presented here, research focuses on utilising a natural, biodegradable polymer produced by bacteria, making it suitable for use in tissue engineering. Poly(gamma-glutamic acid; γ-PGA) is a non-toxic polymer that undergoes enzymatic degradation. This method is advantageous over commonly used polyesters, which undergo random hydrolysis. Polyesters release acidic byproducts that cause a drop in the local pH, leading to a more harsh environment for cells to live in. One example of an adverse reaction to their degradation is cystic formation in bone tissue, where byproducts have a slow rate of removal.[104] Furthermore, this drop in the local pH catalyses the polyester construct degradation, leading to a bulk loss in mechanical properties. It is anticipated that using γ-PGA will degrade in a more controlled manner and the amino acid byproducts released will be more tolerable in the local environment.

The γ-PGA macromolecule contains a simple -COOH side group in the monomer, rendering it highly water soluble, which may be a problem in some tissue engineering applications, particularly when a water-insoluble scaffold is required. Fortunately, this side group can be modified, functionalising of the native polymer and changing its properties. In this work, this -COOH side chain was esterified using three groups, as shown previously[146] to produce a water-insoluble 'scaffold' for use in the human body. Though esterification of γ-PGA has been around for nearly two decades, nobody has investigated this modified material for tissue engineering applications.

All modified polymers were found to be both non-cytotoxic and support human cell growth. This method of chemical modification also enabled the polymer to be drawn using tensile deformation, a common technique used in industry, resulting in mechanical properties that could be tailored over an order of magnitude.

In this thesis, the first chapter serves to provide background information on tissue engineering, including considerations necessary for regenerative medicine, mechanical properties and composition of human tissue, currently used biomaterials, and methods of scaffold fabrication. Chapters 2-6 discuss the experimental results of this thesis, include study-specific experimental methodologies, and provide suggestions for future work. Conclusions and a general overview of future developments are discussed in the final chapter.

Two different methods of γ-PGA modification are described in this thesis. The first technique involves esterification of the -COOH side group and follows the previously described synthesis by Kubota *et al.* to reduce the high water solubility of the native γ-PGA polymer. The second synthesis technique highlights the first time γ-PGA has been

fully conjugated with an amino acid through the side chain via a peptide bond. This novel synthesis paves the way for full functionalisation of γ-PGA with amino acids or peptide sequences. Between the two chapters, disparate functionality of γ-PGA is demonstrated in modifying this polymer for use with tissue engineering applications.
Each experimental chapter highlights are as follows:

Material synthesis and characterisation

Chapter 2 addresses the need for reducing water solubility of the polymer for adequate use in tissue engineering. Using a previously described synthesis method,[146] the γ-PGA was esterified using either an alkyl or aryl group. This chemical modification was structurally and thermally characterised, and results are presented here.

Chapter 3 highlights utilisation of a different modification of γ-PGA, using a two-step carbodiimide synthesis to fully conjugate L-Phenylalanine*HCl, demonstrating amino acid functionalisation. The synthesis, structural and thermal characterisation are discussed in this chapter.

Biological studies and feasibility in tissue engineering

Building on the previous chapter, the feasibility of modified γ-PGA for use in tissue engineering was examined in chapter 4. To assess toxicity of the chemically modified γ-PGA , an international standard pre-clinical test for cytotoxicity (ISO 10993:5) was run on unoriented, modified γ-PGA films. This test is generally used to determine if materials are suitable for *in vivo* studies.[147] For cell viability studies, human foreskin fibroblasts were cultured for 7 days on modified γ-PGA . The ability of this material to support cell viable growth and proliferation was evaluated using a LIVE/DEAD® assay. Immunostaining was performed to image the cytoskeletal organisation of these cells on the polymer.

Dissolution soaking studies were performed for 28 days in three different media to determine any hydrolysis of the modified ester side chain. Mass loss, optical changes, and surface changes were measured and reported in chapter 4.

Increasing mechanical properties and production

Chapter 5 investigates the capability of tailoring mechanical properties of esterified γ-PGA, produced as in chapter 2, by utilising tensile deformation, a powerful method to investigate mechanical properties and produce highly-aligned molecular structures with ultra-high tensile strength.[148] Here, thermal, structural, and mechanical characterisation results are presented, demonstrating tailorability of esterified γ-PGA polymers.

Finally, chapter 6 focuses both on increasing the batch size of esterified γ-PGA and decreasing batch-to-batch variability, employing a different experimental setup to increase yield and repeatability of these batches. Necessary for further translation of this work from the laboratory to industry, this chapter presents the structural and thermal results achieved in scaling the synthesis.

Chapter 2

Reduction of poly-γ-glutamic acid water solubility via side chain esterification

2.1 Introduction

This chapter investigates chemical modification of poly(gamma-glutamic acid) (γ-PGA) to decrease water solubility of the polymer. As discussed in Section 1.3.2, γ-PGA is a water-soluble, edible, nontoxic, and biodegradable poly-γ-amino acid produced by many Bacillus species. Depending on the choice of bacteria, differing enantiomeric positions of γ-PGA can be obtained. For example, *Bacillus subtilis* synthesises γ-D,L-PGA, while *Bacillus anthracis* produces only D-enantiomer γ-PGA[149].

Of particular interest with γ-PGA is the enzymatic[134–136] degradability, while FDA-approved polyesters undergo random hydrolytic degradation. Acidic by-products of polyester degradation can also lead to autocatalysis[150–152] and thus a loss of bulk properties in scaffold material. In contrast, the degradation mechanism of γ-PGA does not experience autocatalysis from polymer by-products.

The high water solubility of γ-PGA limits its' use in tissue engineering scaffold applications as it readily dissolves in minute amounts of water. Thus modification of γ-PGA is necessary to avoid dissolution of fabricated scaffolds. Fortunately, the -COOH side group in γ-PGA provides a site for functionalisation of the polymer, as discussed in Section 1.3.2. To reduce the water solubility for use in scaffolds, this chapter focuses on esterifying the -COOH side chain with either alkyl or aryl groups, as previously reported[146,153]. While Kubota *et al.* pioneered synthesis of water-insoluble γ-PGA, this material has yet to be investigated for tissue engineering applications.

Esterification of biological polymers has become popular in recent years. In the late 1940's and early 1950's, synthesis of methyl esters of hyaluronic acid and chondroitin sulfate were published, though potential applications of these materials were unclear.[154–157] Several decades later, in 1993, esterification of hyaluronic acid was first published for tissue engineering applications under the name HYAFF® (registered by Fidia Farmaceu-

tici s.p.a.)[158] The most popular of esterified hyaluronic acids, HYAFF 11®, is a fully benzyl-esterified polymer that has medical approval for use in Europe.

Similarly, this work aims to utilise esterification to enable γ-PGA for use in tissue engineering. This synthesis chapter presents the chemical, structural, and thermal properties of γ-PGA polymers modified by esterification to limit their water solubility.

2.2 Experimental

2.2.1 Chemical synthesis

General

All starting polymer (γ-D,L-PGA Na^+ salt, produced by *Bacillus subtilis*) was purchased from Natto Biosciences (Shanghai, China). All reagents and solvents were purchased from Aldrich and used as received, unless otherwise specified.

Free acid form of γ-PGA

γ-PGA Na^+ salt (10 g) was dissolved in 250 mL of distilled water. The solution was acidified with HCl 6M to pH 1.5 and lyophilized for at least 96 h. The freeze-dried material resulted in a soft and porous solid.

γ-PGA esterification

γ-PGA free acid (+ NaCl) (2.4 g, 0.01 mol) was introduced into a 250 mL round bottom flask equipped with a thermometer and a magnetic stirrer, and suspended in 180 mL of anhydrous N-Methyl Pyrrolidone (NMP). The suspension was heated by oil bath to 80°C and stirred for 24 h. After that time, the mixture was cooled to 60°C and $NaHCO_3$ (4.3 g, 0.28 M) was added. After 2 h, the corresponding bromide (ethyl, propyl or benzyl bromide to make γ-PGA-Et, γ-PGA-Pr, and γ-PGA-Bn, respectively) was added dropwise to the mixture in a 5x molar excess over 5 min. The mixture was stirred at 60°C for a period of 40 h. The reaction was quenched by removing the round bottom flask from the oil bath, cooling to room temperature and stirring stopped.

For degree of esterification calculation, 3 mL of esterified γ-PGA/NMP solution was precipitated in 30 mL cold HCl (pH 1.5), centrifuged at 4000 R.P.M. for 5 min, supernatant removed, and 30 mL HCl added. This was subsequently repeated twice using diH_2O, and twice with diethyl ether (Et_2O). The resulting polymer was dissolved in 600 μL DMSO-d6 for ^{1}H-NMR, and the degree of esterification was calculated from integration of the NH peak of modified γ-PGA against that of γ-PGA-H (if present) from the ^{1}H-NMR spectra.

If an esterification reaction level was below 100%, the reaction was returned to 60°C, stirring. Once the solution reached 60°C, 2 molar equivalents of the required bromide was added drop wise and allowed to react for 24 h, quenched, another withdrawal for NMR

purified and the level of esterification analysed. This was repeated until either complete esterification was achieved or no change in esterification level was seen with addition of bromide.

Following confirmation of reaction esterification by ^{1}H-NMR, the mixture containing the reacted γ-PGA (in NMP) was decanted and the supernatant was poured into a 2 L beaker containing 1.8 L of cold HCl (pH 1.5) and left to precipitate overnight at 4°C. The remaining salts ($NaHCO_3$ and NaBr) were discarded. The precipitate was filtered on a glass filter (Por 3), washed with cold diH_2O (500 mL) and diethyl ether (500 mL), and finally dried at 40°C overnight under vacuum.

Purification

The esterified γ-PGA was dissolved in DMSO (2% solution) by mild heating (40°C) and stirring. The solution was then precipitated in diH_2O. The solid was filtered on a frit, repeatedly washed with H_2O and Et_2O, and then dried at 40°C overnight under vacuum.

2.2.2 Chemical analysis

Nuclear magnetic resonance

NMR spectra were recorded on a Bruker Biospin GmbH AV500 (operating at 500 MHz for ^{1}H; 125.76 MHz for ^{13}C) using DMSO-d6 as a deuterated solvent. ^{1}H-NMR spectra were referenced to the residual protons in the deuterated solvent. Data are reported as follows: chemical shifts are in ppm in the δ scale; multiplicity (s: singlet, d: doublet, t: triplet, q: quartet, m: multiplet, bs: broad signal); integration; assignment. ^{13}C-NMR spectra were referenced to the solvent chemical shift.

γ-PGA acid form (γ-PGA-H): **^{1}H-NMR** δ: 1.73 (m, 1H, CH β); 1.93 (m, 1H, CH β); 2.19 (t, 2H, CH_2CO); 4.13 (m, 1H, C<u>H</u>NH); 8.21 (d, 1H, NH). **^{13}C-NMR** δ: 27.02 (CH_2 β); 31.59 (<u>C</u>H_2CO); 51.59 (CHNH); 171.66 (COOH); 173.43 (CONH).

γ-PGA Ethyl ester (γ-PGA-Et): **^{1}H-NMR** δ: 1.18 (t, 3H, C<u>H$_3$</u>CH_2O); 1.77 (m, 1H, CH β); 1.95 (m, 1H, CH β); 2.19 (t, 2H, CH_2CO); 4.09 (q, 2H, CH_3C<u>H$_2$</u>O) 4.21 (m, 1H, C<u>H</u>NH); 8.17 (d, 1H, NH). **^{13}C-NMR** δ: 13.87 (<u>C</u>H_3CH_2O); 26.66 (CH_2 β); 31.12 (<u>C</u>H_2CO); 51.49 (CHNH); 60.28 (CH_3<u>C</u>H_2O); 171.37 (COO); 171.68 (CONH).

γ-PGA Propyl ester (γ-PGA-Pr): **^{1}H-NMR** δ: 0.83 (t, 3H, C<u>H$_3$</u>CH_2CH_2O); 1.53 (q, 2H, CH_3<u>C</u>H$_2$$CH_2O$); 1.75 (m, 1H, CH β); 1.94 (m, 1H, CH β); 2.19 (t, 2H, CH_2CO); 3.97 (m, 2H, CH_2O); 4.18 (m, 1H, C<u>H</u>NH); 8.13 (bs, 1H, N<u>H</u>CHCOOH); 8.25 (bs, 1H, N<u>H</u>CHCOOPr). **^{13}C-NMR** δ: 10.11 (<u>C</u>H_3CH_2); 21.45 (CH_3<u>C</u>H_2); 26.71 (CH_2 β); 31.18 (<u>C</u>H_2CO); 51.59 (CHNH); 65.80 (CH_2O); 171.47 (COO); 171.87 (CONH).

γ-PGA Benzyl ester (γ-PGA-Bn): **^{1}H-NMR** δ: 1.77 (m, 1H, CH β); 1.96 (m, 1H, CH β); 2.20 (t, 2H, CH_2CO); 4.25 (m, 1H, C<u>H</u>NH); 5.07 (d, 2H, OC<u>H$_2$</u>Ph); 7.29 (m, 5H, H-Ar); 8.27 (d, 1H, NH,). **^{13}C-NMR** δ: 26.63 (CH_2 β); 31.19 (<u>C</u>H_2CO); 51.66 (CHNH); 65.83 (CH_2O); 127.65-135.89 (C-Ar); 171.54 (COO); 171.69 (CONH).

Film casting

Polymer films for ATR-FTIR, wide-angle x-ray scattering, and contact angle analysis were cast onto a PTFE-lined 6-well polystyrene culture plate from a 5% wt wt^{-1} solution in 1,1,1,3,3,3-hexafluoroisopropanol (HFIP). Well plates were covered loosely and solutions allowed to evaporate for 72 h at RT.

Fourier transform infrared spectroscopy

Fourier transform infrared (ATR-FTIR) spectra were obtained with a Perkin Elmer® Spectrum 100 FTIR Spectrophotometer, from 500 to 4000 cm^{-1} using the Universal diamond attenuated total reflectance (ATR) top-plate.

Wide-angle x-ray scattering

Wide-angle x-ray scattering (WAXS) was performed by Mr. Ryan Bayliss (Materials Department, Imperial College) on polymer films cast on PTFE (as above) using a PANalytical MPD X-ray diffractometer (Almeo, Netherlands), using a Cu K_α source with a secondary graphite monochromator (step size = 0.03 degrees, 50 s count time per step).

Size exclusion chromatography

All measurements were performed by Dr. Thomas Schweizer (ETH) on esterified γ-PGA using a PL-GPC 220 integrated gel permeation chromatograph/size exclusion chromatograph (SEC) fitted with a differential refractometer, a PL-220R viscometer, and a PL-PD2040 light scattering detector (all Varian, Inc.; Palo Alto, CA, USA). Solutions of esterified γ-PGA (1.5 mg mL^{-1} in dimethylformamide (DMF) containing 1 g L^{-1} LiBr) were prepared and injected through two 10 μm PLgel MIXED-B columns connected in series using DMF at a flow rate of 1 ml min^{-1} and a temperature of 45°C. Data was analyzed using Polymer Laboratories Cirrus multi software (Varian, USA) with monodisperse poly(methyl methacrylate) (PMMA) solutions as reference standards. SEC of γ-PGA-H form was performed using sodium polyacrylate standards, in phosphate buffer (pH 7) at Smithers Rapra (UK) under EPSRC.

Thermogravimetric analysis

Dynamic thermogravimetric analysis (TGA) was performed on 5-7 mg γ-PGA polymers at a scanning rate of 2 $°Cmin^{-1}$ under N_2 at 50 ml min^{-1} from 25-300°C on a TGA/SDTA851e instrument (Mettler-Toledo, Greifensee, Switzerland), calibrated with indium and zinc.

Differential scanning calorimetry

Glass transition (T_g), crystallisation (T_c), and melting (T_m) temperatures were determined with a Mettler-Toledo DSC822e differential scanning calorimeter, calibrated with indium and zinc. Samples of 5-7 mg sealed in aluminium crucibles were heated under nitrogen at a rate of 10°C min^{-1} from -25°C until 10-20°C above T_m. All values reported were anal-

ysed using Mettler-Toledo STARe-Software. Melting temperatures reported here refer to the maximum in the endothermal peaks, while crystallisation and recrystallisation (T_{rc} temperatures refer to the minimum value in the exothermal peaks. The second heating on the same sample was treated as melt crystallised, and glass transition temperatures were measured as the midpoint change in slope of this trace.

Contact angle analysis

Static water contact angle analyses were performed on the polymer films using an Easydrop Drop Shape Analysis System (Kruss Surface Science, Germany).

2.3 Results and discussion

2.3.1 Nuclear magnetic resonance

It is possible to identify the chemical structure of the polymer and to calculate the degree of modification achieved during synthesis from the ^{1}H-NMR spectra.

Table 2.1: Degree of esterification as synthesised and calculated from NH peak in ^{1}H-NMR.

Polymer	Batch	Degree of esterification/%	Total reaction time/h
γ-PGA-Et	1	100	40
	2	100	40
γ-PGA-Pr	1	96	110
	2	94	80
	3	93	80
	4	100	60*
	5	100	60*
γ-PGA-Bn	1	99	40
	2	96	40

*Fresh bottle of PrBr used with these synthesis batches

Modification of γ-PGA was achieved using three different bromides. Depending on the bromide used, the total reaction time was found to be between 40 and 110 h. Esterifications using ethyl or benzyl bromide were more successful than that with propyl bromide. Neither γ-PGA-Et nor γ-PGA-Bn required reheating with additional bromide after 40 h of reacting. Across all polymer types, overall yield was found to be between 60-70%.

It was observed that the propyl-esterification of γ-PGA had variable reaction times. Unlike γ-PGA-Et, after 40 h of reacting, not a single batch of γ-PGA-Pr was fully modified. This resulted in subsequent reheating and additional reaction time to increase the esterification. The first synthesis of γ-PGA-Pr was repeated 3 additional times for a total reaction time of 110 h. The degree of esterification did not improve from 96% between the second and third repeat so the reaction was stopped and purified. This was also seen between the

first and second repeated synthesis of γ-PGA-Pr-2 (94%) and γ-PGA-Pr-3 (93%), thus the reaction was stopped after a total time of 80 h. These two batches can be considered to be slightly different from a fully esterified polymer (eg. γ-PGA-Pr-4 and γ-PGA-Pr-5) as the estimated degree of esterification exceeds the error of ^{1}H-NMR integration. The degree of esterification for γ-PGA-Bn batches vary slightly, however they are within the error of ^{1}H-NMR integration (γ-PGA-Bn-1 = 99% and γ-PGA-Bn-2 = 96%).

There are a few limitations of the synthesis and repeatability using this setup. Despite literature stating NMP is the best organic solvent for γ-PGA-H with this reaction, the solution must first be heated to 80°C to partially dissolve γ-PGA-H. Therefore, this varies the actual concentration of starting polymer in solution from batch to batch. While this may adversely affect the reaction reproducibility, γ-PGA-Et polymers were fully esterified, and γ-PGA-Bn within the error of integration, after 40 h of reacting.

Furthermore, the stirrer/hotplate was set to maintain a reaction temperature of 60°C, yet did not have a feedback system to regulate and heat or cool accordingly. Thus, both the oil bath and reaction were liable to environmental variations in temperature associated with a daily reduction in the laboratory's central heating between 11 PM and 7 AM. It would be advantageous to perform synthesis using a temperature regulated, feedback hotplate/stirrer system to compare any batch variability or effect on overall reaction yield.

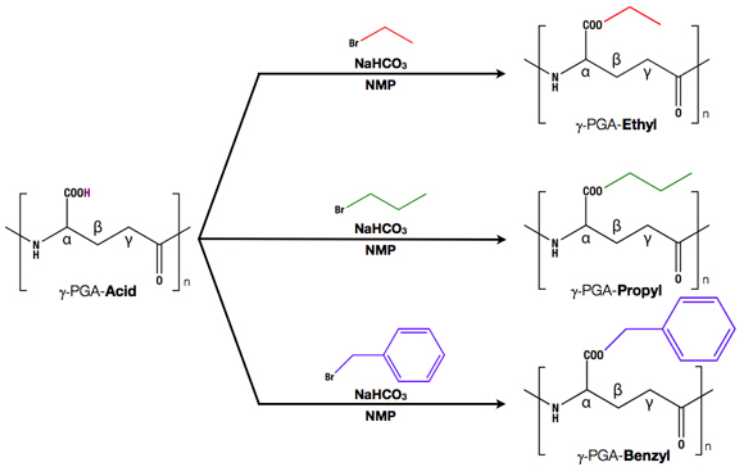


Figure 2.1: Esterification of γ-PGA using ethyl, propyl, or benzyl bromide to produce γ-PGA-Et, γ-PGA-Pr, and γ-PGA-Bn, respectively.

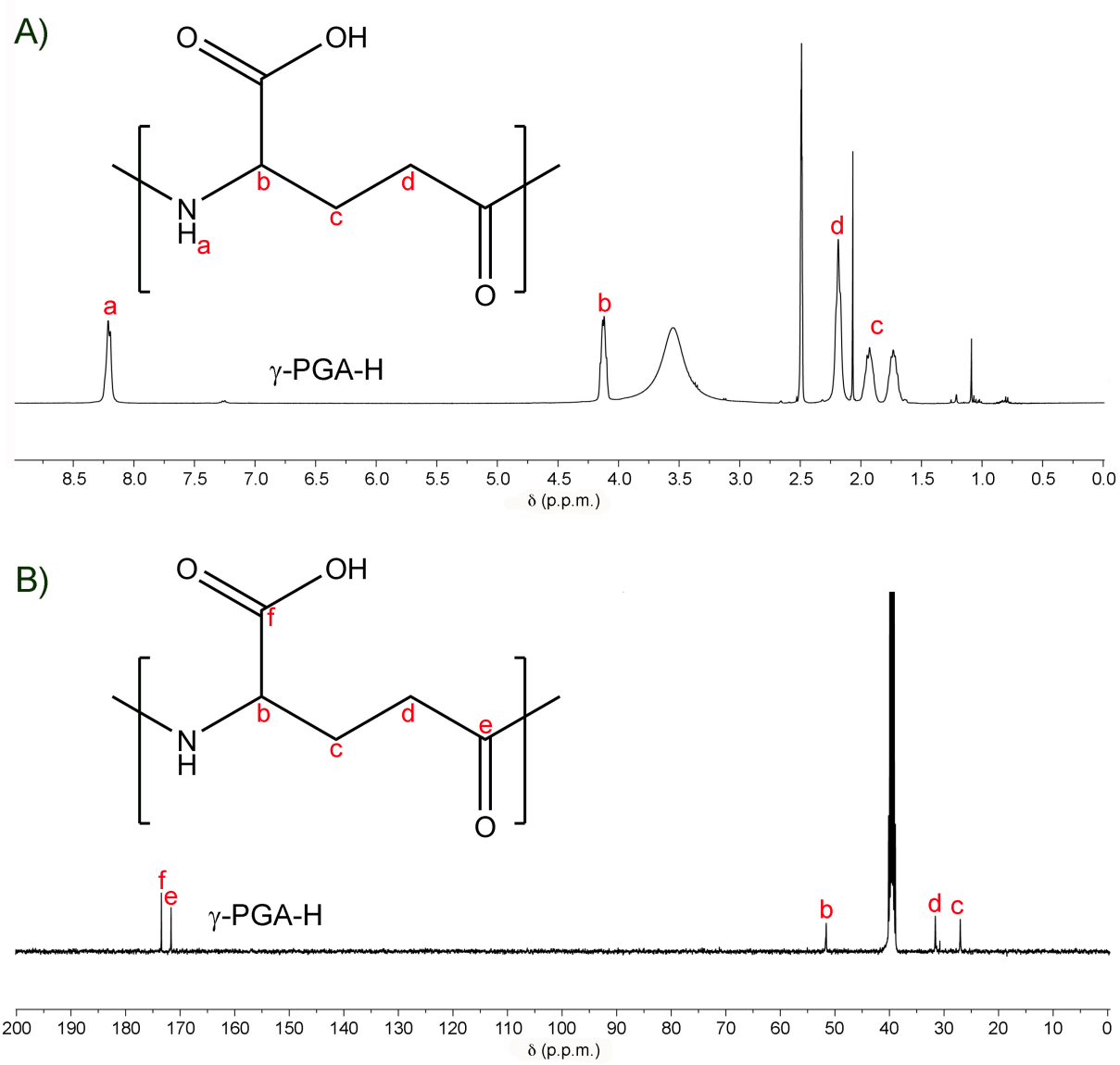


Figure 2.2: A)^{1}H-NMR and B) ^{13}C-NMR spectra for unmodified γ-PGA-H polymer (DMSO-d6, 25°C).

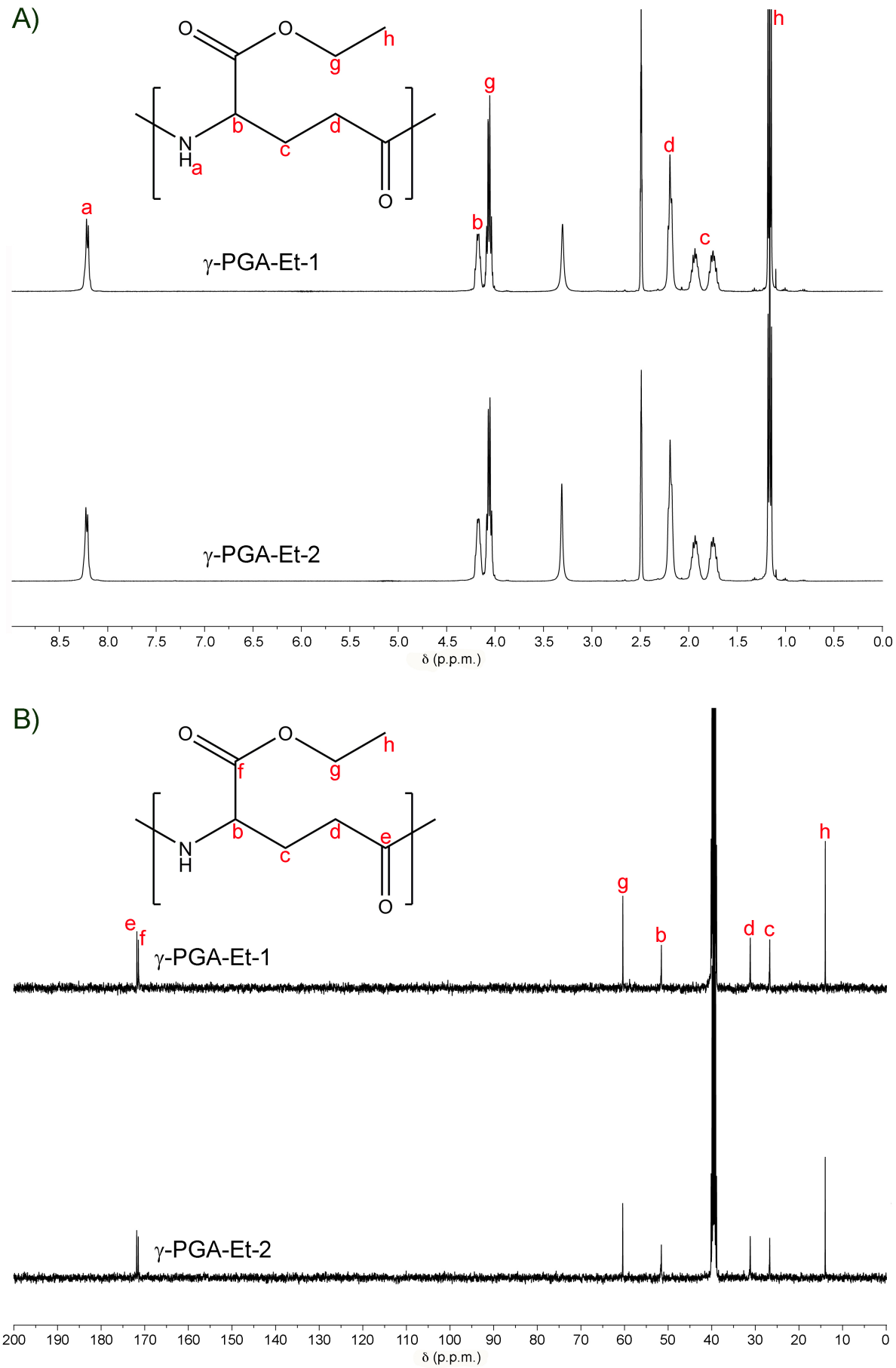


Figure 2.3: A)[1]H-NMR and B) [13]C-NMR spectra for γ-PGA-Et series polymers (DMSO-d6, 25°C).

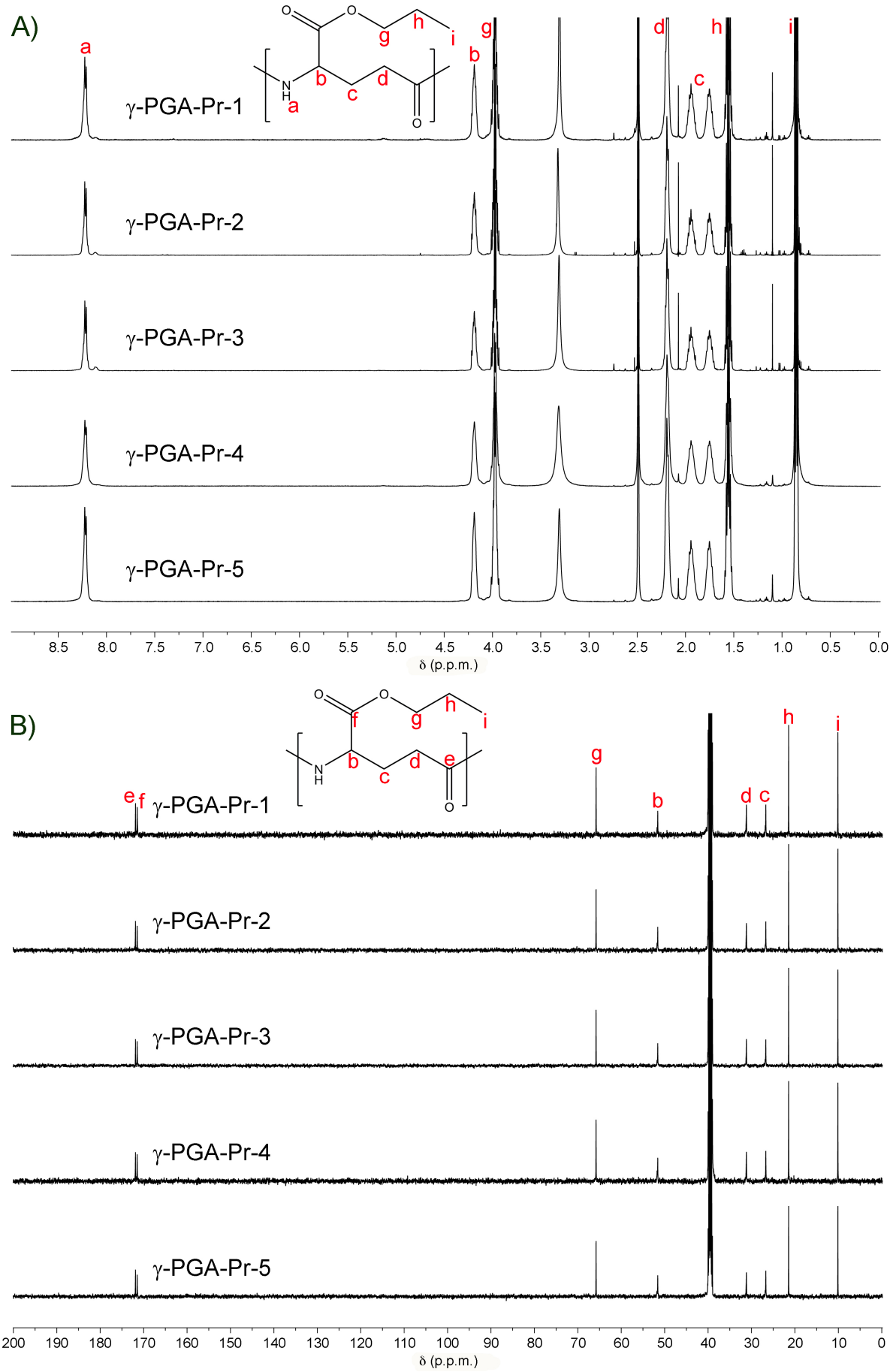


Figure 2.4: A)[1]H-NMR and B) [13]C-NMR spectra for γ-PGA-Pr series polymers (DMSO-d6, 25°C).

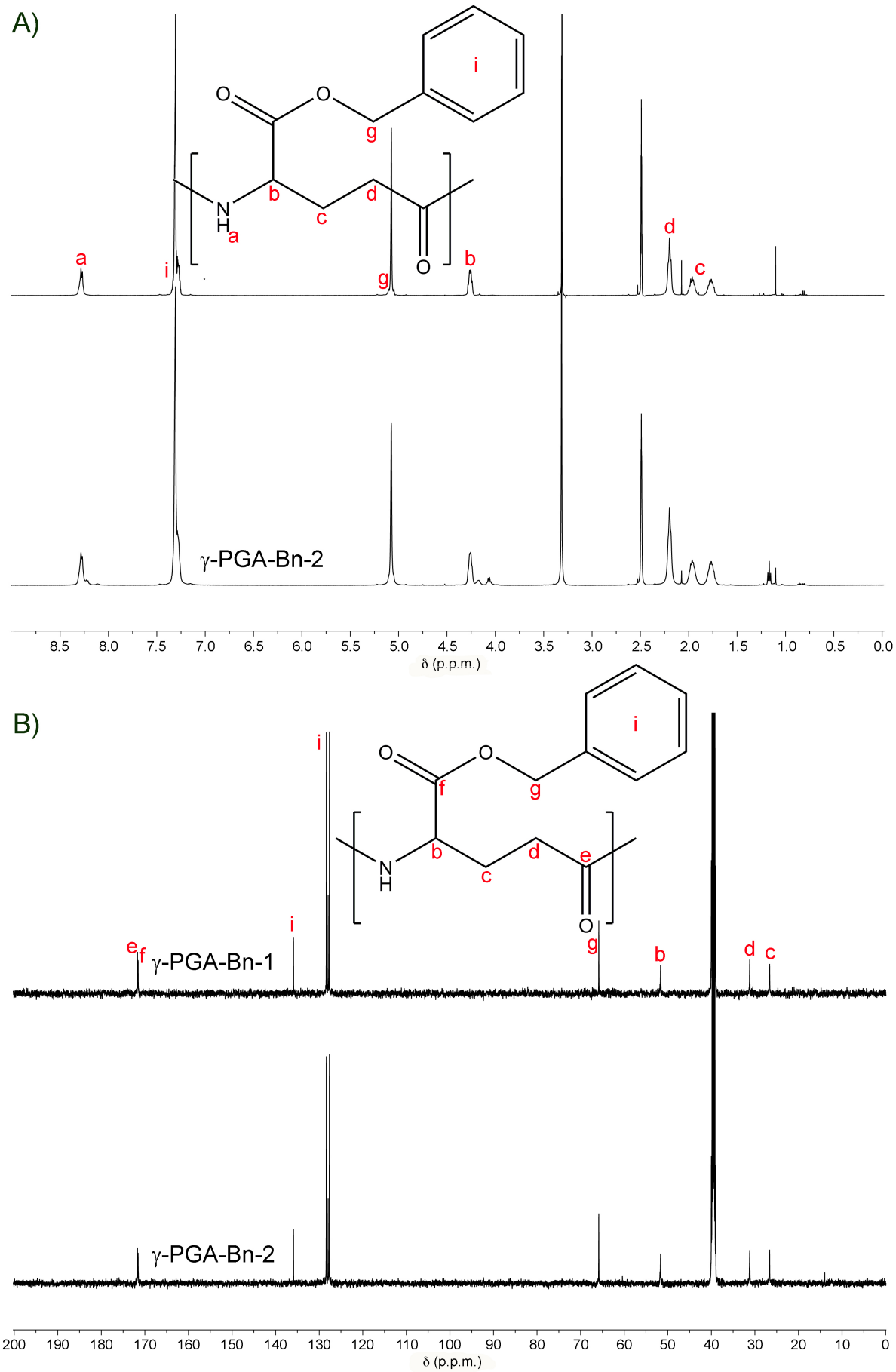


Figure 2.5: A)[1]H-NMR and B) [13]C-NMR spectra for γ-PGA-Bn series polymers (DMSO-d6, 25°C).

2.3.2 Fourier transform infrared spectroscopy

The chemical structure of produced polymers was further confirmed with ATR-FTIR. These spectra are presented in Figures 2.6-2.9. The characteristic bands of interest were identified[25,26] for these polymers and are detailed in Table 2.2.

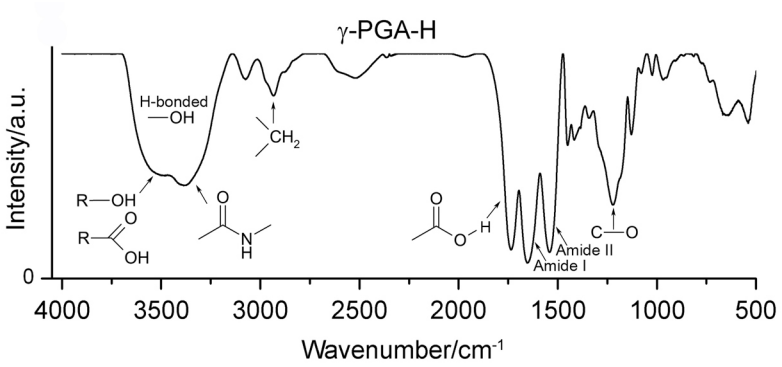


Figure 2.6: Fourier transform infrared spectra of native γ-PGA-H.

As seen in Figure 2.6, there are two peaks in the region of absorption frequencies of single bonds to hydrogen spanning $\nu \approx$ 3600-3200 cm. Two peaks of interest, an -OH peak at 3635 cm^{-1} and an acid (-COOH) peak at 3550 cm^{-1}, are shadowed in the broad peak from $\nu \approx$ 3600-3200 cm^{-1} (H-bonded -OH). These peaks confirm the native γ-PGA-H structure is in the acid form, and there is a large amount of hydrogen bonding between polymer chains. The disappearance of this peak with esterification is visible in Figures 2.7, 2.8, and 2.9. Characteristic peaks are shown for all polymer species with those of the -CONH- displaying a shifted weak absorption in $\nu \approx$ 3460-3400 cm^{-1} range due to the solid state of the polymers. The amide I and amide II bands are sharply visible between 1680-1630 and 1570-1515 cm^{-1}. Finally, the C=O band at $\nu \approx$ 1850-1650 is very strong in all polymers.

Introduction of an alkyl group on the side chains via esterification for γ-PGA-Et and γ-PGA-Pr is visible between $\nu \approx$ 2960-2850 cm^{-1}. The additional carbon alkyl group in γ-PGA-Pr is visible with another shoulder appearing in this range of the γ-PGA-Pr spectra (Figure 2.8) when compared with that of the γ-PGA-Et (Figure 2.7). Other absorption is seen with a sharp peak visible between $\nu \approx$ 1750-1735 cm^{-1}. Lower than this, the esterified alkyl groups are indistinguishable from those in the native polymer chain.

The aryl group of γ-PGA-Bn is visible with a weak absorption from 3040-3010 cm^{-1} (Figure 2.9). The other absorption band from 1225-950 cm^{-1} is difficult to resolve as it conflicts with other groups in the native polymer structure, including the side group ester (C-O) and alkyl groups (-CH_2-) on the polymer backbone.

These infrared spectra for all the polymers further confirm their chemical structure, as was shown with ^{1}H-NMR and ^{13}C-NMR in the previous section. Additionally, the disappearance of the broad peak from 3600-3200 cm^{-1} is consistent with NMR data of

esterified batches.

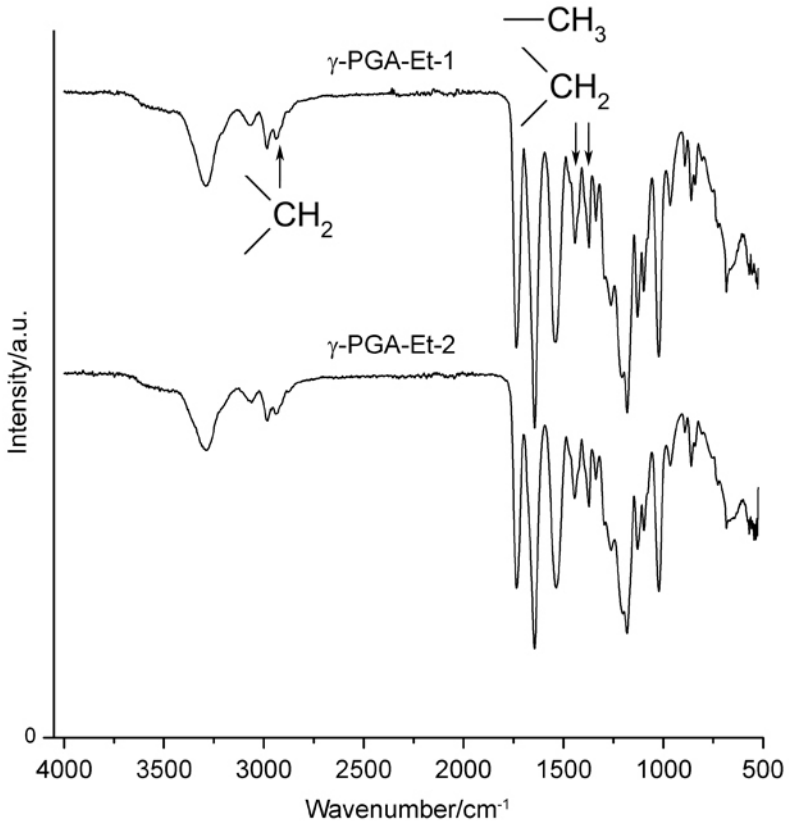


Figure 2.7: Fourier transform infrared spectra of the synthesised γ-PGA-Et series.

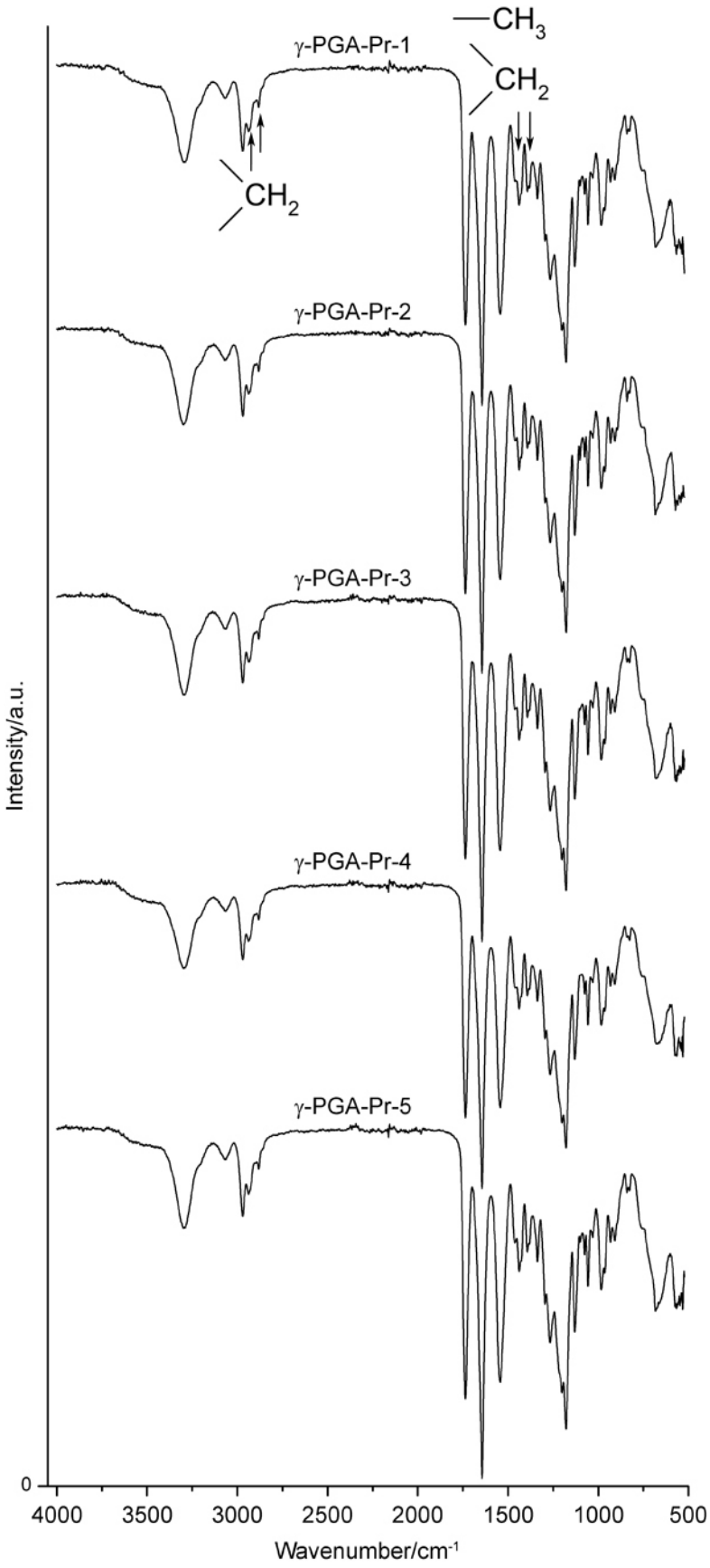


Figure 2.8: Fourier transform infrared spectra of the synthesised γ-PGA-Pr series.

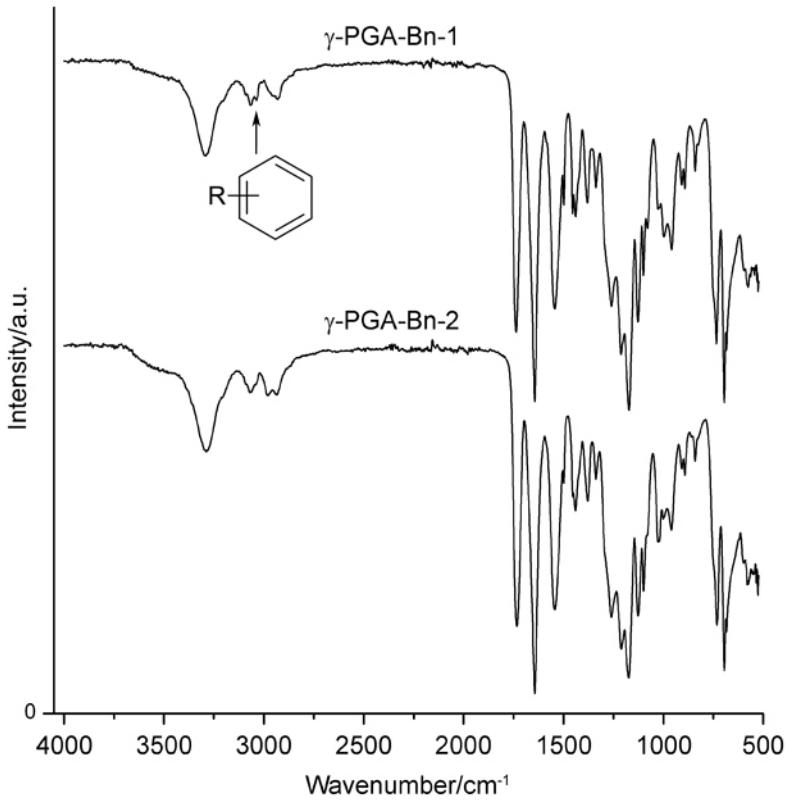
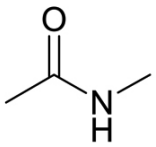
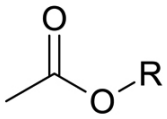
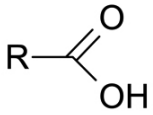
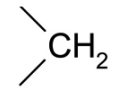
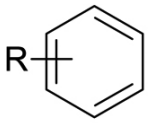


Figure 2.9: Fourier transform infrared spectra of the synthesised γ-PGA-Bn series.

Table 2.2: Fourier transform infrared spectra absorptions and chemical groups of interest for native γ-PGA and esterified polymers. Table generated from values listed in[25,26]

Group		Absorption / cm^{-1}
		3460-3400* 3100-3070
	Amide I	1680-1630
	Amide II	1570-1515 *Shifted to lower values in the solid state
	R = Alkyl	2960-2850 1750-1735 1150-1100
	R = Aryl	1730-1715
	R = H	1725-1700
	Acids	3550
—OH	H-bonded	3600-3200
R—OH		3635
 —CH_3		2960-2850 1470-1430 1390-1370
		3040-3010 1225-950
C—O		1300-1020

2.3.3 Wide-angle x-ray scattering

Wide-angle x-ray scattering (WAXS) was performed on cast films of γ-PGA-H and modified γ-PGA polymers, confirming semicrystalline structures. WAXS spectra are plotted by modified polymer series in Figures 2.10-2.12 and are plotted together with γ-PGA-H in Figure 2.13.

Interatomic distances are presented in Table 2.3, as calculated using Bragg's law (Equation 2.1) where n is the layer line (1 for these calculations), λ is the wavelength of the x-ray source (λ Cu K_α = 1.54439 Å), d represents the interatomic spacing in Å and θ is the scattering angle (°).

$$n\lambda = 2dsin\theta \tag{2.1}$$

Both γ-PGA-Et (Figure 2.10) and γ-PGA-Pr (Figure 2.11) polymer series express some degree of order, shown with two peaks, a slight 200 peak at 8-9° and the more intense 011 peak at 20-21°, corresponding to approximately 10-11 Å and 4.2 Å, respectively. The γ-PGA-Bn (Figure 2.12) series displayed a broader 011 peak than the alkyl-esterified γ-PGA polymers, shifted to lower 2θ values and thus higher interatomic distances. The weak 200 peak was found around 11-12 Å while a broader 011 peak showed some order around 4.5-4.6 Å. This broadening of this 011 peak, when compared to that of γ-PGA-Et and γ-PGA-Pr, indicates the benzyl experiences less order.

Similarly, the γ-PGA-H (Figure 2.13) displayed a very broad 011 peak, slightly shifted to 22° with a d-spacing of 4.03 Å. Several sharp peaks were seen in the γ-PGA-H diffraction, and these are peaks from NaCl, an expected byproduct from the acidification of γ-PGA-Na^+ using HCl.

The results shown here indicate the γ-PGA-H polymer may be mostly amorphous, while all esterified polymers are semicrystalline. This will be investigated using differential scanning calorimetry in the following section, and discussed further in Section 5.4.5.

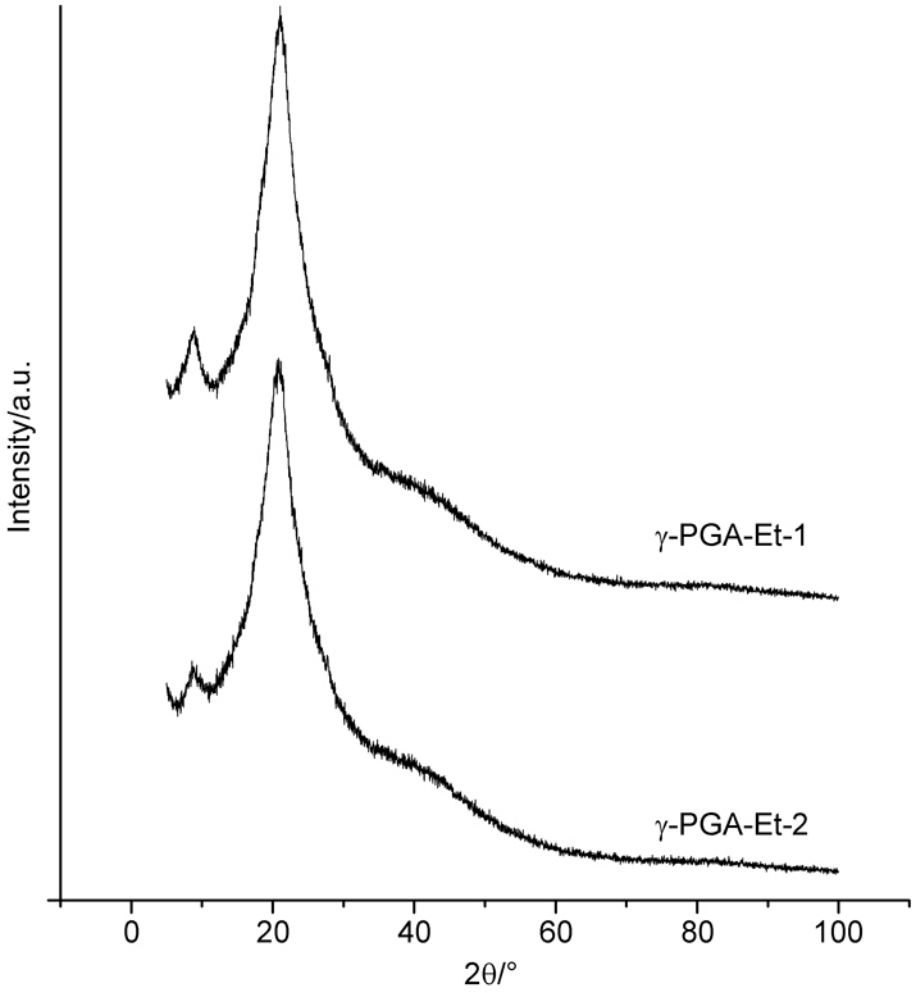


Figure 2.10: Wide-angle x-ray scattering pattern of the synthesised γ-PGA-Et series.

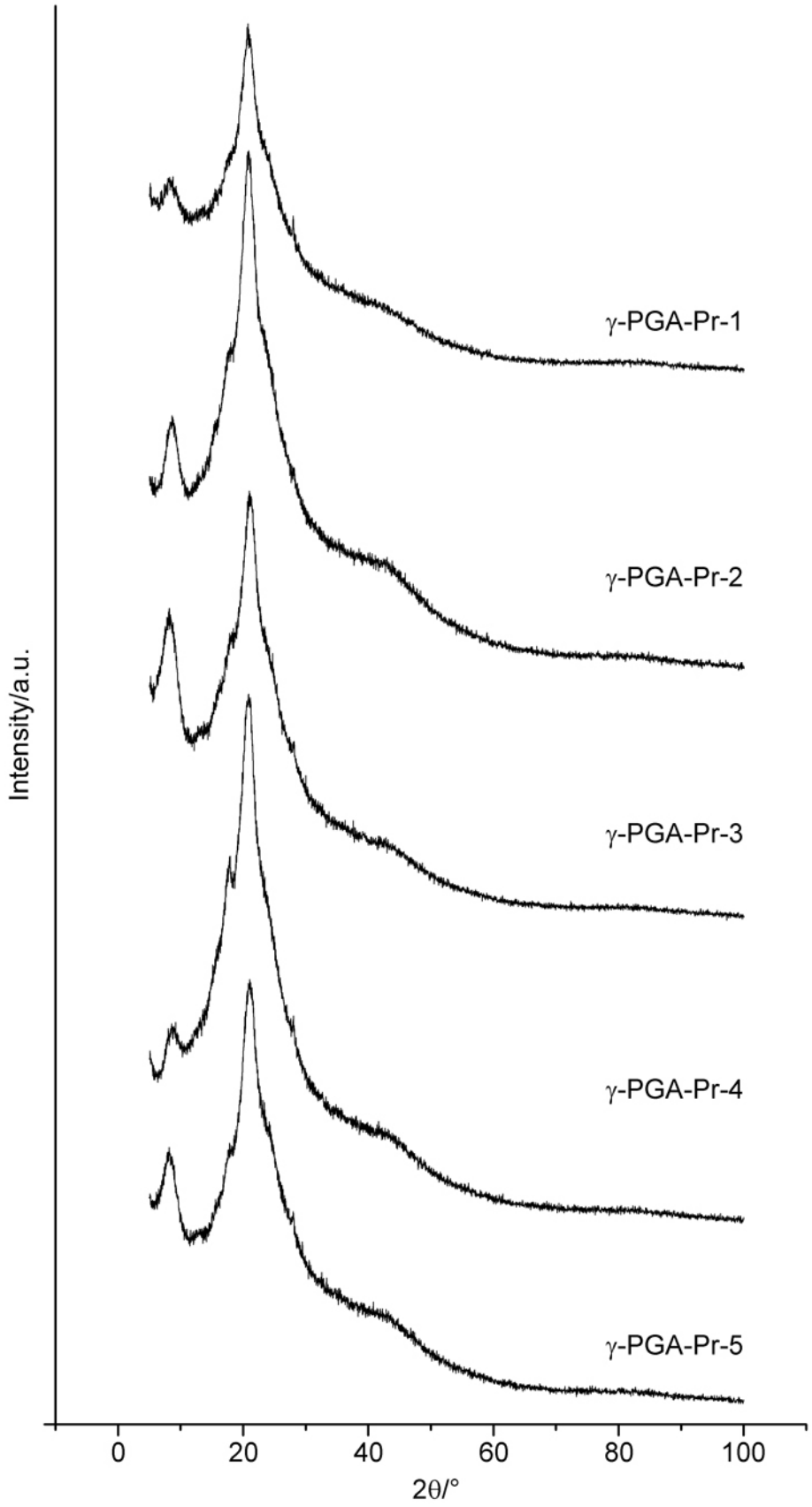


Figure 2.11: Wide-angle x-ray scattering pattern of the synthesised γ-PGA-Pr series.

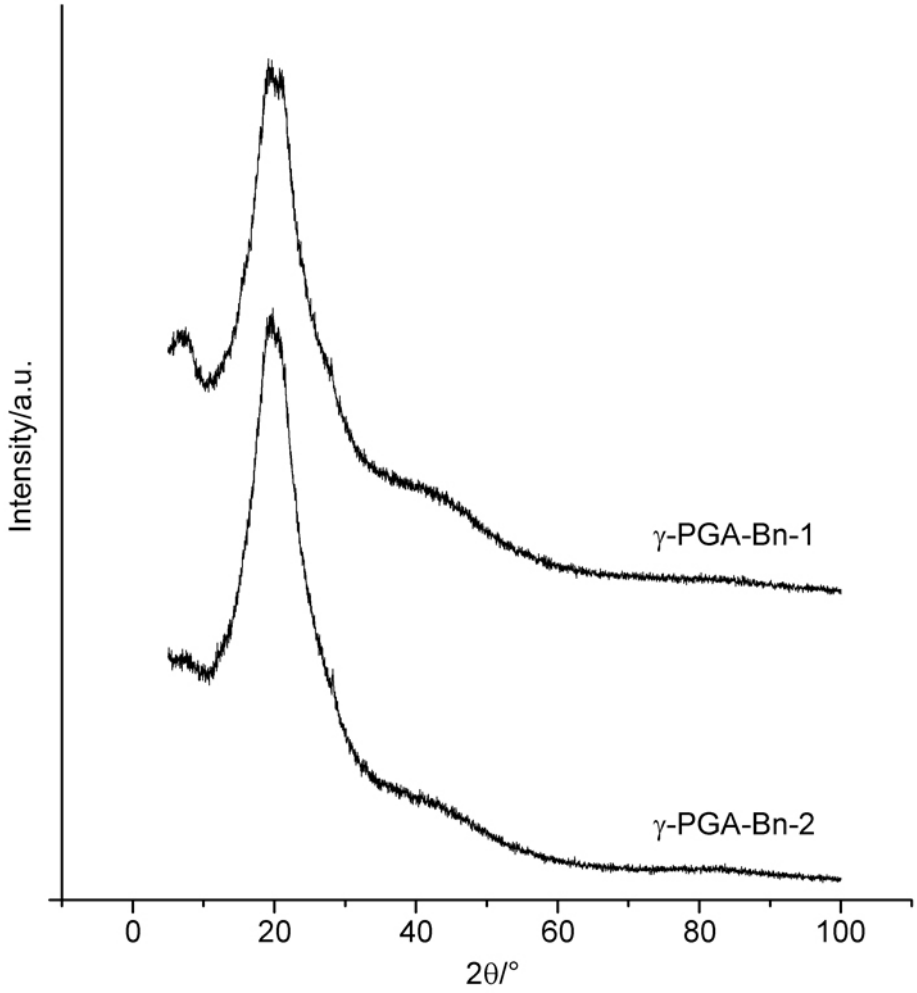


Figure 2.12: Wide-angle x-ray scattering pattern of the synthesised γ-PGA-Bn series.

Table 2.3: Distances between similar atomic planes for batches of γ-PGA polymers.

Polymer	**Synthesis**	**(200)**		**(011)**	
		d / Å	**2θ/°**	**d / Å**	**2θ/ °**
γ-PGA-H	-	-	-	4.03	22.11
γ-PGA-Et	1	9.94	8.91	4.23	21.04
	2	10.33	8.58	4.28	20.81
γ-PGA-Pr	1	10.15	8.72	4.24	20.72
	2	10.31	8.59	4.27	20.86
	3	10.87	8.15	4.25	20.96
	4	9.64	9.19	4.26	20.89
	5	10.81	8.15	4.23	21.06
γ-PGA-Bn	1	11.83	7.49	4.64	19.15
	2	12.62	7.02	4.49	19.79

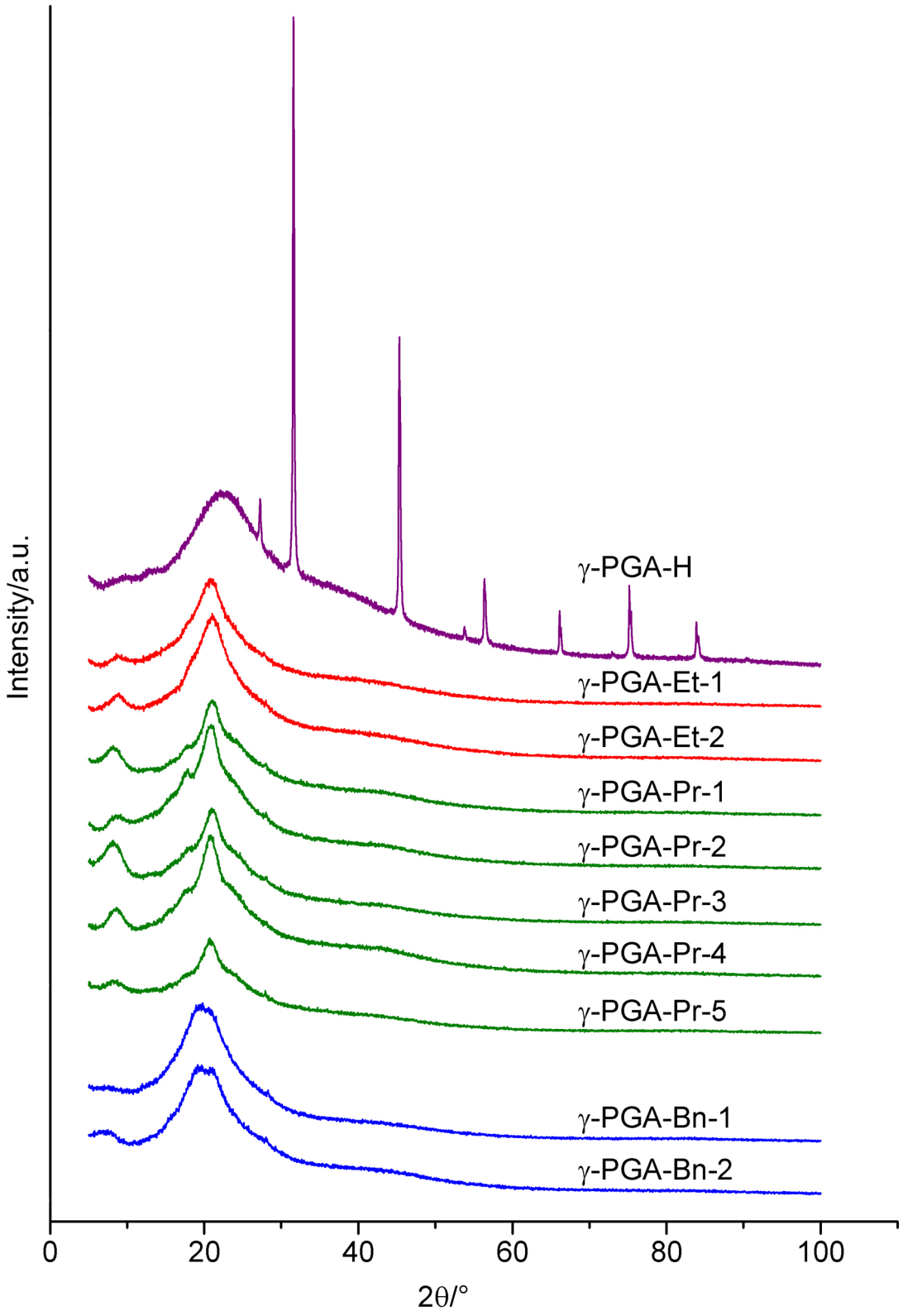


Figure 2.13: Wide-angle x-ray scattering pattern of the all γ-PGA-polymers plotted together.

2.3.4 Size exclusion chromatography

The molecular weight distributions of the starting and modified γ-PGAs were determined using size exclusion chromatography. All esterified γ-PGA polymer results are relative to PMMA standards (in DMF with 1g/L LiBr) while that of γ-PGA-H is relative to sodium polyacrylate (in phosphate buffer, pH 7). The starting γ-PGA-H polymer, as produced by *Bacillus subtilis*, has a high weight-average molecular weight (M_w) of 2.83 x 10^5, with a fairly broad distribution as shown in its' polydispersity index (PDI, 2.40).

Esterification of γ-PGA caused a slight decrease in molecular weight of polymers, but this was maintained above 10^5 kDa for all batches except γ-PGA-Bn-1 (8.67 x 10^4). A variation in molecular weight distribution and PDI was observed across the synthesis batches, as seen in Table 2.2. Longer reaction times resulted in a lower average M_w and higher PDI for some polymer batches (notably γ-PGA-Pr-1 and γ-PGA-Pr-4), though this was not uniform for the entire series.

The SEC for γ-PGA-H was performed in an aqueous solvent as they were not soluble in organic solvents like modified γ-PGAs. Therefore, the M_w of γ-PGA-H is 2.83 x 10^5, relative to sodium polyacrylate. While the specific results cannot be directly compared between the different conditions, they provide an order of magnitude estimate about the polymers' weight-average molecular weights.

Table 2.4: SEC results for differing batches of γ-PGA esterifications.

Polymer	Synthesis	M_n/g mol^{-1}	M_w/g mol^{-1}	P.D.I.	Total reaction time/h
γ-PGA-H*	-	1.18 x 10^5	2.83 x 10^5	2.40	-
γ-PGA-Et	1	6.16 x 10^4	1.40 x 10^5	2.28	40
	2	6.31 x 10^4	1.38 x 10^5	2.18	40
γ-PGA-Pr	1	3.93 x 10^4	1.62 x 10^5	4.12	110
	2	8.30 x 10^4	1.99 x 10^5	2.39	80
	3	1.03 x 10^5	2.69 x 10^5	2.62	80
	4	5.35 x 10^4	1.62 x 10^5	3.02	60
	5	8.01 x 10^4	1.81 x 10^5	2.26	60
γ-PGA-Bn	1	3.24 x 10^4	8.67 x 10^4	2.67	40
	2	5.08 x 10^4	1.46 x 10^5	2.88	40

*SEC performed in aqueous solvents by Smithers Rapra

2.3.5 Thermogravimetric analysis

Dynamic thermogravimetric analyses (TGA) were performed on all polymers to determine temperatures of thermal degradation. The temperatures at which polymers experienced 5% decomposition is presented in Table 2.5. The native γ-PGA-H form experiences decomposition early at 165°C, though a gradual weight loss is seen at from slightly lower temperatures. All the esterified polymers experience degradation at much higher temper-

atures (> 230°C).

Table 2.5: Thermogravimetric analysis of esterified γ-PGA polymers.

Polymer	Synthesis	5% Decomposition/°C
γ-PGA-H	-	165
γ-PGA-Et	1	244
	2	242
γ-PGA-Pr	1	235
	2	231
	3	231
	4	243
	5	245
γ-PGA-Bn	1	245
	2	236

Esterification improves heat stability of γ-PGA, up to 245°C. This is likely due to the degradation mechanism of the native γ-PGA polymer. Assuming the polymer undergoes the proposed degradation mechanism as published by Melis *et. al*,[159], a five-membered ring is formed from an intramolecular nucleophilic attack of the NH onto the CO ester carbon at the chain end. Introduction of a side group leads to a higher M_w of the monomer, requiring more energy to volatilise and thus increasing the onset of thermal degradation.

2.3.6 Differential scanning calorimetry

Differential scanning calorimetry (DSC) was employed to determine the transition temperatures of the polymers. DSC was performed on purified powders and the heating/cooling rates were kept at 10°C min^{-1}. All heating traces of esterified polymers are presented in Figures 2.14-2.16 and the results tabulated in Table 2.6.

As the γ-PGA used here is purchased in the Na^+ form (γ-PGA-Na^+) and then acidified (yielding γ-PGA-H) prior to esterification, DSC was performed on both polymers to investigate their respective T_g and T_m. These values are presented in Table 2.6. The γ-PGA-Na^+ had a T_g of 93°C while that of γ-PGA-H was found to be 124°C. This increase in T_g is attributed to the nature of the side chain. At neutral pH, the -O^- is charge balanced by the Na^+ ion, but at acidic pH below the pKa (pH = 4.0), the oxygen is saturated (- OH). This introduces hydrogen bonding between polymer chains, resulting in restriction of bond rotation and a higher T_g.

The DSC analyses indicate that esterification of γ-PGA results in a much lower T_g than γ-PGA-H, as shown in Table 2.6. Introduction of the esterified group reduces hydrogen bonding between polar -OH groups and allows more chain mobility at lower temperatures. Glass transition temperatures were found to be relatively consistent among batches of γ-PGA-Et and γ-PGA-Bn, while γ-PGA-Pr batch T_g values range from 23-47°C. This

range may be attributed to degradation experienced in the first heating, as both batches experienced 5% degradation at 231°C. A lower degree of esterification, and thus less chain regularity, also contributes to a lower T_g than that of fully modified batches.

Interestingly, however, γ-PGA-Bn did not display a much higher T_g than alkyl esterified batches. The presence of bulky side groups, such as the benzyl group, disrupt hydrogen bonding. This may interfere with chain packing which increases the amorphous volume fraction, and result in a restriction of bond rotation[160,161], effectively increasing T_g more than flexible side groups like the two short alkyl groups used in this study. Thus it is hypothesised the T_g may be due to the level of esterification being 99% and 96% (as determined by ^{1}H-NMR for γ-PGA-Bn-1 and γ-PGA-Bn-2 respectively).

Upon the first heating, only γ-PGA-Pr polymers experienced recrystallisation. All γ-PGA-Et and γ-PGA-Pr polymers displayed a sharp melting peak while γ-PGA-Bn either had a double melting peak (γ-PGA-Bn-1) or a shoulder peak (γ-PGA-Bn-2). T_m was found to increase with decreasing size of the esterified group. γ-PGA-Bn polymers had the lowest value of T_m, which may be attributed its' side group introducing disruptions into the polymer crystals[102].

All polymers experienced degradation with melting. This was more prominent in γ-PGA-Pr batches, notably γ-PGA-Pr-2. Degradation during the first heat resulted in a change upon the second heat, as shown in the plotted DSC curves (2.14-2.16) and the values tabulated in Table 2.6. This degradation had a destructive effect on γ-PGA-Et and γ-PGA-Pr polymers, which have a 5% T_d near or below their respective T_m. Upon the second heating, melting peaks appeared slightly rounded, less intense and had a lower melting peak temperature. In particular, γ-PGA-Pr-2 was significantly affected, as seen in the second heating. This effect was less prominent with γ-PGA-Bn polymers, as the T_m lies 15-20°C below the 5% T_d.

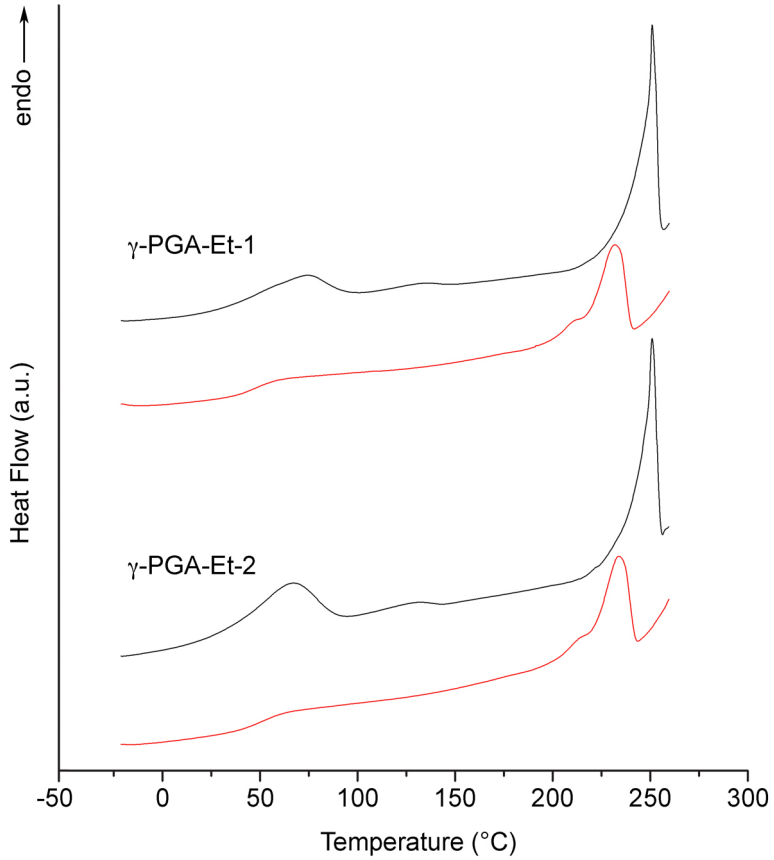


Figure 2.14: DSC heating traces of synthesised γ-PGA-Et series, where black indicates first heating and red is the second.

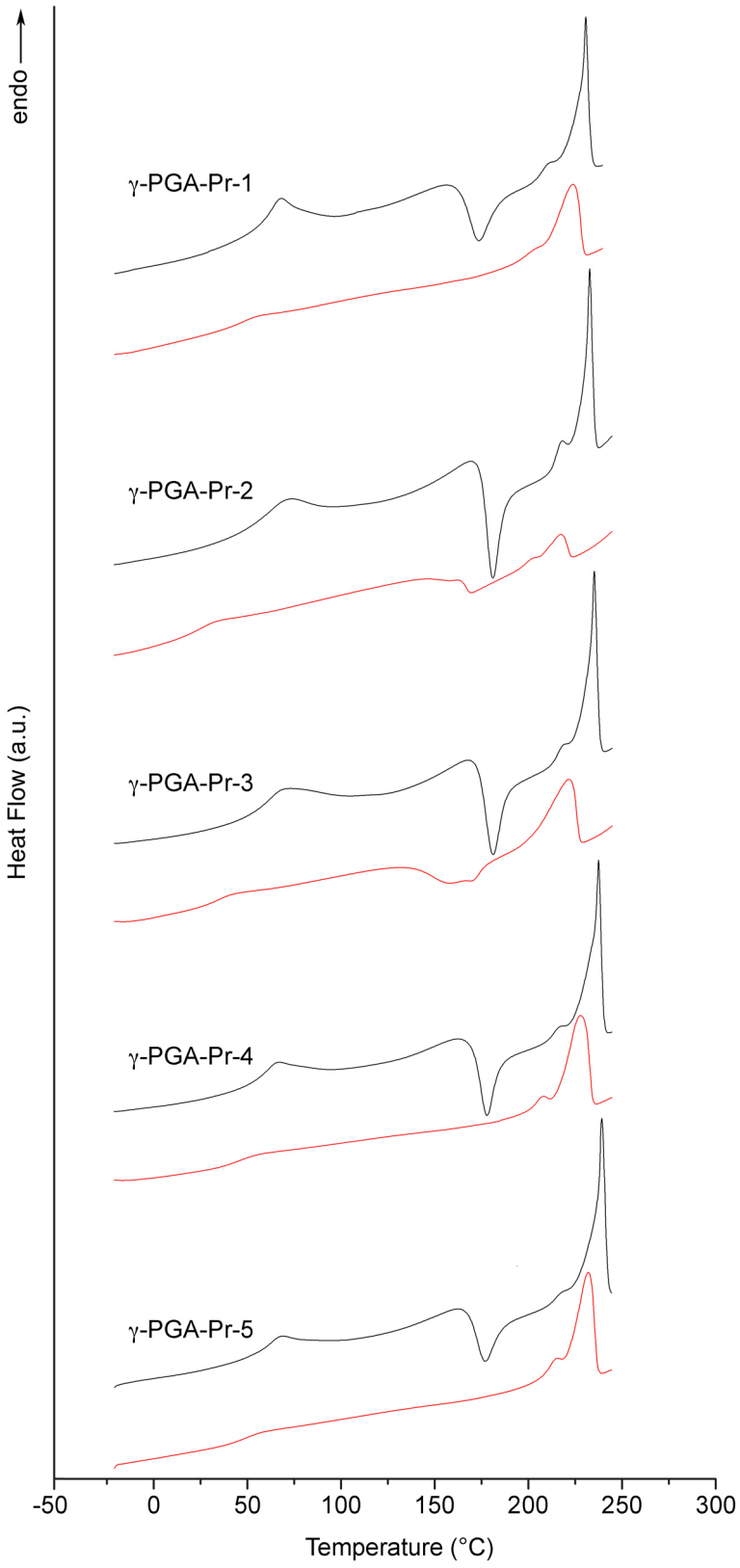


Figure 2.15: DSC heating traces of synthesised γ-PGA-Pr series, where black indicates first heating and red is the second.

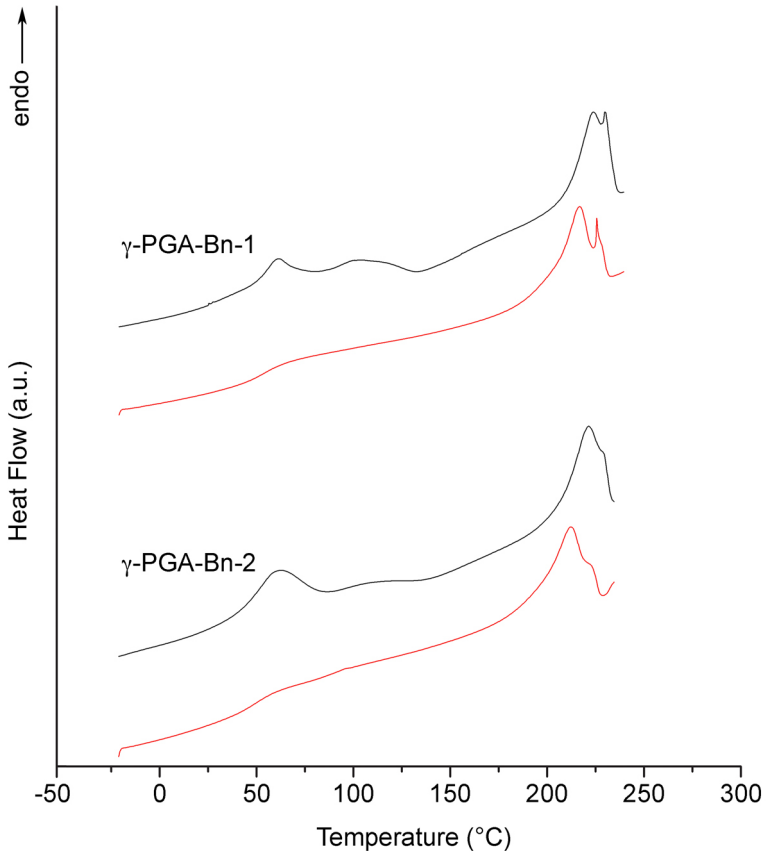


Figure 2.16: DSC heating traces of synthesised γ-PGA-Bn series, where black indicates first heating and red is the second.

Table 2.6: Thermal results for all γ-PGA polymers obtained via DSC, where T_{rc} is measured during heating and T_c from cooling.

Polymer	Synthesis	T_g /°C	T_{rc} /°C	T_c /°C	T_m 1 /°C	T_m 2 /°C
γ-PGA-Na^+	-	93	-	-	203	-
γ-PGA-H	-	124	-	-	-	-
γ-PGA-Et	1	48	-	177	251	232
	2	49	-	180	251	234
γ-PGA-Pr	1	44	174	170	231	224
	2	23	181	147	233	217
	3	31	181	152	235	221
	4	43	178	172	237	228
	5	47	177	182	239	232
γ-PGA-Bn	1	55	-	163	224	217
	2	50	-	156	221	212

Table 2.7: Thermal results for all γ-PGA polymers obtained via DSC in K.

Polymer	Synthesis	T_g /K	T_m 1 /K	T_g/T_m
γ-PGA-Na^+		366	476	0.77
γ-PGA-H		397		
γ-PGA-Et	1	321	524	0.61
	2	322	524	0.61
γ-PGA-Pr	1	317	504	0.63
	2	296	506	0.58
	3	304	508	0.60
	4	316	510	0.62
	5	320	512	0.63
γ-PGA-Bn	1	328	497	0.66
	2	323	494	0.65

When presented in Kelvin, the value of T_g is generally between 0.5 and 0.8 T_m [102], thus showing the strong relationship between the T_g and T_m. The results obtained from the modified γ-PGA polymers are tabulated in Table 2.7 and plotted in Figure 2.17

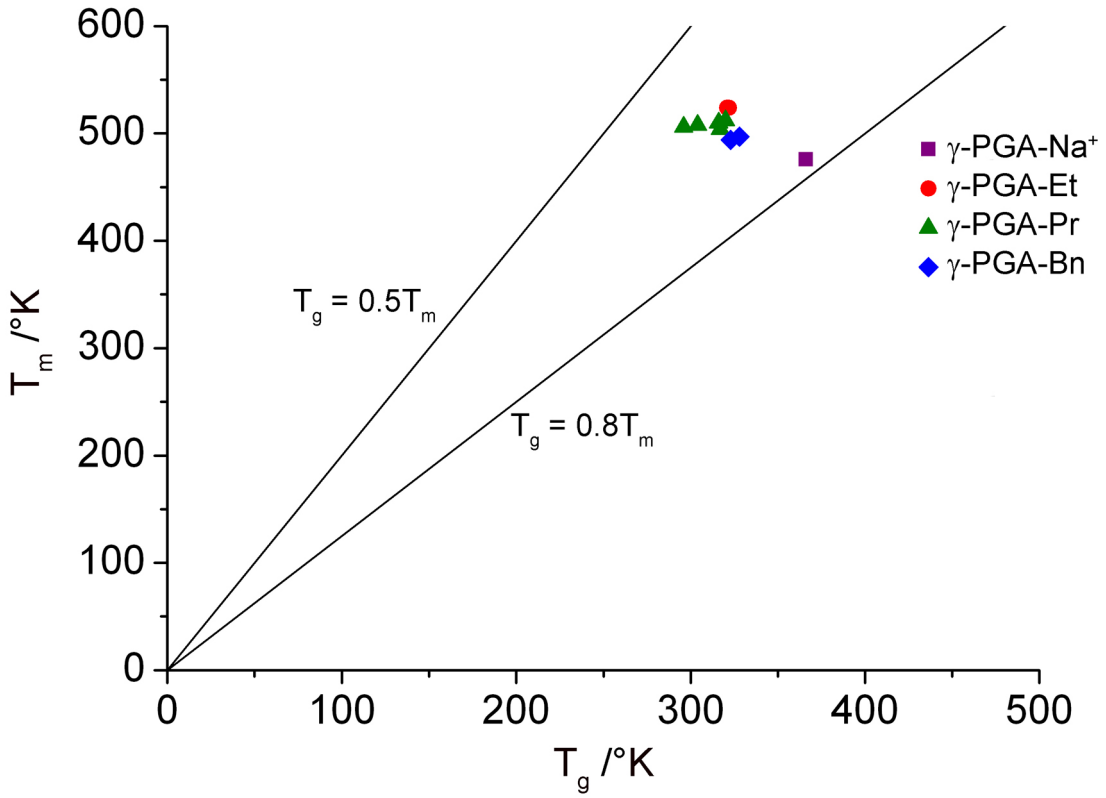


Figure 2.17: Plot of T_m as a function of T_g for γ-PGA-Na^+ and modified γ-PGA polymers.

2.3.7 Contact angle

Finally, water contact analysis was performed to examine the hydrophobicity of the various γ-PGAs. The measurement was conducted with t = 0, 1 min, as it was observed that a water droplet became stable after this period of time. Expectedly, water contact angle (WCA) measurements show that the esterified γ-PGAs are more hydrophobic than the unsubstituted γ-PGA-H, with γ-PGA-Bn displaying a contact angle higher than γ-PGA-Et and γ-PGA-Pr (Figure 2.18). Data for all polymers are deemed statistically significant both from the two time scales and between each polymer species, with the exception of γ-PGA-Bn and poly(L-lactic acid; PLLA)($p < 0.001$; Two-way ANOVA with Tukey post-hoc test).

As noted above, the contact angle increased with increasing hydrophobicity of the side group. Interestingly, the highest contact angle, that of γ-PGA-Bn, is similar to that of the highly-characterised, FDA-approved PLLA, which is widely used in tissue engineering.

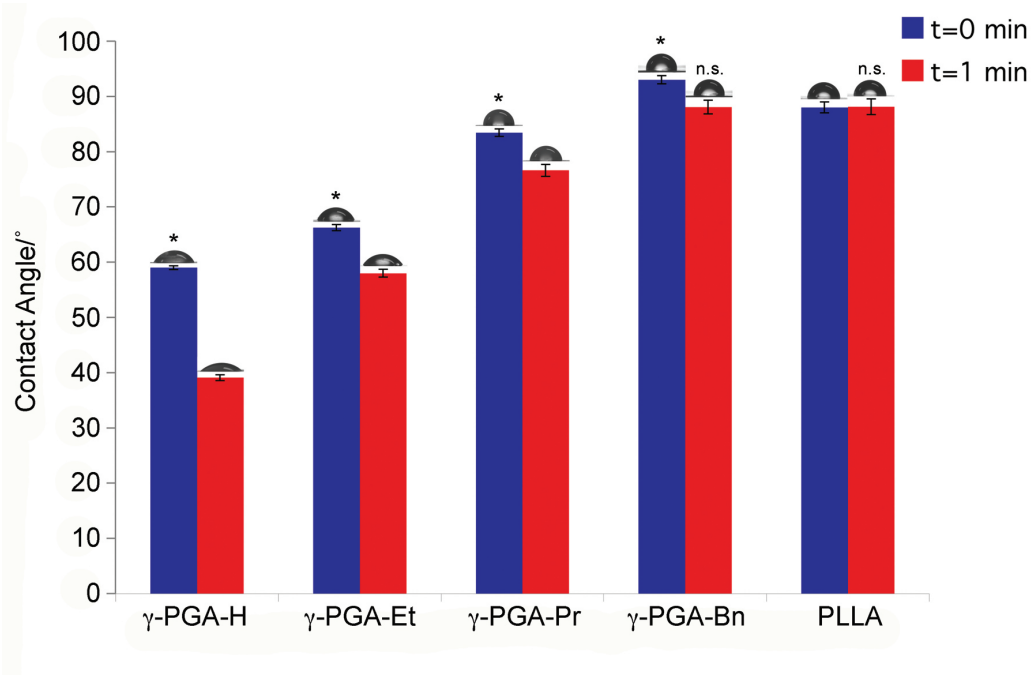


Figure 2.18: Contact angle analysis for for as-cast, dried γ-PGA films compared to PLLA(* $p < 0.001$, n.s. = not significant).

2.4 Conclusions

In this chapter, the water solubility of γ-PGA was diminished by esterification with alkyl or aryl groups, enabling the polymer for use in tissue engineering applications. Full modification of the γ-PGA-H was achieved using either ethyl bromide or benzyl bromide, while >90% modification was possible using propyl bromide with an approximate yield of 60-70% for all polymers. Polymers were fully characterised for their chemical, structural, and thermal properties. All produced polymers were found to be semicrystalline and

synthesis resulted in a relatively polydisperse polymer (PDI 2-3, with one batch having a PDI of 4.12), yet molecular weights were maintained above 10^5 kDa for all but one batch. Esterification led to a decrease in glass transition temperature while the the degradation temperature increased, widening the thermal processing window for all polymers.

The synthesis would benefit from scaling up, as each batch produces roughly 1.6 grams of material and batch-to-batch variation inhibits combining multiple syntheses for one application. Variability between batches is attributed to the experimental equipment, which may be improved by using a temperature-regulated feedback system with future syntheses.

Esterification of the non-toxic, enzymatically degradable γ-PGA-H expectedly shielded of the H-bonds present in the unmodified form, rendering the polymer water insoluble in powder form. Furthermore, the water contact angle increased with increasing hydrophobicity of the side chain. The fully esterified γ-PGA polymers, would be excellent candidates for tissue engineering. Thus it is of particular interest for this thesis to focus on utilising these polymers to investigate their mechanical properties and biocompatibility. Given the high M_w maintained in the esterification, it would be useful to utilise techniques to tailor the mechanical properties to target specific tissues, which is the main focus of the next chapter.

Chapter 3

Modification of γ-PGA with Phenylalanine

3.1 Introduction

This chapter investigates chemical modification of poly (gamma-glutamic acid; γ-PGA) using an amino acid both as an alternative method to esterification for decreasing γ-PGA water solubility and as a strategy to increase functionality of the polymer. In the previous chapters, γ-PGA was esterified using alkyl or aryl groups. Esterification with benzyl bromide displayed the most promise, and was focused on with cell and dissolution studies. It has been shown in Chapter 6 that this synthesis may be scaled to produce larger quantities with higher yields by modifying the experimental setup.

A main focus of this thesis is modifying the -COOH side group in γ-PGA, which provides a site for functionalisation of the polymer, as discussed previously in Section 1.4 and Chapter 2. Instead of creating an ester bond which may be liable to random hydrolysis, the synthesis within this chapter focuses on coupling a modified phenylalanine to the side chain using a carbodiimide coupling agent. The side group of phenylalanine has an aromatic ring, which should help to provide water resistance to the γ-PGA-H like that of the benzyl group in γ-PGA-Bn. It is anticipated that the phenylalanine-modified polymer may be more stable over time as the peptide bond will be less liable to hydrolysis than an ester. Furthermore, modification with an amino acid paves the way for coupling peptide sequences with specific targeting abilities, as discussed in Section 1.2.4, to γ-PGA.

To date, no work has been published on using γ-PGA-conjugated with phenylalanine for tissue engineering applications. The Akashi group from Osaka university have recently published several papers on γ-PGA partially grafted (53%) with L-phenylalanine ethyl ester[162–170] to generate amphiphilic nanoparticles for vaccination or drug delivery. Their work provides hydrophobicity by utilising a water soluble 1-ethyl-3-(3-dimethylaminopropyl) carbodiimide (WSC) to couple phenylalanine to the γ-PGA. Therefore, coupling phenylalanine to γ-PGA-H should still provide the polymer with water resistance,

making it an excellent candidate for tissue engineering applications.

This chapter presents the synthesis, chemical, and thermal properties of phenylalanine modified γ-PGA for tissue engineering applications.

3.2 Experimental

3.2.1 Chemical synthesis

General

All starting polymer (γ-D,L-PGA Na^+ salt, produced by *Bacillus subtilis*) was purchased from Natto Biosciences (Shanghai, China). All reagents and solvents were purchased from Aldrich and used as received, unless otherwise specified.

Free acid form of γ-PGA

γ-PGA Na^+ salt (10 g) was dissolved in 250 mL of distilled water. The solution was acidified with HCl 6M to pH 1.5 and lyophilized for at least 96 h. The freeze-dried solid resulted soft and porous.

γ-PGA-H N-terminus protection

For N-terminus protection, γ-PGA free acid (+ NaCl) (2.5 g, 0.08 M) was introduced into a 250 mL round bottom flask equipped with a magnetic stirrer, and suspended in 180 mL of diH_2O at room temperature. Once dissolved, the pH was adjusted to 4 using NaOH. Subsequently, 0.25 molar equivalents of Boc anhydride (0.78 mL) was added dropwise, the flask vented to allow CO_2 release, and the solution left to react for 24 h at room temperature. Upon completion, the solution was dialysed (Molecular weight cut off = 50,000 Da; SpectraPor, SpectrumLabs via VWR) against water for two days, changing every 12 h. The dialysed solution was frozen at -80°C and lyophilized for at least 96 h, resulting in a soft, porous solid.

One-step phenylalanine coupling

For one-step amino acid coupling four separate reactions were performed. Boc-protected γ-PGA-H (0.5 g, 0.091 M) was suspended in 30 mL anhydrous N-Methyl Pyrrolidone (NMP). The suspension was heated by oil bath to 60°C and stirred for 24 h. Meanwhile, 1.3, 2, 4, and 5 equivalents of L-Phenylalanine amide hydrochloride (Phe-$CONH_2$; Merck Chemicals, Nottingham, UK) were dissolved separately in 5 mL NMP and neutralised with 1 molar equivalent (to Phe-$CONH_2$) of N,N-diisopropylethylamine (DIPEA).

After 24 h, 1.3 molar equivalents of N,N'-dicyclohexylcarbodiimide (DCC) in NMP (0.68 M) was added drop wise to the Boc-γ-PGA-H mixture and allowed to react for 30 min at 60°C. Following this time, the neutralised amino acid solutions were added drop wise, NMP supplemented to make a final volume of 70 mL, and left to react for 48 h.

For degree of conversion calculations, 3 mL of the solution was precipitated over ice

in a 1:1 mixture of acetone and diethyl ether, as the solution did not precipitate in cold HCl (pH 1.5). This was centrifuged at 4000 R.P.M. for 5 min, supernatant removed, 30 mL cold diethyl ether added, and repeated four times. The resulting polymer was dissolved in 400 μL DMSO-d6 for ^{1}H-NMR, and the degree of coupling was calculated from integration of the NH peak of modified γ-PGA against that of γ-PGA-H from the ^{1}H-NMR spectra.

Two-step phenylalanine coupling

In another approach to the amino acid coupling, Boc-protected γ-PGA-H (128 mg) was suspended in a 3:1 mixture of PBS:NMP. Solutions of EDC:NHS (1:2 molar equivalents of polymer) in PBS and 11.7 molar equivalents of Phe-$CONH_2$ in 3:1 PBS:NMP were added drop wise to the stirring polymer suspension for a final volume of 28 mL, and allowed to react at room temperature. After 48 h, the solution was transferred to dialysis tubes (as before) and dialysed against water for 48 h, changing every 12 h. Following dialysis, the product was frozen and lyophilized for 96 h, yielding 150 mg porous solid product. Finally, 10 mg of the partially modified, lyophilized polymer was dissolved in 500 μL DMSO-d6 and ^{1}H-NMR confirmed the product was approximately 30% coupled.

For the second coupling step, the polymer produced from the previous step was dissolved (150 mg, 0.04M) in 25 mL NMP. Meanwhile, 1.3, and 5 molar equivalents of DCC and Phe-$CONH_2$ (neutralised 1:1 with DIPEA), respectively, were dissolved separately in NMP. The DCC solution was added, and after 30 min the neutralised Phe added drop wise and allowed to react. After 48 h, the solution was transferred to dialysis bags as before and dialysed against water for 72 h, changing every 12 h.

Two-step phenylalanine coupling purification

Polymer precipitated by dialysis was centrifuged at 4000 R.P.M., the supernatant removed, and washed repeatedly with cold HCl (pH 1.5) to remove the Boc protecting group. This was followed by repeated washes with H_2O and finally diethyl ether. The product retrieved was redissolved in DMSO (2% w/v), filtered through cotton, precipitated into cold HCl, and centrifuged. The polymer was then repeatedly washed with sonication in methanol and subsequently washed in diethyl ether before drying at 40°C. Finally, 10 mg of produced polymer was dissolved in 500 μL DMSO-d6 and ^{1}H-NMR performed.

3.2.2 Chemical analysis

Nuclear magnetic resonance

NMR spectra were recorded on a Bruker Biospin GmbH AV500 (operating at 500 MHz for ^{1}H; 125.76 MHz for ^{13}C) using DMSO-d6 as a deuterated solvent. ^{1}H-NMR spectra were referenced to the residual protons in the deuterated solvent. Data are reported as

follows: chemical shifts are in ppm in the δ scale; multiplicity (s: singlet, d: doublet, t: triplet, q: quartet, m: multiplet, bs: broad signal); integration; assignment. ^{13}C-NMR spectra were referenced to the solvent chemical shift.

Phenylalanine coupled γ-PGA (γ-PGA-Phe): **^{1}H-NMR** δ: 1.75 (m, 1H, CH β [backbone]); 1.91 (m, 1H, CH β [backbone]); 2.07 (t, 2H, CH_2CO); 2.72 (m, 1H, CH β [side chain]); 3.08 (m, 1H, CH β [side chain]); 4.07 (m, 1H, C<u>H</u>NH [backbone]); 4.39 (m, 1H, C<u>H</u>NH [side chain]); 7.19 (m, 5H, H-Ar); 7.42 (d, 1H, NH [side chain]); 7.85 (m, 1H, NH β [side chain]); 7.94 (m, 1H, NH β [side chain]); 8.23 (d, 1H, NH [backbone]).

^{13}C-NMR δ: 27.75 (CH_2 β [backbone]); 31.50 (<u>C</u>H_2CO); 37.24 (CH_2 β [side chain]); 52.87 (CHNH [backbone]); 53.87 (CHNH [side chain]); 126.30-137.97 (C-Ar); 171.22 ($CONH_2$); 171.74 (CH_2<u>C</u>ONH); 173.00 (CH<u>C</u>ONH).

3.2.3 Thermal analysis

γ-PGA-Phe produced was thermally characterised as previously stated in Chapter 2 using TGA and DSC. The glass transition temperature (T_g) was measured from the second run in a program of heating to 120°C, cooling to -25°C, and heating to 245°C, all at 10°C min.

3.3 Results and discussion

3.3.1 One-step γ-PGA-Phe coupling

To couple the phenylalanine to γ-PGA, a one-step reaction was attempted to limit purification steps and overall synthesis time. However, it was found that if the cloudy reaction of Boc-γ-PGA-H in NMP was cooled to room temperature, the polymer crashed out of solution prior to adding the carbodiimide (DCC). After addition of DCC and the neutralised phenylalanine, the cloudy solution became more transparent over time as the degree of coupling increased.

NMR withdrawals for all four reactions of one-step γ-PGA-Phe coupling in NMP were unable to be precipitated in cold HCl (pH 1.5), which was the method used for fully esterified γ-PGA polymers. Instead, a cold 1:1 mixture of acetone:diethyl ether was employed for purification of the polymer. Figure 3.1 displays the most pure NMR spectrum of the four obtained for the coupling reactions. Very little product was able to be retrieved through repeated washing, resulting in low intensity of the polymer peaks, as shown in Figure 3.1. Also visible in Figure 3.1 are numerous impurities, shown by the number of peaks, whose signal intensity overpowers that of the polymer.

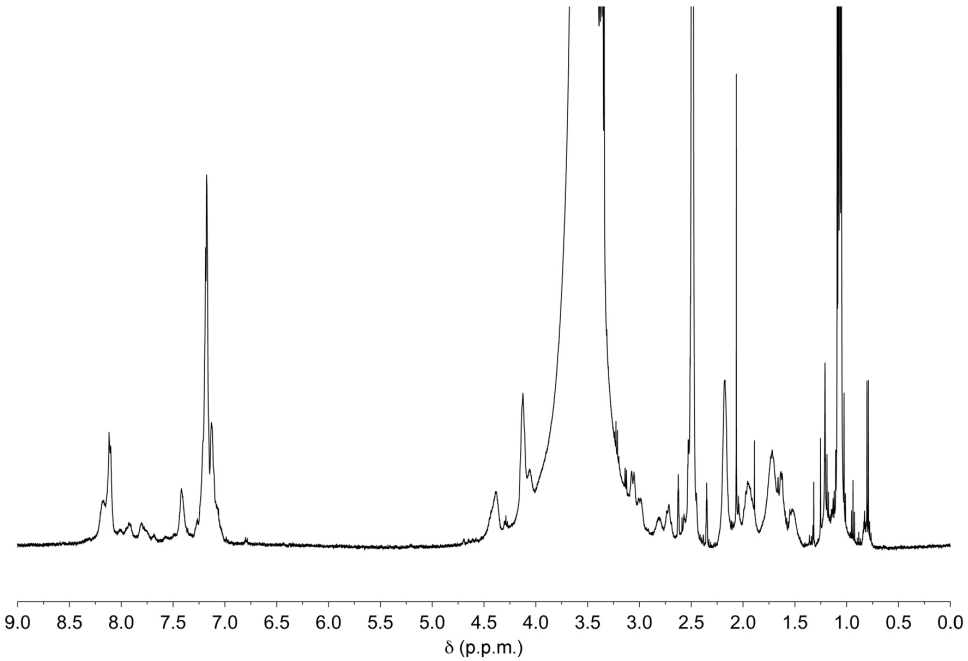


Figure 3.1: ^{1}H-NMR for retrieved γ-PGA-Phe polymer coupled using DCC and 5 molar equivalents of phenylalanine.

None of the four reactions performed were able to be modified above 30% using this one-step synthesis in NMP, as determined by ^{1}H-NMR. This is speculated to be caused by the initial poor solubility of Boc-γ-PGA-H in NMP. Furthermore, the cloudy reaction indicates that the actual polymer concentration in solution is unknown.

It is anticipated that performing this coupling in two steps may be better for obtaining 100% modification. Partially modifying the Boc-γ-PGA-H using EDC/NHS chemistry in an aqueous/organic solvent mix first may help with Boc-γ-PGA-H solubility. The mixture of solvents will solubilise the un- and partially modified polymer in the aqueous and organic phase, respectively. Following purification of this, an organic solvent should dissolve the partially modified starting polymer, allowing a more reliable calculation of polymer concentration in the solution.

3.3.2 Two-step γ-PGA-Phe coupling

By performing the synthesis in two separate steps, full coupling of phenylalanine to Boc-γ-PGA-H was achieved. The first step, performed in a mixture of PBS/NMP using EDC/NHS chemistry, resulted in approximately 30% coupling according to ^{1}H-NMR. This product was then purified from the water-soluble urea byproducts via dialysis and lyophilized for preparation of the second synthesis step.

Once partially modified, the Boc-[γ-PGA-Phe]$_m$-[γ-PGA-H]$_n$ polymer readily dissolved in NMP. The reaction was transparent, unlike the cloudy solution of Boc-γ-PGA-H in NMP. By improving the initial solubility in NMP from the partial modification step, the polymer concentration in NMP is more accurately determined and may help with repro-

ducibility of the reaction. This time using DCC, a highly efficient coupling reagent, a large excess of phenylalanine was used to push the reaction to full modification.

Upon completion of the second synthesis step, ^{1}H-NMR confirmed that 100% coupling of phenylalanine had been accomplished. Unfortunately, the NMR spectra also displayed numerous impurities, mainly attributed to a synthesis byproduct, dicyclohexylurea (DCU), as highlighted in Figure 3.2.

A relatively pure, 100% coupled product was obtained from the two-step synthesis after repeated washing. Using NMR techniques including ^{13}C-DEPT 135 and ^{13}C-COSY NMR, the new, relevant peaks from the phenylalanine were identified for this polymer. All NMR spectra obtained from the two-step coupling are presented in the following section.

3.3.3 Nuclear magnetic resonance

As anticipated, one byproduct of the DCC coupling reaction is DCU, a compound that is only soluble in a few alcohols or chloroform. Once fully modified, the γ-PGA-Phe also is slightly soluble in these solvents, thus removing DCU is difficult. Following filtration through cotton, purification washing steps were repeated for a total of three cycles, performing NMR analysis after each ”wash”. With each cycle, the spectral intensity decreased for impurities, as shown in Figure 3.2.

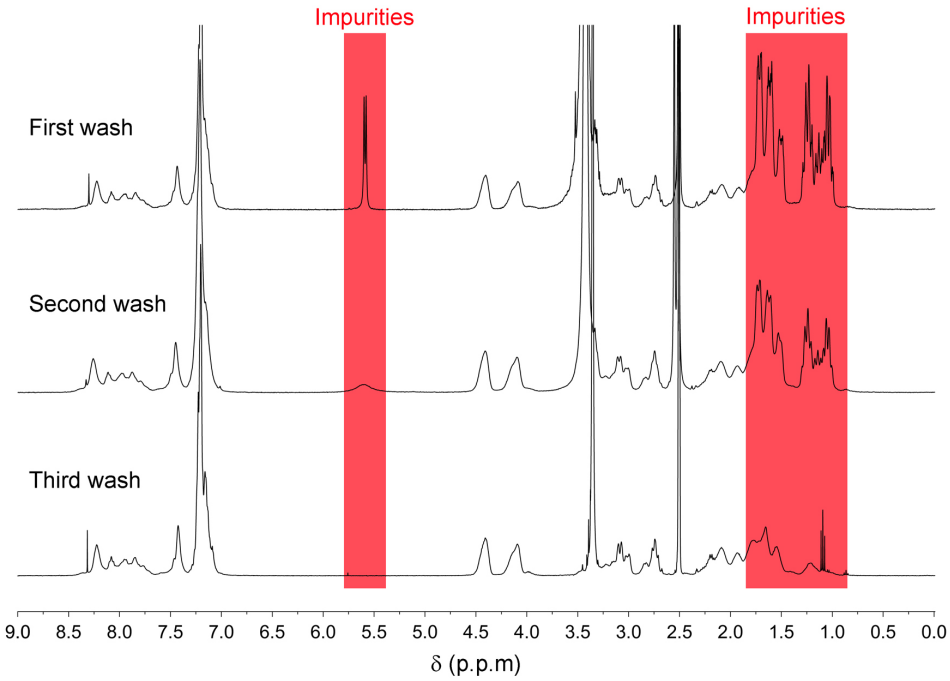


Figure 3.2: ^{1}H-NMR for fully coupled γ-PGA-Phe polymer, where impurities (DCU) indicated in red diminish with repeated wash steps.

^{1}H- and ^{13}C-NMR were used to determine the chemical structure of the γ-PGA-Phe polymer, as shown in Figure 3.3. This was further distinguished using ^{13}C- DEPT NMR, which shows CH and CH_3 pulse intensities as positive, while those of CH_2 are negative

(Figure 3.4). The ^{1}H- ^{13}C- COSY NMR correlation spectrum was also elucidated by interpreting the identification of protons with their corresponding carbon atoms in the structure (Figure 3.5).

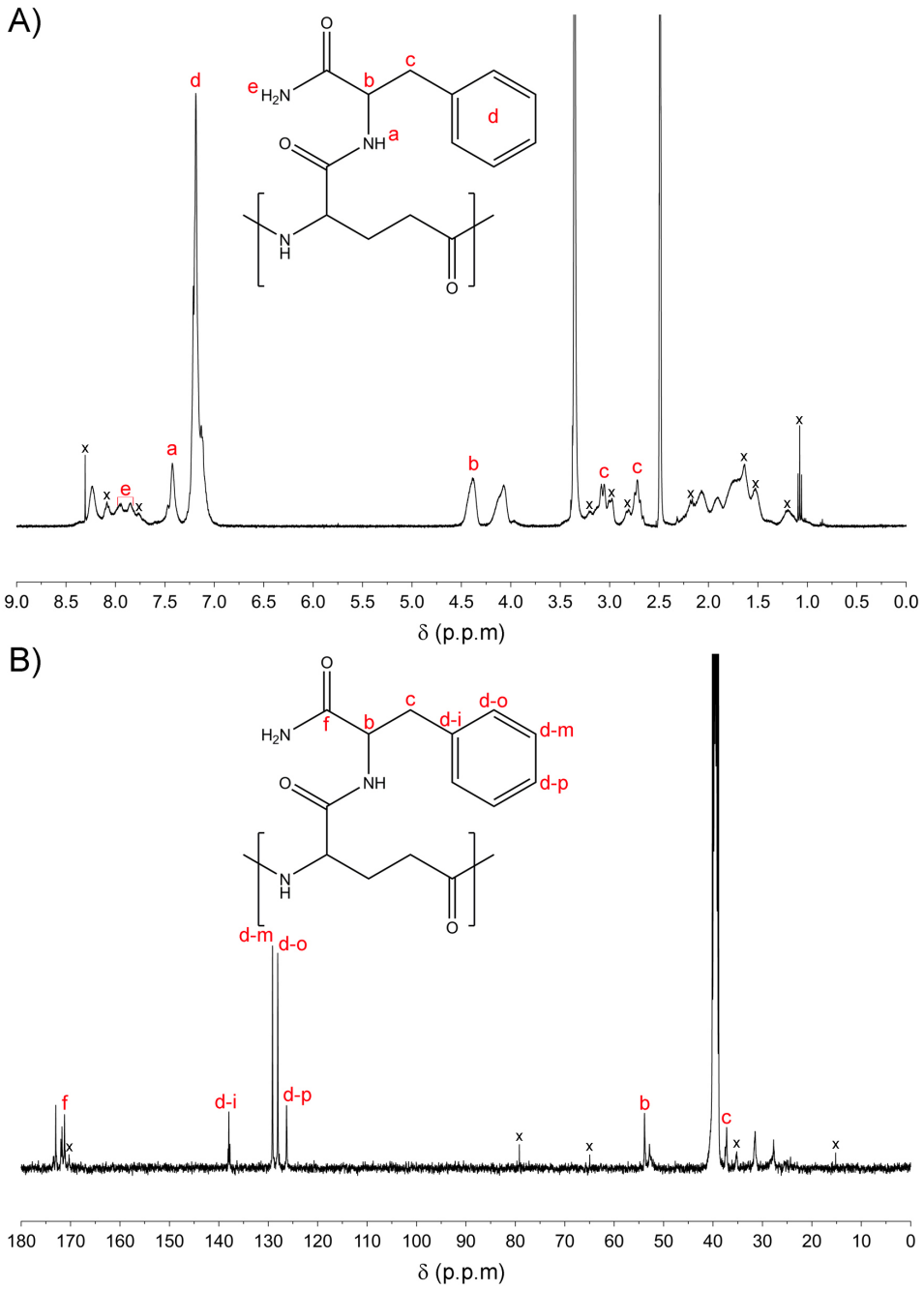


Figure 3.3: A) ^{1}H-NMR and B) ^{13}C-NMR for fully coupled γ-PGA-Phe polymer. Side group peaks are labeled in red lettering while peaks from impurities are indicated with black ”x” symbols.

3.3.4 ^{13}C- DEPT NMR

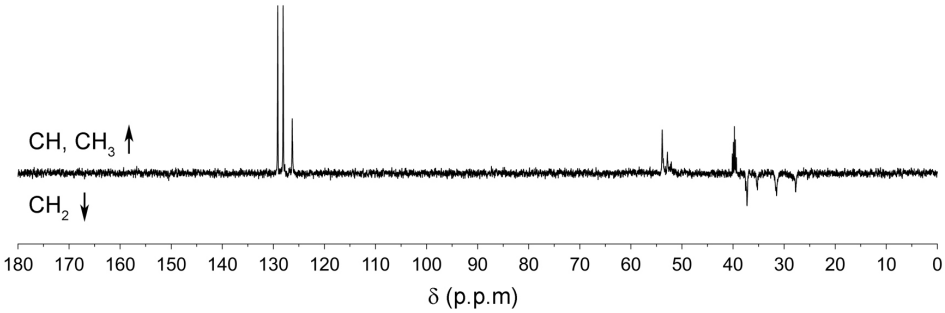


Figure 3.4: ^{13}C- DEPT 135 NMR for fully coupled γ-PGA-Phe polymer.

3.3.5 ^{1}H-^{13}C- COSY NMR

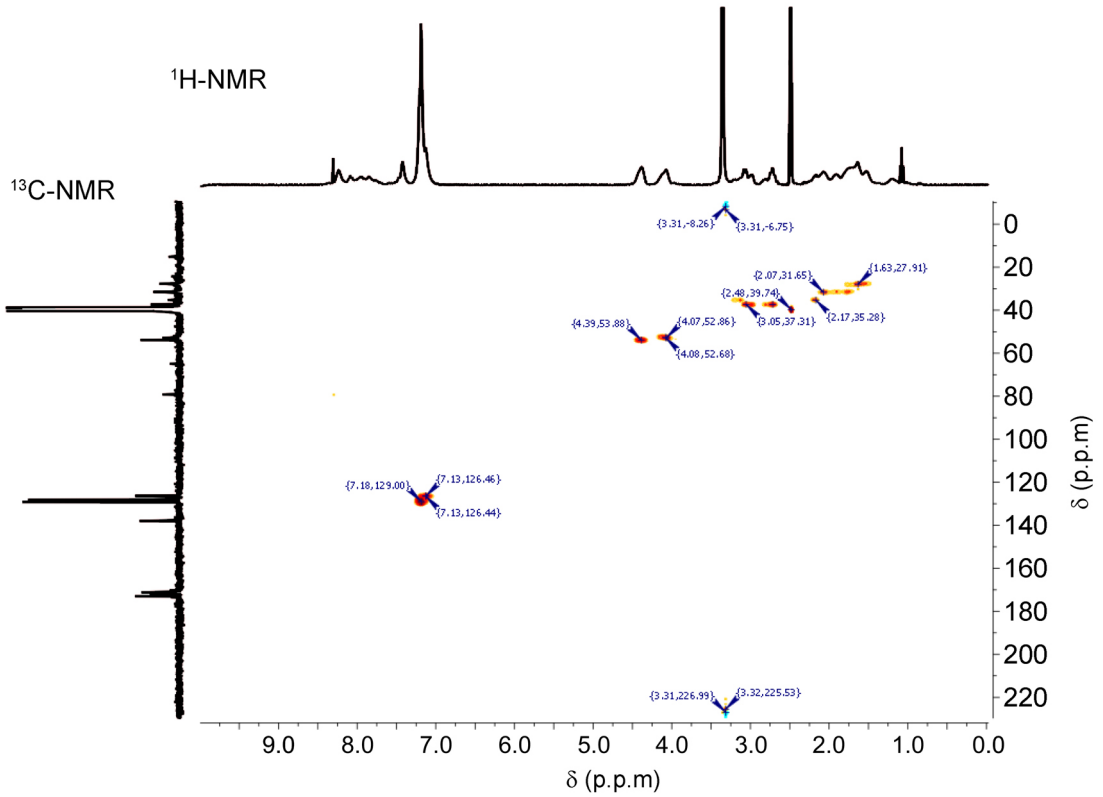


Figure 3.5: ^{1}H-^{13}C-COSY NMR for fully coupled γ-PGA-Phe polymer.

3.3.6 Thermal analysis

Dynamic TGA was performed on γ-PGA-Phe to the determine the temperature at which the polymer experienced 5% decomposition. DSC was then employed to determine the transition temperatures of the polymers. Performed on the purified powder, the DSC

heating/cooling rate was kept at 10°C min^{-1}. Both heating traces of esterified polymers are presented in Figure 3.6 and thermal results are tabulated in Table 3.1. In order to obtain the T_g, a shortened heating run was performed from -25°C to 120 °C, cooled to -25°C, and then the T_g was measured as before from the full heating run of -25°C to 245°C.

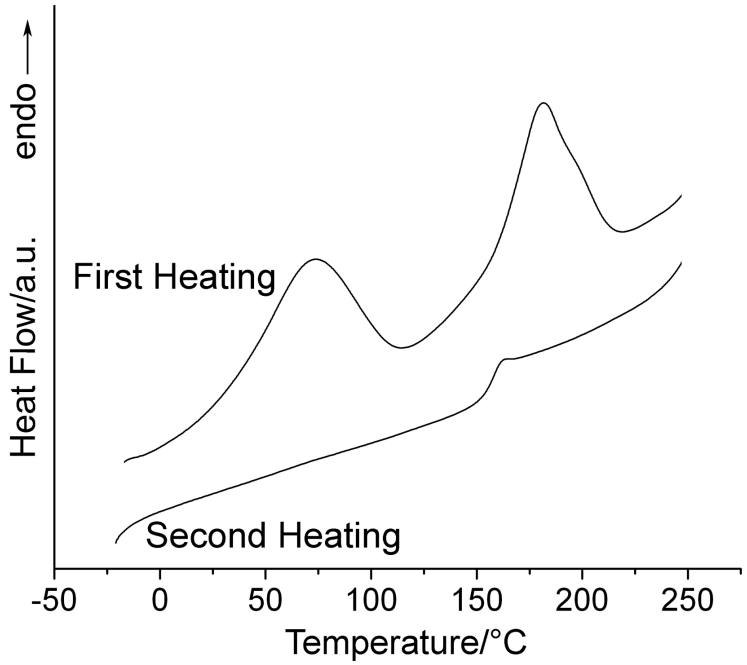


Figure 3.6: First and second heating DSC traces for fully coupled γ-PGA-Phe polymer, with excess solvent visible in the first heating, thus a separate, pre-heat run was performed to 120°C for the second heating trace to remove excess solvent for accurate T_g calculation.

Table 3.1: Thermal characterisation of coupled γ-PGA-Phe.

Synthesis	**T_g /°C**	**T_m /°C**	**5% T_d /°C**
γ-PGA-Phe	156	not visible	255

Though two peaks were visible in the first heating trace, no melting or recrystallisation was seen on the DSC traces for coupled γ-PGA-Phe. These endothermic peaks are thought to be a result of residual solvent evaporation. This polymer was found to have a very high glass transition temperature (156°C), which is most likely due to the chemical nature of the side chain. The additional amine and $CONH_2$ groups encourage more hydrogen bonding between chains than the native γ-PGA-H, restricting motion even further and increasing the T_g.

The glass transition temperatures and mechanical properties of γ-PGA-H and γ-PGA-Bn polymers shown in Chapter 5 are presented in Table 3.2. γ-PGA-H was found to be very brittle at room temperature, with a modulus of 4.7 GPa, tensile strength of 94 MPa,

and strain at break of 2%. This was attributed to two factors, the H-bonding between chains that limits chain motion and the T_g (124°C). While these are interrelated, testing performed at room temperature was in the glassy state of γ-PGA-H, leading to brittle behaviour.

Table 3.2: Thermal and mechanical properties of γ-PGA polymers as presented in Chapter 5.

Polymer	**T_g/ °C**	**E/ GPa**	**σ_y/ MPa**	**σ/ MPa**	**ϵ/ %**
γ-PGA-H	124	4.99	-	94	2
γ-PGA-Bn	40	1.24	28.1	20.3	106

With introduction of the benzyl ester on the side chain, H-bonds between chains of γ-PGA-H were diminished. This allowed for more chain motion, and the bulky benzyl side group may have created more void volume, leading to a large drop in T_g. When testing at room temperature, γ-PGA-Bn was found to be ductile, breaking at 106%, with a decreased modulus and tensile strength when compared with the brittle γ-PGA-H (1.24 GPa and 28.1 MPa, respectively).

By comparing the relationship of thermal and mechanical properties of γ-PGA-H and γ-PGA-Bn, the produced γ-PGA-Phe, with a high T_g of 156°C, should be brittle at room temperature. The introduction of more hydrogen bonding per monomer is expected to increase the mechanical properties, and it is speculated that γ-PGA-Phe would have a higher modulus than that of the native γ-PGA-H polymer.

Properties of nylon 12 and nylon 6,6 are presented in Table 3.3, as reported in the *Springer Handbook of Condensed Matter and Materials Data*[27]. Though both polymers have twelve carbon atoms, one main difference between them is that nylon 6,6 has twice as many N-H and C=O groups as nylon 12. According to[27], nylon 6,6 has a higher T_g and yield stress than nylon 12 and is twice as stiff. This is an encouraging example for γ-PGA-Phe, thus it would be advantageous to produce more material and perform thorough mechanical tests.

Table 3.3: Thermal and mechanical properties of nylon polymers as presented in[27].

Polymer	**T_g, °C**	**E, GPa**	**σ_y, MPa**
Nylon 12	50	1.3 - 1.6	45 - 60
Nylon 6,6	80	2.7 - 3.3	75 - 100

3.4 Conclusions

This study focused on coupling an amino acid to γ-PGA-H, yielding γ-PGA-phenylalanine. Initially a one-step synthesis was performed, yielding a polymer of approximately 30% modification. Full modification to γ-PGA-Phe was only achieved through a two-part synthesis containing urea impurities from the reaction. This may benefit from using a different carbodiimide coupling agent, such as N,N'-Diisopropylcarbodiimide (DIC), in the second synthesis step that will react to form a urea which will be easier to purify from the polymer. The chemical structure of γ-PGA-Phe was identified and confirmed using ^{1}H-NMR, ^{13}C-NMR, ^{1}H-^{13}C- COSY NMR and ^{13}C-DEPT-135 NMR.

The polymer experienced 5% weight loss at 255°C and no melting was seen before this temperature was reached. With introduction of an amino acid side group, the T_g increased to 156°C, caused by more hydrogen bonding between polymer chains. The increased number of interchain hydrogen bonds of γ-PGA-Phe means tensile deformation would not be a possible processing method. However, it is anticipated this bonding will increase the mechanical properties when compared with those of γ-PGA-H and γ-PGA-Bn polymers.

This synthesis chapter highlights the ability to fully modify γ-PGA-H using an amino acid, which opens the possibility for functionalisation of γ-PGA with other amino acids or short peptide sequences. Various extracellular matrix protein-mimicking peptides may be of interest for better cell incorporation in a scaffold of this material. This work helps pave the way to targeting specific tissue engineering applications using γ-PGA polymers, showing that γ-PGA is a versatile polymer whose functionality may be highly controlled and tuned through chemical modification.

Chapter 4

Cytotoxicity and culture stability of esterified γ-PGA

4.1 Introduction

As reviewed in Section 1.3.1, scaffolds produced for tissue engineering must fulfil as many as possible of the characteristics listed in Table 1.2, most notably biocompatibility and biodegradability. Previously discussed in Section 1.3.2, non-toxic, naturally produced γ-PGA is an excellent candidate for tissue engineering. In the preceding two chapters, γ-PGA was esterified to reduce the water solubility. There is a distinct lack of publications on the biocompatibility of esterified γ-PGA. Therefore, this chapter aims to assess the biocompatibility of these modified γ-PGA polymers.

While the native γ-PGA polymer backbone is enzymatically degraded,[134–136] the side groups introduced to reduce the water solubility are coupled through an ester bond. Similar to the degradation of FDA-approved polyesters like polycaprolactone and poly-L-lactide, this bond may be subject to random hydrolysis. Released side groups, now alkyl or aryl alcohols, may have an adverse effect on biocompatibility. Furthermore, the polymer scaffold may lose water resistance, allowing dissolution of the construct and thus a loss of mechanical properties. Therefore another focus of the work presented in this chapter is to determine and quantify whether or not any side chain hydrolysis or overall dissolution of the modified polymer takes place.

4.2 Experimental

All reagents for cell culture were used as purchased from Invitrogen (Paisley, UK) unless stated otherwise. Salts were purchased from Sigma-Aldrich (Gillingham, UK), the Triton X-100 from BDH laboratories (Poole, UK). Aluminum Scanning Electron Microscopy (SEM) pin stubs and adhesive carbon discs were purchased from Agar Scientific (Standsted, UK).

4.2.1 ISO 10993:5 pre-clinical cytotoxicity test

Modified γ-PGA films were sterilised for 2 h on each side under UV light and prepared with a material surface area to culture medium ratio of 6 cm^2 mL^{-1} according to thin-film requirements outlined in ISO10993:12. Similarly, controls were calculated with an extraction ratio of 3 cm^2 mL^{-1} [negative, non-toxic PVC (Med7539 noDop) tubing; positive, organo-tin stabilised PVC sheet, t > 0.5 mm; both kindly supplied by Raumedic (Munchberg, Germany)] and sterilised using 70% ethanol for 40 min and allowed to air dry.

The mouse osteoblast cell line MC3T3-E1 (European Collection of Cell Cultures; Salisbury, U.K.) was routinely cultured under standard conditions (37°C, 5% CO_2, 100% humidity) in Alpha Minimum Essential Medium (α-MEM) supplemented with 10% (v/v) foetal bovine serum (FBS) and 2 mM L-glutamine (all Invitrogen; Paisley, U.K.).

Sterile samples were soaked in α-MEM for 7 days at 37°C, 5% CO_2 to make the conditioned media. MC3T3-E1 cells were seeded into 96 well plates at a density of 20,000 cells cm^{-2} in standard culture medium (as above). Cells were imaged on an Olympus IX51 epifluorescence microscope fitted with a DP-70 camera (London, U.K.). After 24 h, the medium was exchanged with conditioned culture medium (supplemented with 10% v/v FBS and 1% v/v L-glutamine) and diluted by factors of 2, 4, 8, or 16 with standard culture medium for 24 h, upon which the cellular metabolic activity was assessed using MTT (3-(4,5-Dimethylthiazol-2-yl)-2,5-diphenyltetrazolium bromide). For the assay, 20 μL of a sterile-filtered 5 mg mL^{-1} solution of MTT in Dulbecco's phosphate buffered saline (DPBS, pH 7.4) was added to the culture media and incubated for 2 h. Upon completion of incubation, media was removed, cells washed with PBS, and 200 μL DMSO was pipetted in wells to dissolve the formazan product. Finally, 150 μL of formazan/DMSO was transferred to a fresh 96 well plate and read on a colorimetric plate reader at 592 nm (background subtraction at 620 nm). All results are normalised to negative control conditioned, media-treated MC3T3-E1 cell metabolic activity.

4.2.2 LIVE/DEAD® assay

Cell viability on esterified γ-PGA samples was evaluated using a LIVE/DEAD® stain assay (Invitrogen). Primary human foreskin fibroblast cells-1 (HFF-1; ATCC, Virginia, USA) were routinely cultured under standard conditions (37°C, 5% CO_2, 100% humidity) in grown in Dulbecco's Modified Eagles Medium (DMEM) supplemented with 15% v/v FBS and 1% v/v antibiotic-antimycotic (all Invitrogen).

Round samples 8 mm in diameter were punched and sterilised by UV light (2 h per side) in polystyrene petri dishes. Following sterilisation, samples were transferred to 12 well plates containing 1 mL DPBS and soaked for 1 h at RT. After pre-wetting, HFF-1 cells (passage two, P2), were seeded at a density of 20,000 cells cm^{-2} with 50 μL cell

suspension per film. Cells were allowed to attach for 1 h before 2 mL fresh media was added. Samples were cultured, changing media every 2 days, for 1 and 7 days. Upon completion of time points, cells were washed with DPBS and 1 mL sterile LIVE/DEAD® solution (0.5 μM calcein AM and 0.5 μM ethidium homodimer-1 (EthD-1) in DPBS) was added to each well. Plates were incubated at 37 °C for 30 min, after which fluorescence was imaged on an Olympus IX51 epifluorescence microscope fitted with a DP-70 camera (calcein peak excitation 494 nm, peak emission: 517 nm; EthD-1 peak excitation: 528 nm, peak emission: 617 nm).

4.2.3 Immunofluorescence staining

HFF-1 (P2) cells were cultured as above and seeded onto unoriented γ-PGA-Bn films (r = 6 mm) in 12-well plates at a low density of 3000 cells cm^{-1} in 50 μL volumes. Cells were given 1 h to attach before adding 2 mL media into wells. Films were cultured at 37°C, 5% CO_2 for 4 days, refreshing culture media at day 2. After culture period, the films were stained as below and imaged using a Leica TCS SP2 upright confocal microscope (Leica Microsystems GmbH, Wetzlar, Germany).

Cultured films were removed from the well plate, washed three times with DPBS (0.1 M, pH 7.4), and subsequently fixed with a solution of 4 % (w/v) paraformaldehyde in DPBS for twenty min at room temperature. Films were then rinsed 3 times in DPBS and then permeabilized using a Triton x-100 solution (0.25% v/v in DPBS) for five min at RT, and washed 3 times. A 3% (w/v) solution of bovine serum albumin (BSA; Sigma) in DPBS was applied and samples were allowed to block non-specific protein binding for 1 h at RT. All subsequent steps were performed with samples protected from light to preserve fluorescence.

After removal of the BSA solution, focal adhesions were stained with a 1:400 solution of vinculin (primary antibody, raised in mouse; Abcam, Cambridge, U.K.) in DPBS, added to cover films and left to bind at RT for one h. Samples were washed three times with DPBS and the secondary antibody, a goat α-mouse conjugated with Alexafluor 568 (Molecular Probes, Invitrogen), was added at a concentration of 1:400 in DPBS for 1 h at RT. The secondary antibody solution was removed, films washed three times with DPBS, and conjugated Phalloidin-AlexaFluor 488 solution (1:400 in DPBS; Invitrogen) was added to stain actin filaments for thirty min at RT. Samples were then rinsed three times in DPBS, and a 1:1000 solution of 4'-6-Diamidino-2-phenylindole (DAPI) in DPBS was added for 5 min to stain cell nuclei. Finally films were rinsed three times with DPBS, placed on slides, mounted with a drop of ProLong® mounting medium (Invitrogen), covered with a cover slip, and sealed using clear nail varnish.

4.2.4 Dissolution soaking study

For dissolution studies, unoriented γ-PGA-Bn films were cast as described in Section 5.2.2 and samples punched in two sizes, r = 4 and 9 mm for SEM and ^{1}H-NMR characterisation, respectively. Films were incubated in an orbital shaker (R.P.M. = 120; Weiss Gallenkamp, Loughborough, UK) at 37°C for 7, 14, 21, and 28 days in diH_2O, DPBS (PBS), and simulated body fluid (SBF, as prepared according to Kokubo and Takadama[171]) Soaking volumes (V) were calculated based on surface area (S.A.) from the following equation[171]:

$$V(ml) = \frac{S.A.(mm^2)}{10} \tag{4.1}$$

The medias were changed every 7 days, reserving 1 mL of supernatant for UV-Vis measurements, stored at RT.

UV-Visible spectroscopy

UV-Visible measurements were carried out on a JASCO-V-630 Spectrophotometer, collecting spectra from 200-300 nm and using quartz cuvettes (optical pathway = 10 mm). A calibration curve of benzyl alcohol was obtained by measuring absorbance at λ = 257 nm of 1, 2, 2.5, 4 and 5 mM solutions in diH_2O, as shown in Figure 4.1.

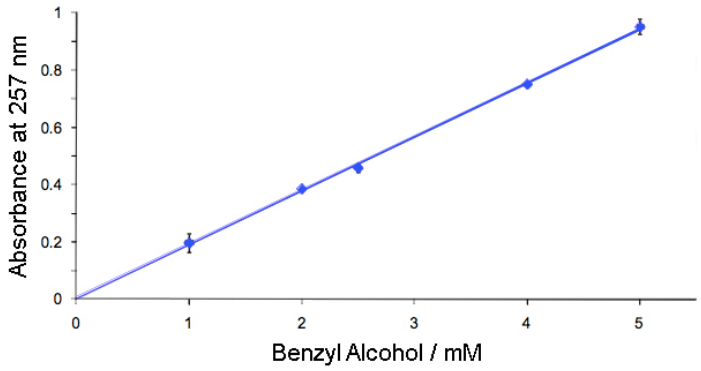


Figure 4.1: UV-Vis calibration curve for benzyl alcohol absorbance at λ = 257 nm.

For each soaking time point, 1 mL of film supernatant (n = 3) was transferred into the cuvette and absorbance measured using the corresponding blank (H_2O, PBS, or SBF). For time points over seven days, cumulative values of individual samples were averaged across media types.

Scanning electron microscopy

Upon time point completion, films were gently washed with diH_2O and air dried at room temperature for 24 h, followed by 72 h at 40°C under vacuum. After drying, smaller film samples (r = 4 mm) were massed and mounted on SEM stubs, sputter coated with

chromium (75 μA, 1.5 min) and imaged using a Leo 1525 Gemini scanning electron microscope operated at an accelerating voltage of 5 kV.

Optical photography

Upon time point completion, films were gently washed with diH_2O and air dried at room temperature for 24 h, followed by 72 h at 40°C under vacuum. Larger samples (r = 9 mm) were massed and then photographed using a Canon EOS 350D with a 24-70 mm 2.8f L-series Canon lens.

^{1}H-NMR

Following optical photographs, films were cut and approximately 10 mg of the film was dissolved in 500 μL DMSO-d6 for ^{1}H-NMR to assess any side chain hydrolysis.

4.3 Results and Discussion

Though γ-PGA is non-toxic, the biocompatibility of the esterified polymers has yet to be reported in the literature. Thus, cell culture studies were performed to assess if esterified γ-PGA films are also non-cytotoxic and support cell attachment.

4.3.1 ISO 10993:5 pre-clinical cytotoxicity test

In order to assess the feasibility of modified γ-PGA films for use in tissue engineering applications,[147] the ISO 10993:5 test was employed, a step often used prior to *in vivo* animal studies. This test assesses if any toxic dissolution products are released, as they will cause a detectable reduction in cellular metabolic activity level. Polymer films were soaked in cell culture medium at 37°C for 7 days. Murine pre-osteoblastic cells (MC3T3-E1) were then cultured in the conditioned medium overnight and their metabolic activity assessed.

For the ISO 10993:5 test, cell metabolic activity was measured using an MTT [3-(4,5-Dimethylthiazol-2-yl)-2,5-diphenyltetrazolium bromide] assay. The MTT assay is a colourimetric assay that measures the enzymatic reduction of the yellow tetrazolium salt (MTT) into an insoluble purple formazan product. This is performed by dehydrogenases in the mitochondria of living cells and more enzymatic reduction reflects more cellular metabolic activity.

MC3T3-E1 cells cultured in conditioned medium soaked with either the negative control or esterified γ-PGA films appeared morphologically normal (Figure 4.2, panels A-D, F), while those exposed to positive control conditioned medium displayed a rounded, abnormal morphology (Figure 4.2-C). Activity of cells exposed to all experimental film soaked media were similar to that of the negative control as shown in Figure 4.3. The MTT activity of positive control treated cells was significantly lower than all other tested groups ($p < 0.001$).

These results indicate that dissolution products released from soaked films did not have

a negative effect upon cell metabolic activity. Thus all esterified γ-PGA polymers pass the international standard test for assessing *in vitro* mammalian cell cytotoxicity and have good potential for use in tissue engineering applications. As this method of assessment is performed with murine cells, it is of great interest to assess human cell viability directly on the modified γ-PGA polymers, which will be described in the following sections 4.3.2 and 4.3.3.

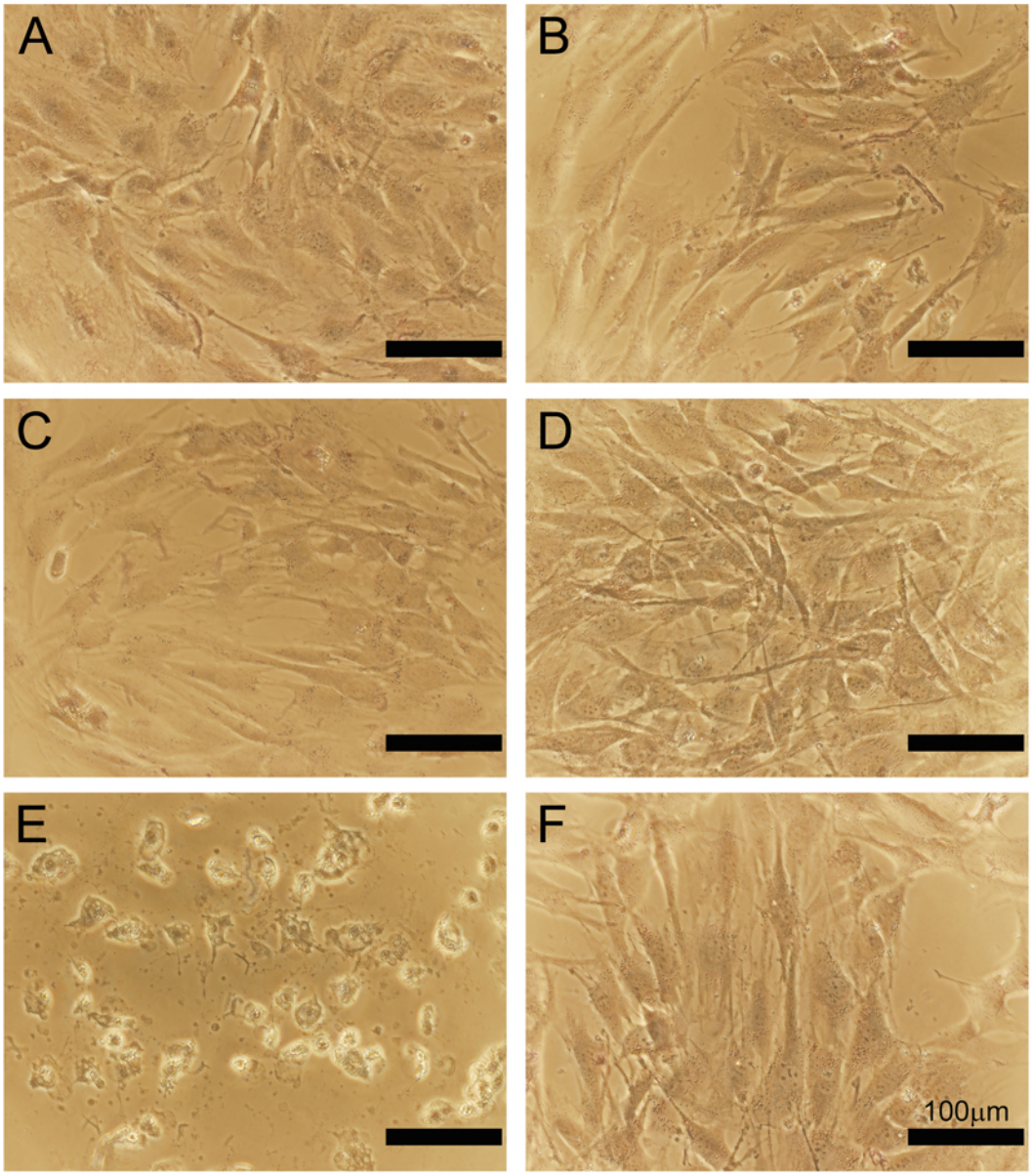


Figure 4.2: MC3T3-E1 cells exposed to conditioned media for 24 h. A) Tissue culture plastic (blank control), B) γ-PGA-Et, C) Negative control, D) γ-PGA-Pr, E) Positive control, F) γ-PGA-Bn.

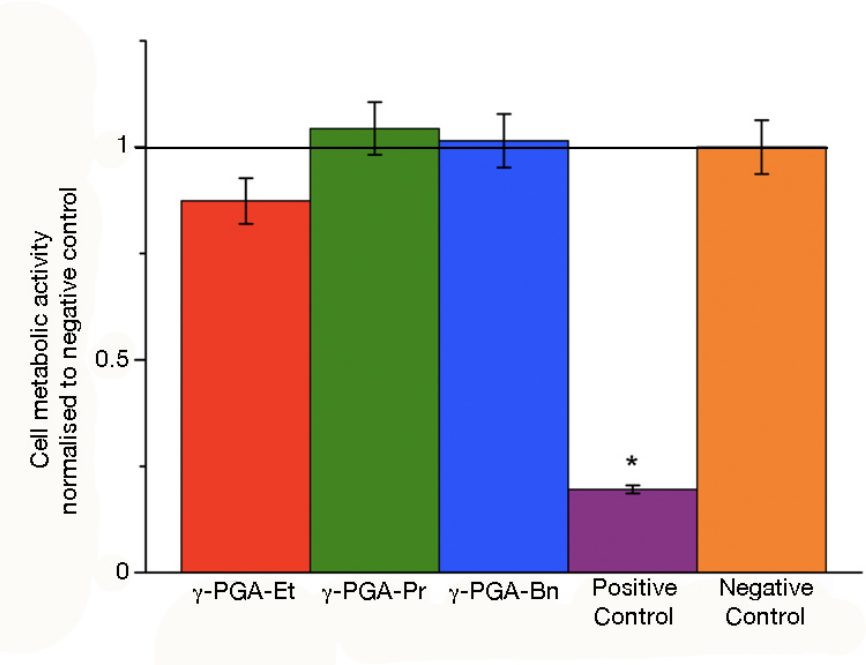


Figure 4.3: ISO 10993:5 pre-clinical test of esterified γ-PGA films, normalised to negative control. All polymers passed and metabolic activities were not significantly different to the negative control, but were significantly different from the positive cytotoxic sample (* $p < 0.001$).

4.3.2 LIVE/DEAD® assay for cell viability

As the ISO 10993:5 test uses mouse cells for testing cytotoxicity, γ-PGA films were then cultured to assess their ability to support human cell attachment and growth. Viability of human foreskin fibroblast-1 (HFF-1) cells (P2) cultured on esterified γ-PGA films was assessed using a LIVE/DEAD® assay at days 1 and 7 (Figure 4.4). The assay shows live cells with intact cell membranes, which only fluoresce green from esterase cleaved calcein AM in the cytoplasm. Meanwhile, ”dead” cells, which have compromised cell membranes, allow EthD-1 to label nucleic acids with red fluorescence.

Day 1 images are shown at 10x magnification to display initial cell morphology after 24 h adhesion in areas of low-density, while Day 7 images are shown at 4x magnification to show cell viability on a wider scale. All polymer films were found to have a large amount of autofluorescence with both the blue and green excitation filters. At 24 h, all films supported sparse cell attachment, while cells on γ-PGA-Et films appeared more round while those on γ-PGA-Pr and γ-PGA-Bn were more spread.

Fibroblasts on all polymer types remained viable at both time points assessed in this study, as confirmed by the LIVE/DEAD® stain. Visual examination of the images taken at lower magnification on day 7 shows that cells spread and proliferated over time on all three polymer types. These results, taken together with those from the ISO test indicate that all three γ-PGA modifications have potential to be candidates for tissue engineering.

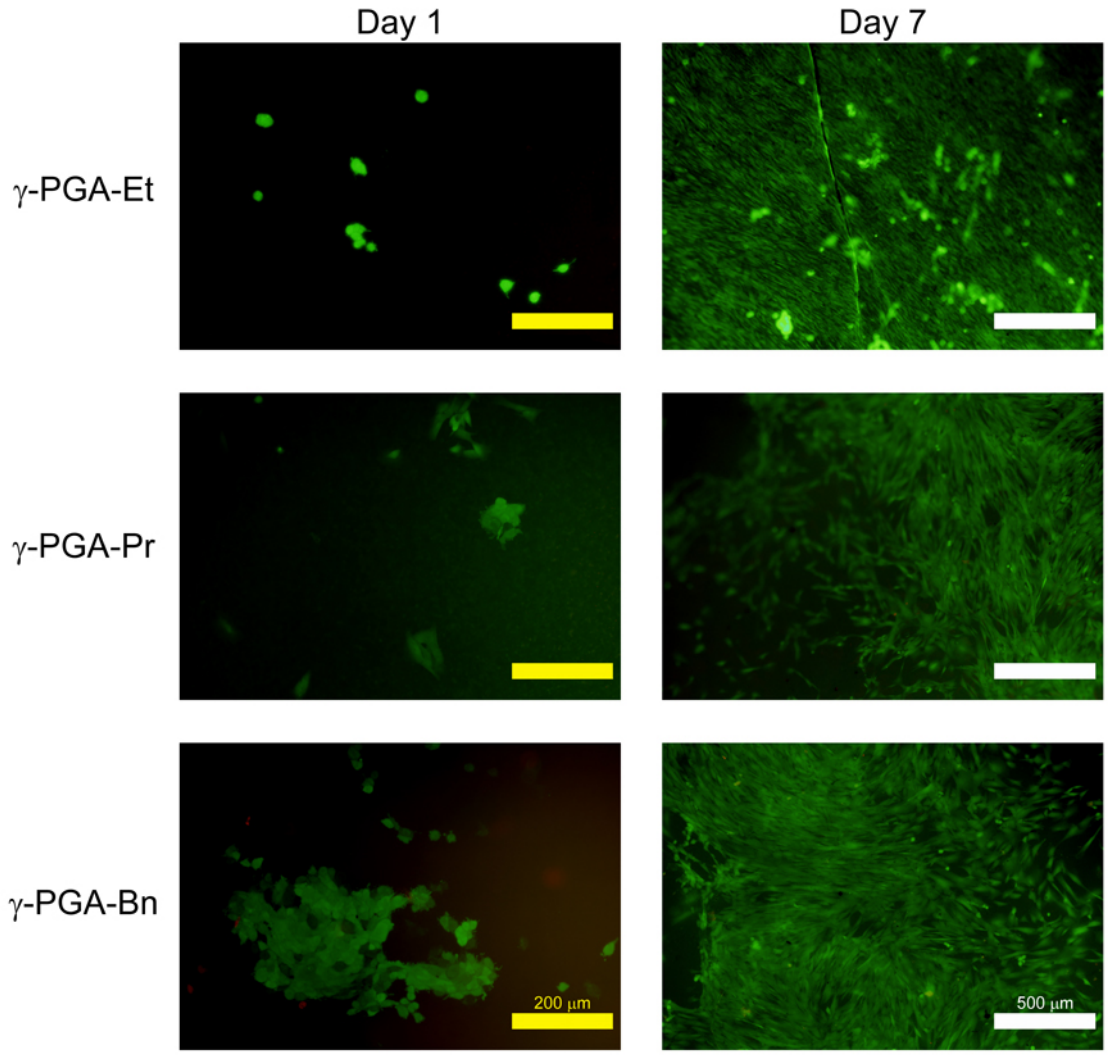


Figure 4.4: LIVE/DEAD® assay of human foreskin fibroblasts (P2) cultured for 1 and 7 days on esterified γ-PGA films at 10x and 4x magnification, respectively.

As reported in the previous chapter, the contact angles of γ-PGA-Et, γ-PGA-Pr, and γ-PGA-Bn were found to be 58.0° ± 0.7, 76.6° ± 1.1, and 88.1° ± 1.2 (not significant from PLLA, 88.1° ± 1.4), respectively. Recently, Joy *et* al.[172] studied a focused library of methacrylate terpolymers to investigate surface chemistry effects on cell function, ranging in contact angle from 61° ± 2.37 to 96° ± 1.28.[172] Their group found that polymers with contact angles ≥ 92.0° (± 1.8) had significantly higher cell attachment and proliferation than those with lower contact angles.[172]

They also demonstrated a positive correlation for both cell attachment and proliferation with increasing contact angle. For polymers with contact angles (61° ± 2.37 and 75° ± 2.37)[172] similar to those of γ-PGA-Et and γ-PGA-Pr, the measured percentages of cells undergoing proliferation were found to be 24 % ± 3.06 and 29% ± 9.27, respectively.[172] This level of proliferation was far lower than that of a polymer with a similar contact angle (92.0° ± 1.83)[172] to γ-PGA-Bn (88.1° ± 1.2). This polymer with a larger contact

angle displayed 78 ± 5.01% cells proliferating.[172] Therefore, the γ-PGA-Bn polymer has been chosen to focus specifically on with further studies to look at cell attachment and cytoskeletal organisation on this polymer using immunostaining techniques.

4.3.3 Immunostaining of cells

Following on the results from contact angle analysis as discussed in the previous section, HFF-1 cells were seeded onto γ-PGA-Bn films and cultured for 4 days. Following completion of the time point, cells were stained to investigate their adhesion onto the polymer substrate (Figure 4.5). HFF-1 cells grown on γ-PGA-Bn films stained positive for F-actin, vinculin, and DNA, allowing the cytoskeleton and nucleus to be imaged. The cells were found to be spread on the films with a large amount of actin fibre organisation in the direction of cell elongation. It was also seen that vinculin was colocalised with actin stress fibres (highlighted in Figure 4.6), indicating the fibroblasts are bound to the substrate by focal adhesions.

The cells displayed F-actin stress fibres (green), a major component of the fibroblast cytoskeleton which is linked to the cell membrane in focal adhesions[173]. In fibroblast cells, actin exists primarily in three structures: the most prominent form of actin stress fibres[174], cell surface protrusions including membrane ruffles and microspikes, and in the cortical actin network.[173]. Stress fibres originate from focal adhesions, areas where integrins cluster and bind to the extracellular matrix, as discussed in Section 1.2.4. Depending on the cytoskeletal organisation, it is possible to determine if the cells are motile or stationary on substrates.

In 1978, Heath and Dunn[175] used electron microscopy to discover that some actin bundles did not pass through the perinuclear region and had focal contacts associated with both ends of the bundles. These cytoskeletal patterns were found to be more common in cells with decreased motility.[175] This organisation was seen in some cells on the γ-PGA-Bn films, as seen in Figure 4.5-B and highlighted in Figure 4.6-A. Heath and Dunn also observed that some cells possessed a star-shaped organisation of filament bundles where bundles terminate at focal adhesions and were radially arranged from a common centre,[175] as seen in some HFF-1 cells grown on γ-PGA-Bn films in Figure 4.5-D and highlighted in Figure 4.6-B.

The organisation and staining observed for F-actin and vinculin indicate that the human fibroblast cells are well adhered to the γ-PGA-Bn films. This is a promising result for human tissue engineering applications as cell adhesion plays a significant role in numerous cell processes.

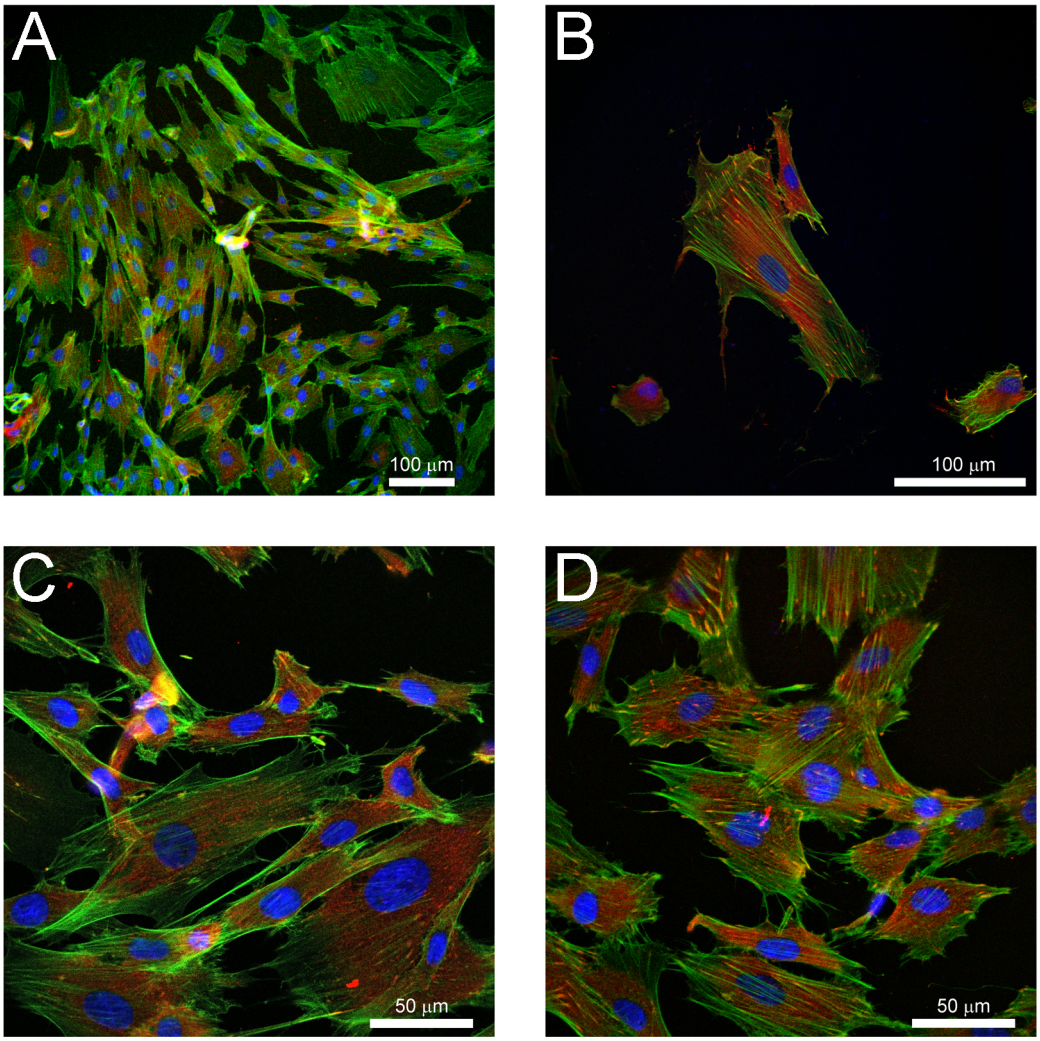


Figure 4.5: Immunostained images of HFF-1 (P2) cells cultured on γ-PGA-Bn films for 4 days at 37°C, 5%CO_2. Confocal images taken at 20x (A), 40x (B), and 63x (C-D) magnification. Blue represents cell nuclei, green shows F-actin filaments and red displays vinculin-positive focal adhesions.

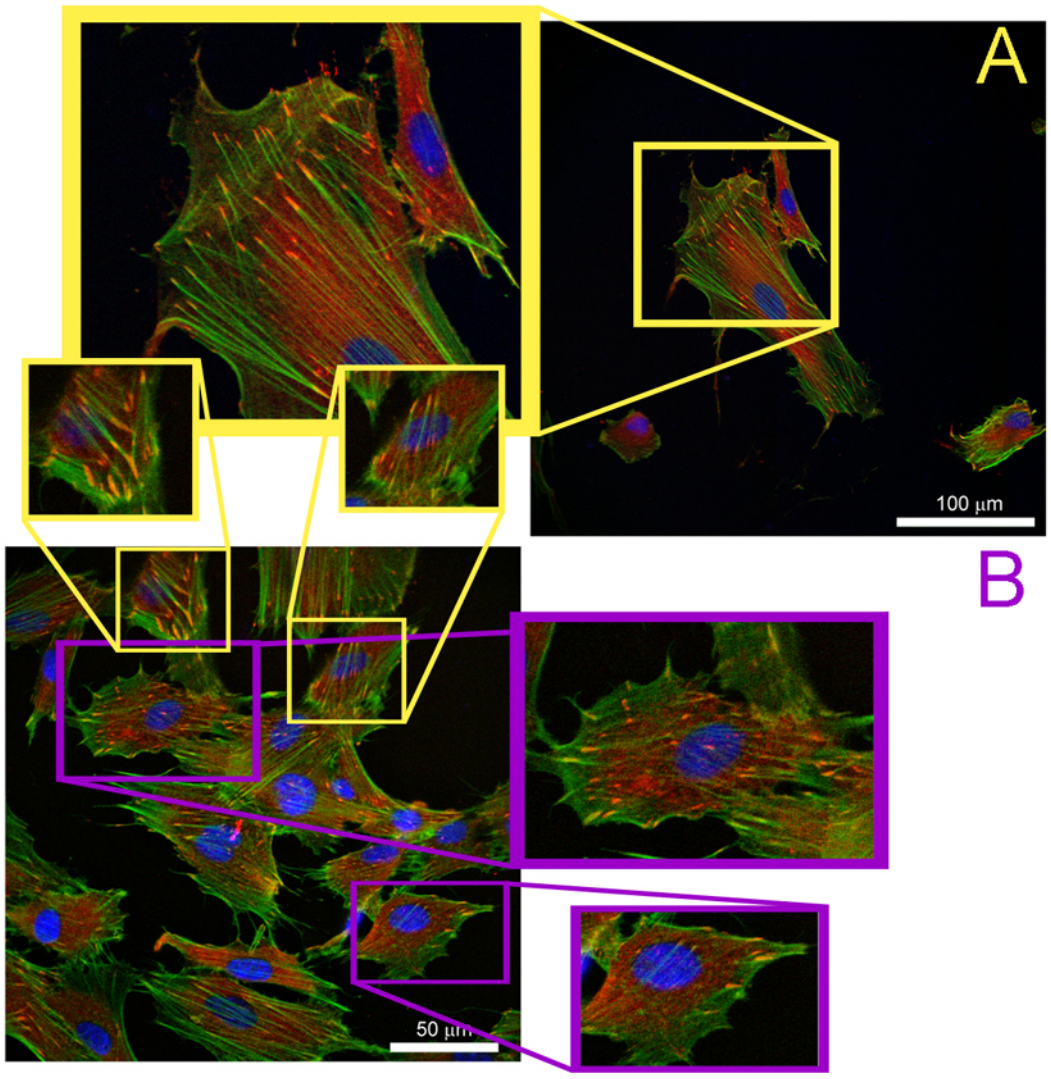


Figure 4.6: Areas of interest from immunostained images shown in Figure 4.5 of HFF-1 (P2) cells cultured on γ-PGA-Bn films for 4 days (37°C, 5%CO_2), displaying F-actin stress fibres associated with focal adhesions at both ends of the fibres highlighed in yellow boxes (A) or radially arranged focal adhesions highlighted in purple boxes (B). Blue represents cell nuclei, green shows F-actin filaments and red displays focal adhesions.

4.3.4 Dissolution soaking study

Following cell cytocompatibility and viability tests, a dissolution study was performed to investigate the stability of γ-PGA-Bn films. While the native γ-PGA is enzymatically degraded, the ester group on the side chain can still be subject to random hydrolysis, yielding benzyl alcohol byproduct and rendering the main chain more soluble. Films were soaked for 7, 14, 21, and 28 days at 37°C to assess any side chain hydrolysis and resultant dissolution.

Mass retained

Over the soaking period, all films had significantly less mass than starting, experiencing a loss of 3-4%, as shown in Figure 4.7. The largest drop in mass occurred in the first seven days, independently of soaking media.

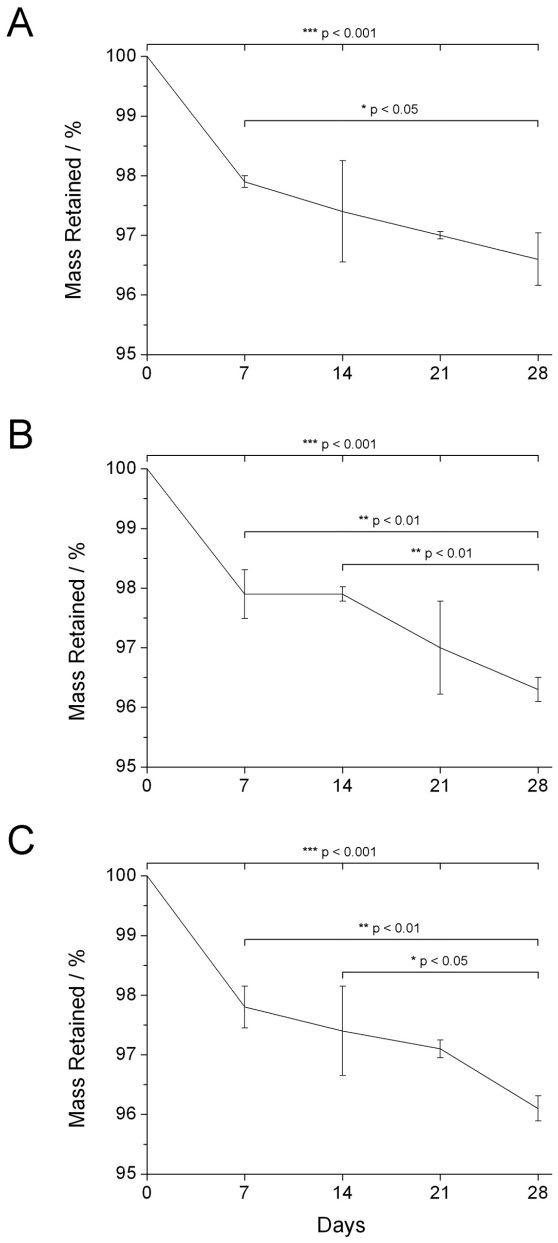


Figure 4.7: Mass retained for films soaked in a) H_2O, B) PBS, or C) SBF for 7, 14, 21, and 28 days at 37°C. Significance determined by One-way ANOVA (Tukey post-hoc) and as indicated in figure.

Side chain hydrolysis

Supernatants from the soaking media at each time point and media changes were run under UV-Visible spectroscopy (UV-Vis) to test for any optical change due to benzyl alcohol

being released in the solution. The absorbance levels detected were below that of the lowest concentration in the calibration curve (1 mM BnOH) and appear to be instrumental noise. Therefore, if any benzyl alcohol was released, the concentration is less than 1 mM BnOH and too low to detect using this method.

Alternatively, dried films from each time point were sent for ^{1}H-NMR analysis to detect any change in esterification level of the films. No change was detected in any of the samples at any of the time points. Thus it may be concluded that if any side chain hydrolysis occurs, it is below a level which the instrument can detect.

Optical photographs

Polymer film transparency decreased upon soaking after 7 days in all three media. Some films were curled upon retrieval, while others remained flat. There was no visible change in colour or opacity after 7 days, and all films maintained their integrity throughout the soaking experiment duration. This optical change is from the unsoaked films is shown in Figures 4.8 and 4.9. The T_g of batches is 62°C, as determined by DSC, so the observable change is not due to crystallisation of the polymer film. Scanning electron microscopy was employed to investigate this change further and see if any microscale changes took place.

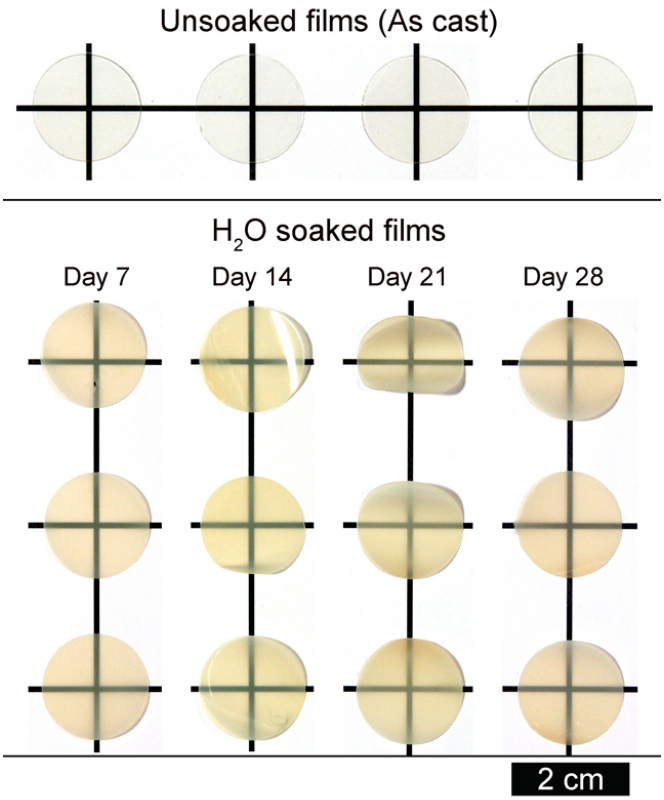


Figure 4.8: Optical photographs of films as cast or soaked in H_2O for 7, 14, 21, and 28 days at 37°C.

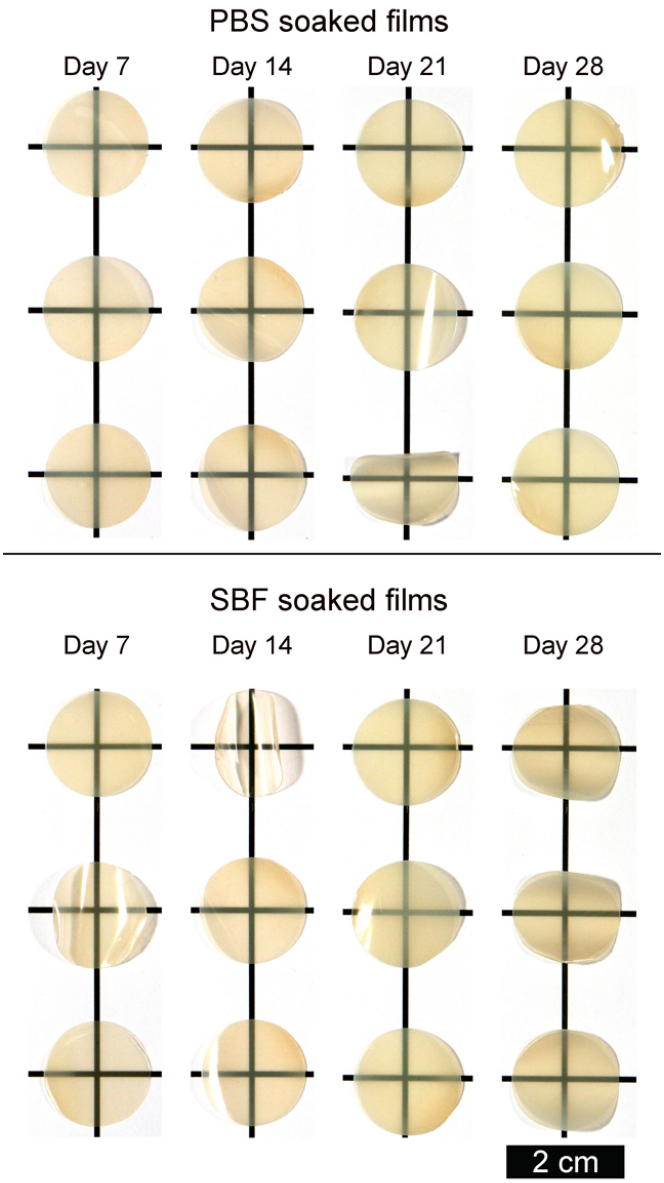


Figure 4.9: Optical photographs of films soaked for 7, 14, 21, and 28 days in PBS or SBF at 37°C.

Scanning electron microscopy

As shown in Figure 4.7, all films experienced around a 2% mass loss by day 7. A change in opacity is also observed optically as shown in Figures 4.8 and 4.9. Scanning electron microscopy images of pristine, as cast films (Figure 4.10) show no obvious defects, such as holes or cracks at 10,000 and 25,000x magnification.

By day 7, however, soaked films start to develop submicron sized holes which appear lighter in contrast than the film surface. These defects may cause a refraction of light, distorting its path through the polymer film and causing a visible change in transparency. Later time points show more occurrence of these defects. By day 28 in the SBF solution, widespread surface dissolution takes place, shown by a large change in contrast of the film surface. Backscattering SEM confirmed there was no mineralisation on the films soaked in SBF, and there was no precipitation of salt or mineral from any of the soaking media. This method also confirmed the holes were a direct result of dissolution from the film surface.

These defects appeared more frequently in the salt-containing solutions (PBS and SBF) than H_2O. While the γ-PGA-Bn is water resistant, the native γ-PGA-Na^+ salt form is extremely soluble at neutral pH. If any side chain hydrolysis occurred, the hydrolysed regions would be charge balanced by the ions in the PBS or SBF solutions. It is speculated that this may introduce even more water to the local environment, causing further hydrolysis of nearby polymer regions.

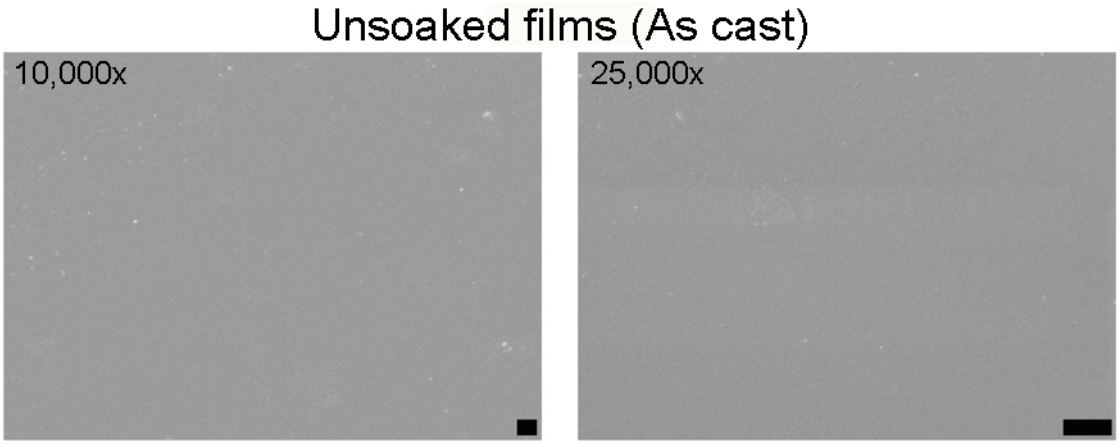


Figure 4.10: Scanning electron microscope photographs of films as cast. Scale bars = 1 μm.

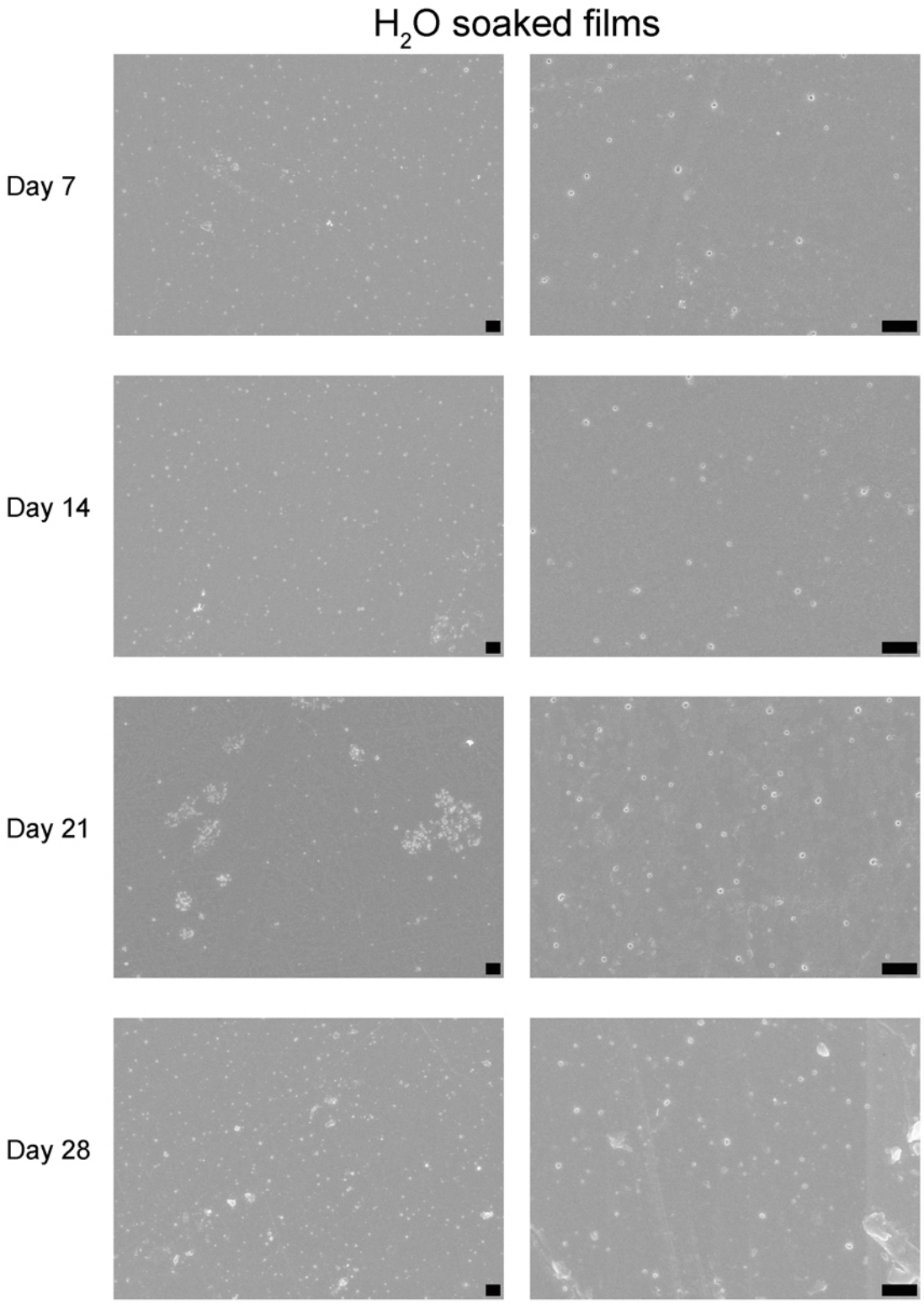


Figure 4.11: Scanning electron microscope photographs of films soaked for 7, 14, 21, and 28 days in H_2O at 37°C. Scale bars = 1 μm.

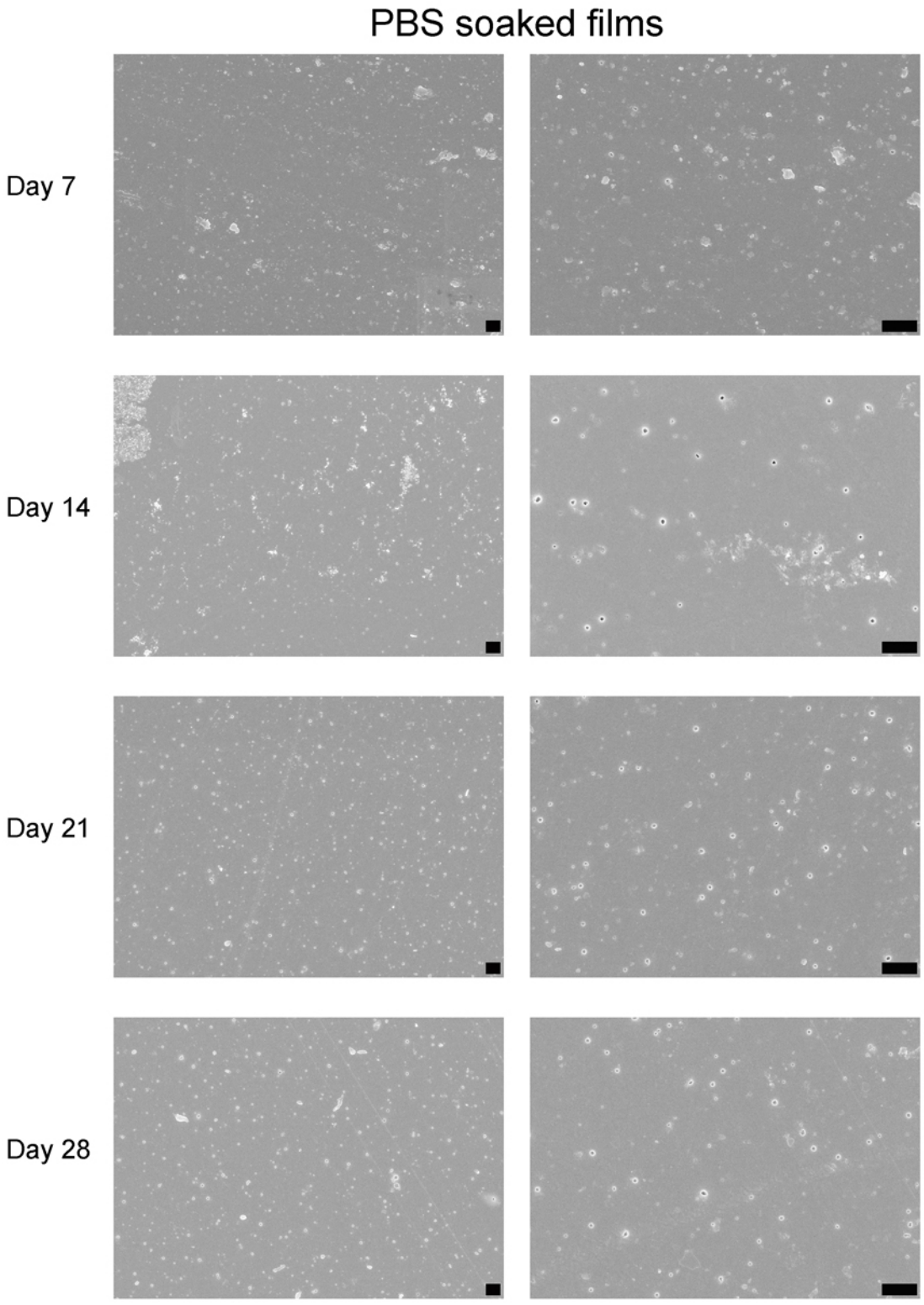


Figure 4.12: Scanning electron microscope photographs of films soaked for 7, 14, 21, and 28 days in PBS at 37°C. Scale bars = 1 μm.

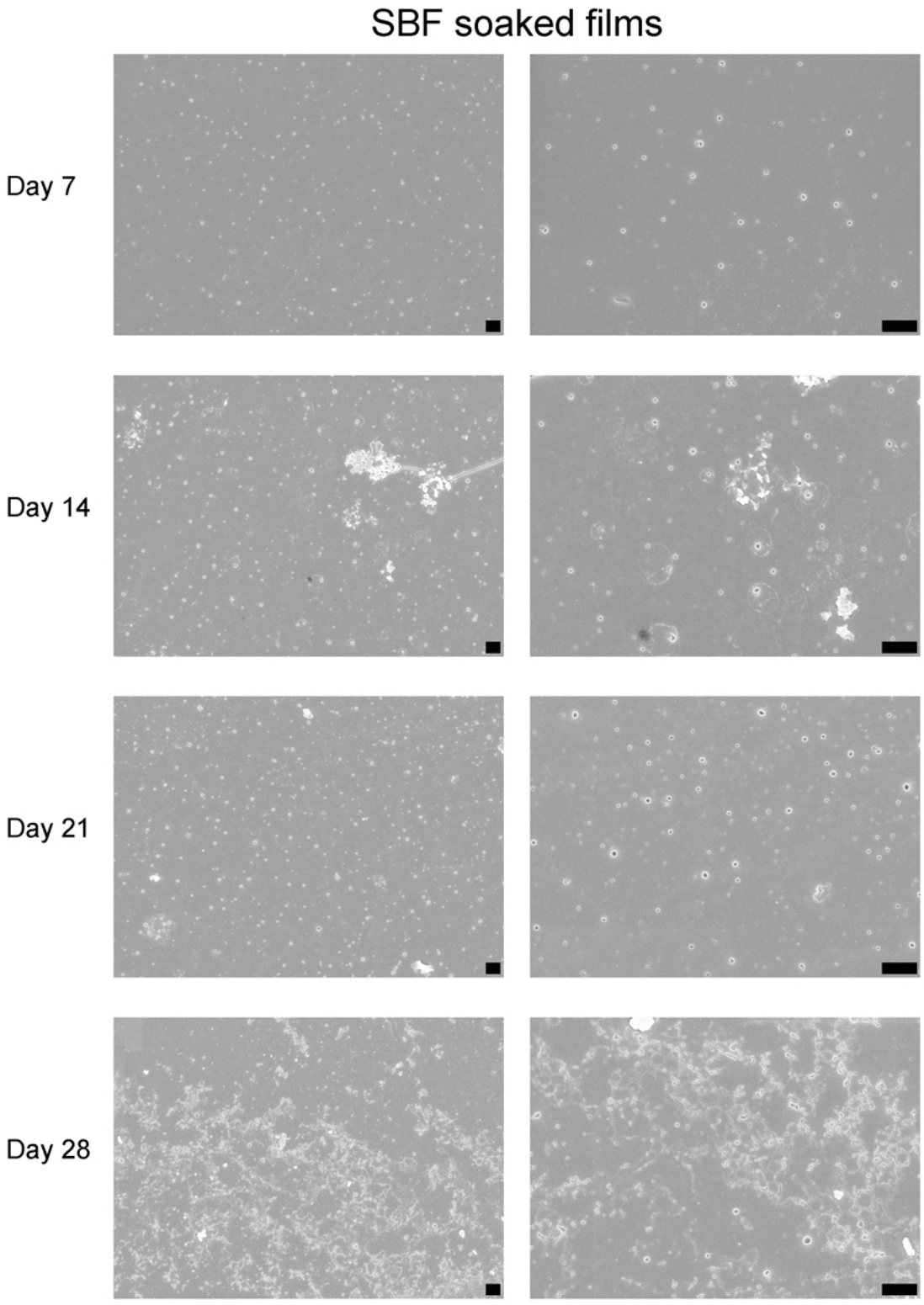


Figure 4.13: Scanning electron microscope photographs of films soaked for 7, 14, 21, and 28 days in SBF at 37°C. Scale bars = 1 μm.

Since their FDA approval, the dissolution of biodegradable polyesters has been well documented over the decades. Depending on the polymer backbone, these polymers can

take anywhere from days up to 2 years to dissolve in the body. In 28 days, no side chain hydrolysis of benzyl-esterified γ-PGA could be detected using UV-Vis and ^{1}H-NMR, indicating this polymer is likely to maintain the same level of water resistance. This is encouraging for tissue engineering applications as this polymer resists dissolution and should still be mainly enzymatically degraded like the native starting polymer.

4.4 Conclusions

All esterified γ-PGA films passed the ISO 10993:5 test, indicating they are non-cytotoxic. Human fibroblast cells were supported on all polymer types and viable for up to seven days. Fibroblasts cultured on γ-PGA-Bn films showed cytoskeletal organisation including stress fibres and focal adhesions, indicating they adhered well to the films. Soaked films of γ-PGA-Bn significantly lost 3-4% mass in 28 days, independent of soaking media. Opacity of all films increased slightly and submicron surface holes were detected after seven days using SEM. These surface defects appeared more prominent in salt containing soaking medias (PBS and SBF), with widespread surface changes visible on SBF soaked films at 28 days. This change was undetectable using UV-Vis, indicating less than 1 mM BnOH was released, and any change in esterification level was indistinguishable by ^{1}H-NMR. Therefore, as expected, the majority of γ-PGA-Bn degradation should be enzymatic and fair, ideal degradation testing is reliant on future *in vivo* studies.

It would be advantageous to have a larger amount of synthesised product to perform more extensive mechanical characterisation, as well as cellular differentiation studies using stem cells. To do so, the synthesis must be scaled up, which is the focus of the next chapter.

Chapter 5

Enhancing mechanical properties of esterified γ-PGA polymers using tensile deformation

5.1 Introduction

For regenerative medicine applications, γ-PGA was esterified as described in the previous chapter to increase the water resistance of the polymer and make it a suitable candidate for scaffold fabrication. Designing products with appropriate mechanical properties presents a challenge for tissue engineers as these properties vary depending on the target replacement tissue (shown in Figure 1.5). Therefore, due to natural variation between patients, the ability to tailor scaffold properties may offer a wider market for customised medical product commercialisation.

One widely used technique to enhance mechanical properties of polymeric materials is tensile deformation. This method utilises mobility within amorphous regions of semicrystalline polymer chains, when above the glass transition temperature and in Van der Waals bonded crystalline entities, subjecting them to a uniaxial tensile force, inducing orientation in the direction of tension. Tensile deformation relies on a phenomenon known as cold drawing, pioneered by Carothers and Hill in 1932, whose work led them to propose orientation was "probably necessary for great strength and pliability."[176] Since then, the polymer industry has investigated and refined making ultra-high strength fibres and films by orienting polymer chains and inducing macromolecular order for various applications. For instance, fibres made from ultra-high molecular weight polyethylene, nowadays are produced with a Young's modulus of over 100 GPa,[148] allowing adaptation for numerous applications ranging from bullet-proof vests to high-performance surgical sutures.

This chapter focuses on mechanical properties of the γ-PGA polymers, as produced in Chapter 2, and exploring how to tailor these properties for appropriate tissue engineering applications. Very recently, de Oca *et al.* performed degradation studies on highly

oriented poly(glycolic acid) fibres they produced using the above-referred tensile deformation process to investigate the effect on mechanical properties.[177] When included in a copolymer, this biodegradable polyester could be highly oriented, yielding Young's moduli of over 20 GPa.[178,179] This work represents the first time mechanical potential of enzymatically degradable polymers is investigated in this manner, as well as the first time modified γ-PGA is tailored using tensile deformation.

As discussed in sections 2.3.5 and 2.3.6, esterification decreased the water resistance while the polymer thermal processing window between the glass transition temperature and the onset of 5% degradation beneficially increased. Unfortunately, however, the discovery of thermal degradation upon the onset of melting precludes traditional polymer processing from the melt. Therefore, in order to orient these modified γ-PGA polymers, solution-processing techniques, followed by tensile deformation, were employed to produce oriented, esterified γ-PGA polymers.

As discussed in the previous chapter, esterification of γ-PGA yielded limited quantities of material with large batch inconsistency. This variability, seen in degree of esterification, thermal properties, and notably, weight average molecular weight (M_w), is well known to have a significant effect on orientation potential, and thus maximal achievable mechanical properties.[180,181]

It is anticipated that separate synthesis batches will display differing mechanical properties. In order to limit these variables, the results presented here are obtained with a single synthesised batch of each modification, using the method described in Chapter 2.

5.2 Experimental

5.2.1 Materials

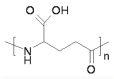
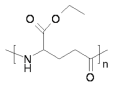
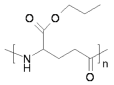
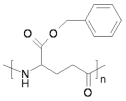
Esterified γ-PGA polymers were used as synthesised (γ-PGA Na^+ salt purchased as before) according to Chapter 2 and are characterised in Section 5.1. Perfluorotrichlorosilane was purchased and used as received from ABCR (Karlsruhe, Germany). Unless indicated otherwise, all other reagents and solvents were purchased from Sigma-Aldrich and used as received.

5.2.2 Sample preparation

Esterified γ-PGA samples were dissolved at room temperature in HFIP (2% wt wt^{-1}) subsequently poured into the fluorinated glass petri dishes, covered and the solvent was allowed to evaporate at RT for 48 h, followed by 24 h under vacuum at 60°C to remove any remaining solvent. γ-PGA-H was dissolved in diH_2O (2% wt wt^{-1}), allowed to evaporate at RT for 96 h, and then placed under vacuum to prevent rehydration. Sample concentrations were calculated to produce films approximately 100 μm thick.

N.B. For convenient removal of solution cast films, glass petri dishes (r = 3.5 cm)

Table 5.1: Structure and properties of polymers used in this work as produced in Chapter 2. Glass transition temperature, $\mathbf{T_g}$, and melting temperature, $\mathbf{T_m}$, of native powder were determined by differential scanning calorimetry; average molecular weight, $\mathbf{M_w}$, calculated from size-exclusion chromatography.

Chemical structure	Polymer	T_g /°C	T_m /°C	M_w /g mol^{-1}
	γ-PGA -H[1]	124	240[2]	4.89x10^5
	γ-PGA -Et	66	260	2.75x10^5
	γ-PGA -Pr	40	228	1.97x10^5
	γ-PGA -Bn	40	226[3]	3.22x10^5

[1]SEC performed under different conditions than esterified γ-PGA s (refer to Chapter 2.2.2)
[2]Degradation detected in TGA prior to melting
[3]Double endotherm, second peak at 240°C

were treated with a fresh Piranha solution of 70/30 sulphuric acid/hydrogen peroxide for 1 h and subsequently washed with excess water. The petri dishes were then placed in a dessicator with a few drops of perfluorotrichlorosilane, evacuated to 20 mbar, left under vacuum to fluorinate overnight, and annealed at 100°C for one h in vacuum.

5.2.3 Room temperature tensile testing and tensile deformation

Initial mechanical testing of as-cast, dried films was performed at room temperature with an Instron Tensile Tester Model 5864 (Norwood, USA) with hydraulic clamps (5 bar) at a cross-head speed of 2 mm min^{-1}. Dumbbell shaped strips of 1.2 mm width and 4.5 mm gauge length were cut from the dried films.

In a second series of experiments, tensile deformation of the dried esterified γ-PGA films was performed above their respective T_g, using a using an Instron Tensile Tester (Model 5864) fitted with an environmental chamber (Model EC43) at a cross-head speed of 2 mm min^{-1}. Dumbbell shaped strips were cut as for RT testing; ink marks were printed at 1 mm intervals prior to drawing to determine draw ratios (λ = final/initial length) from their displacement. γ-PGA-Et and γ-PGA-Pr samples were drawn at 125°C while γ-PGA-Bn samples were drawn at 115°C, as maximum draw ratios (λ_{max}) were achieved at these respective temperatures.

5.3 Analysis

5.3.1 Mechanical testing

Following tensile deformation above T_g and determination of the draw ratios from the ink mark displacements, samples were then cut and glued using Al-Fix glue (Novatio; Olen, Belgium) between card frames (separation distance = 10 mm), and allowed to dry for 2 h under 200 g weights to ensure a strong bond. Sample width was measured using an optical microscope, while thickness was determined using a micrometer. Mechanical testing of the different samples was then performed at RT using hydraulic clamps as above, at a cross-head speed of 5 mm min^{-1}.

5.3.2 Optical microscopy

Optical microscopy was carried out with a Leica DMRX polarising microscope equipped with a Leica DFC 480 Camera (both Wetzlar, Germany).

5.3.3 Wide-angle x-ray scattering (WAXS)

WAXS experiments were performed by Y. Odarchenko and Dr. D. Ivanov (Institut de Sciences des Materiaux de Mulhouse, UHA Mulhouse) on the BM26 beamline of the ESRF (Grenoble, France) using a Frelon detector positioned at approximately 6 cm from the sample. This sample-to-detector distance allowed recording of the signals in the s-range ($s = 2 \sin \theta/\lambda$, where θ is the Bragg angle) from 0.03 to 0.52 $Å^{-1}$ using the wavelength of 1.04 Å. Additional measurements were carried out on a custom-build SAXS/WAXS machine (Molecular Metrology) coupled to a Rigaku MicroMax-007HF rotating anode generator. The 2D WAXS data were collected in vacuum using Fuji image plates with the pixel size of 100 x 100 μm^2. The modulus of the scattering vector was calibrated using diffraction orders of silver behenate in both setups. The measurements were performed in transmission mode on the oriented samples (films with a thickness in the range 0.1-0.3 mm).

5.3.4 Polarised Raman spectroscopy

Raman measurements were performed by Y. Odarchenko and Dr. D. Ivanov (Institut de Sciences des Materiaux de Mulhouse, UHA Mulhouse), and carried out on a confocal Raman microspectrometer Labram-BX 40. The 632.81 nm excitation polarised light from a HeNe laser light source was focused through a 50 x/0.95 objective (Olympus; Japan) onto flat oriented films fixed in a holder specially designed to eliminate the signal from the substrate. The laser power was 5 mW. The device calibration was conducted using the Si peak at 520 cm^{-1}. A single spectrum was recorded after integration of 50 measurements.

The direction of polymer chain orientation was parallel to the X direction of the incident beam. The polarisation direction of the incident beam was rotated with the help of a

λ/2 plate by 90° (Y direction). In total, four Raman spectra were acquired with polarisation geometries X|X, X|Y, Y|X and Y|Y, using the notation incident polarisation|emitted polarisation as shown in Figure 5.1.

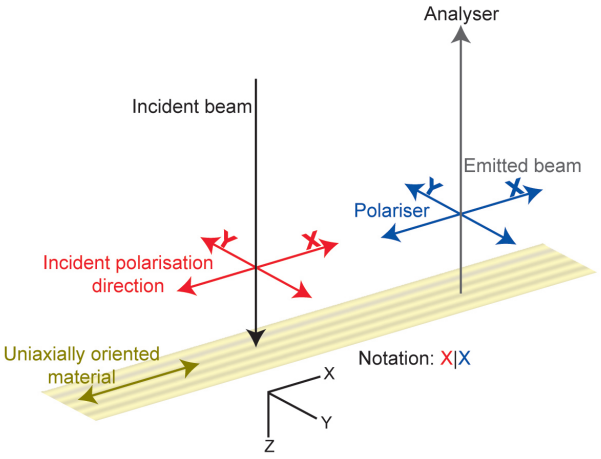


Figure 5.1: Coordinate system used for recording of the polarised Raman spectra of the glutamate films. The incident beam is polarised in the X-direction or Y-direction.

5.3.5 Thermal analysis

Polymer films were characterised in the same manner as synthesised powders in Section 2.2.2. Drawn samples were tightly rolled and the rolls were flattened to maintain alignment throughout DSC analysis until complete melting occurred.

5.4 Results and discussion

5.4.1 Room temperature tensile properties of as-cast films

Initial tensile tests were performed at RT to determine mechanical characteristics of the isotropic, as-cast, dried films, both of the native γ-PGA-H and its esterified forms. Typical stress-strain curves recorded for the polymers are presented in Figures 5.2 and 5.3, while their corresponding mechanical properties, Young's modulus E, yield stress σ_y, tensile strength σ, and strain at break ϵ, are presented in Table 5.2.

As expected, due to hydrogen bonding between carboxylic groups, the native γ-PGA-H films were found to be brittle when tested at room temperature (Figure 5.2 and Table 5.2). As shown in the nominal stress-strain plots in Figure 5.3, esterification of the γ-PGA-H side chain resulted in highly enhanced ductility, as seen in a dramatic increase in the strain at break of as much as 50, 150, and 250 times that of γ-PGA-H in γ-PGA-Bn, γ-PGA-Pr, and γ-PGA-Et, respectively (Figure 5.3). As expected, however, this highly beneficial enhancement was accompanied by a decrease in values of the stiffness E, and of the yield- and tensile strength (Table 5.2).

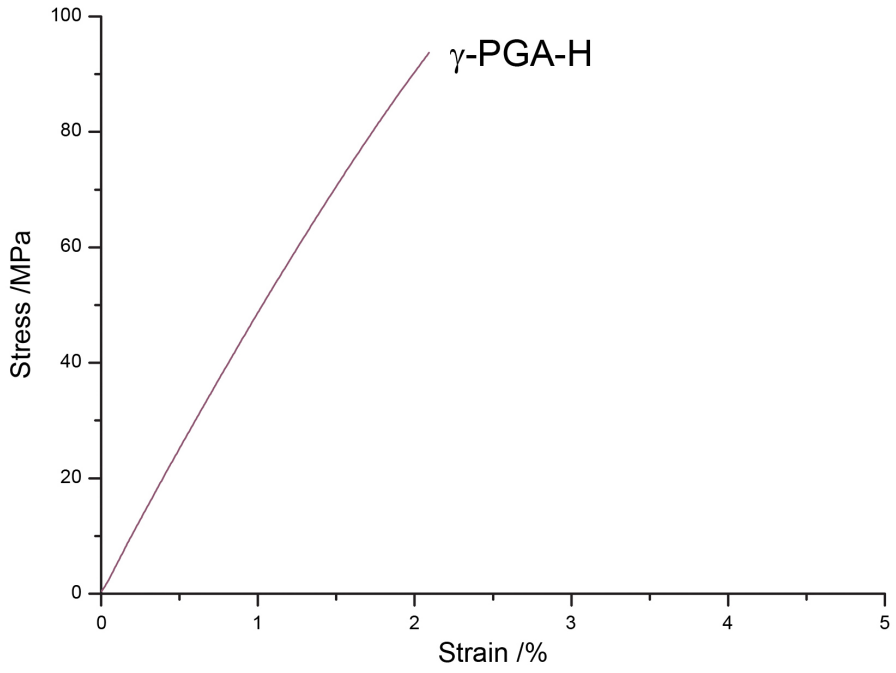


Figure 5.2: Typical nominal stress/strain curve recorded at room temperature for the native γ-PGA-H films.

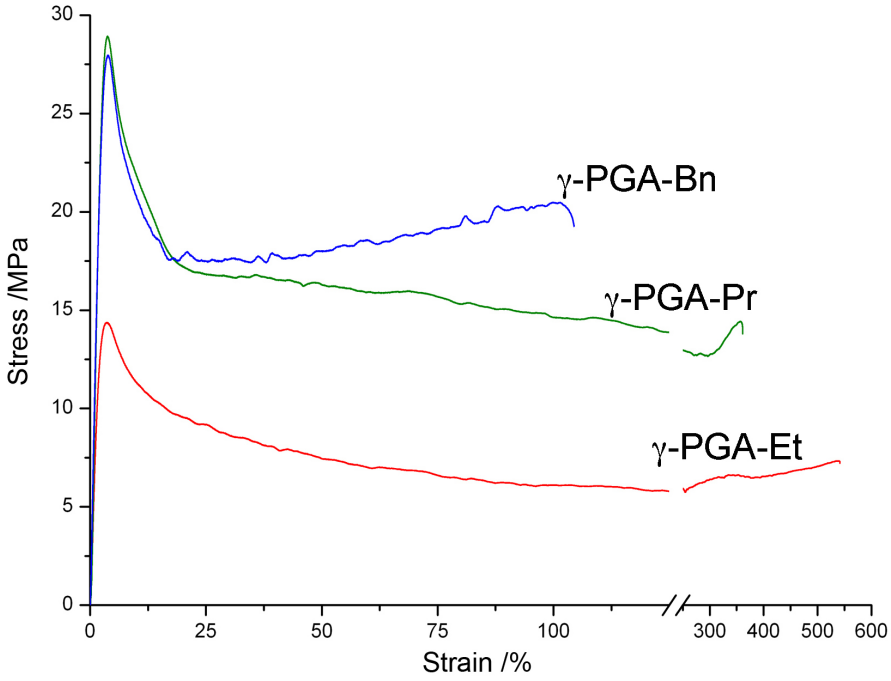


Figure 5.3: Nominal stress/strain curves recorded at room temperature for esterified γ-PGA films.

Table 5.2: Mechanical characteristics at room temperature of differently esterified γ-PGA films tested at room temperature.

Polymer	**E/ GPa**	**σ_y/ MPa**	**σ/ MPa**	**ϵ/ %**
γ-PGA-H	4.99	-	94	2
γ-PGA-Et	0.85	14.7	7.33	542
γ-PGA-Pr	1.37	29.2	14.4	361
γ-PGA-Bn	1.24	28.1	20.3	106

5.4.2 Tensile deformation

As a first step, stress-strain curves were recorded in the temperature range from RT-T_m in order to establish the maximum draw ratio ($\lambda_{max} = \epsilon/100 + 1$) for subsequent tensile deformation experiments. It was found that all modified films could be drawn to remarkably high draw ratios, generally above $\lambda \geq 10$ at the optimum temperature (125°C for both γ-PGA-Et and γ-PGA-Pr, and 115°C for γ-PGA-Bn). Above these temperatures, λ_{max} rapidly reduced due to excessive macromolecular mobility, as is commonly observed for weakly interacting polymers, such as polyethylene[148,182]. It was found that γ-PGA-H film could not be drawn to appreciable draw ratios; this is likely due to a high T_g and the limited temperature window between T_g and the onset of degradation, caused by hydrogen bonds between the chains.

5.4.3 Mechanical properties of drawn films

The different esterified γ-PGA films were drawn at their optimum deformation temperatures to various draw ratios and subsequently subjected to tests at room temperature to determine their mechanical properties. Polymer films were drawn to $\lambda \leq 10$ to produce a comparable set of results between the polymers with different side chains. Nominal stress-strain curves of these drawn films are presented in Figures 5.4, 5.5, and 5.6 for γ-PGA-Et, γ-PGA-Pr, and γ-PGA Bn, respectively. In all cases, the draw ratio was measured from initial ink mark displacement as indicated in these graphs. Common to all esterified polymer samples, both Young's modulus and tensile strength rapidly increased with increasing draw ratio, while the strain at break decreased, as is commonly observed for oriented polymers.

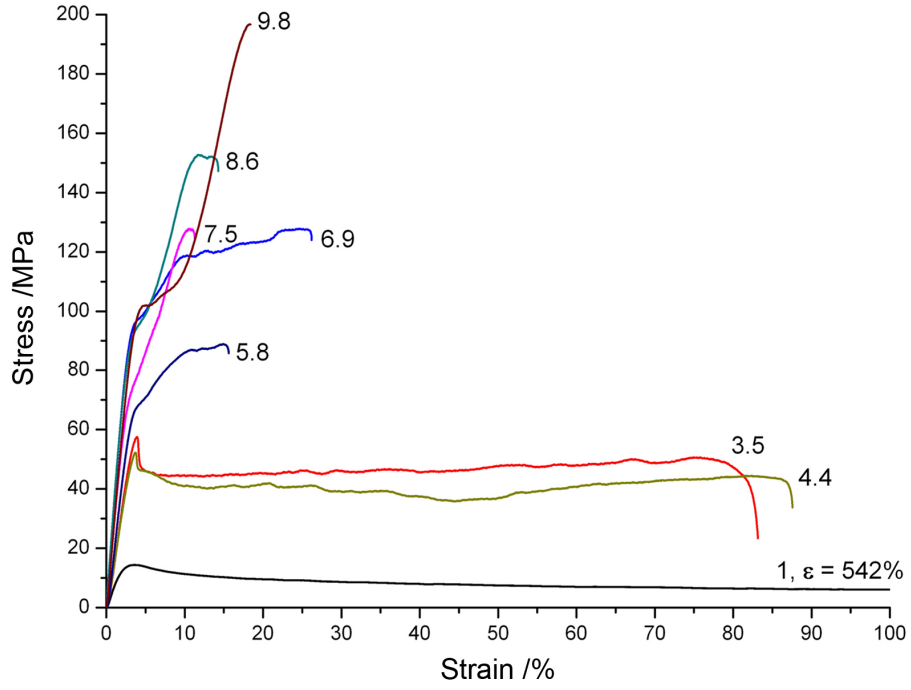


Figure 5.4: Nominal stress/strain curves recorded at RT of drawn γ-PGA-Et films drawn at 125°C. Draw ratios are indicated in the figure.

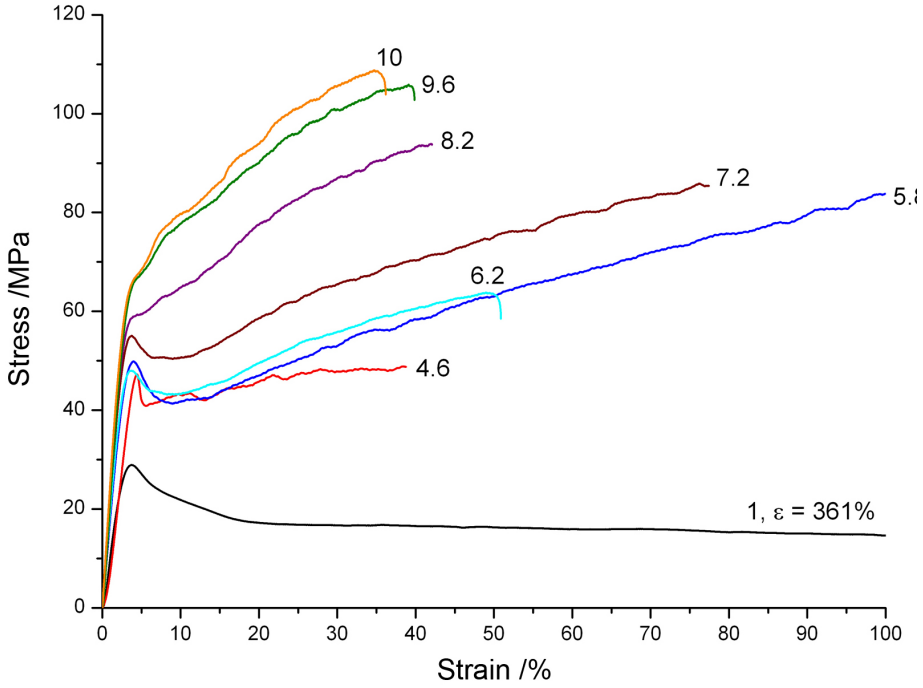


Figure 5.5: Nominal stress/strain curves recorded at RT of drawn γ-PGA-Pr films drawn at 125°C. Draw ratios are indicated in the figure.

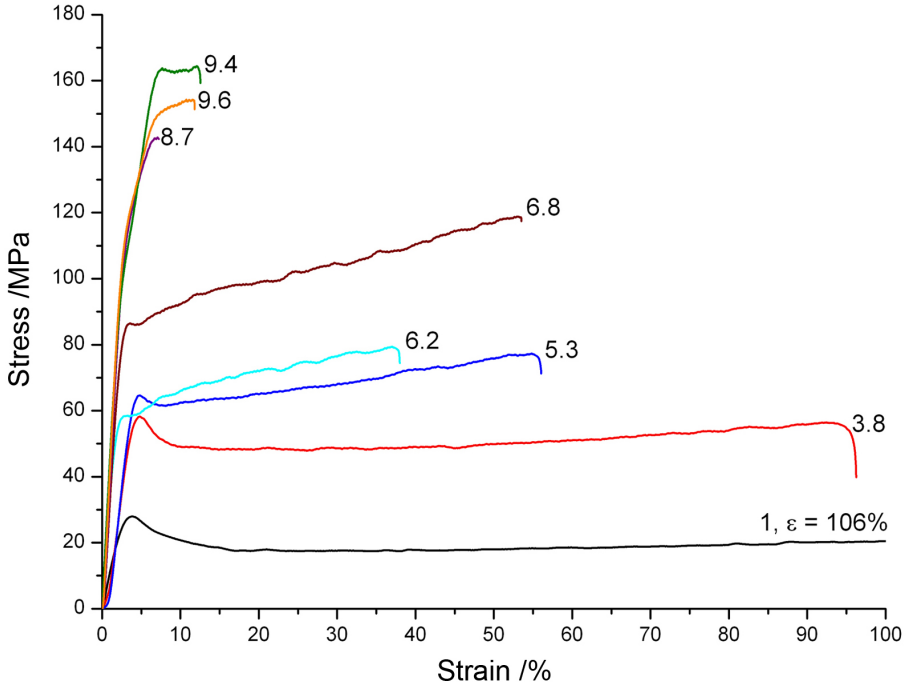


Figure 5.6: Nominal stress/strain curves recorded at RT of drawn γ-PGA-Bn films drawn at 115°C. Draw ratios are indicated in the figure.

These characteristic trends are more quantitatively shown in Figure 5.7, in which the values of E, σ, and ϵ are plotted as a function of the draw ratio, λ, for all three γ-PGA films. These plots display the positive relationship between λ and E, as well as the negative

development of ϵ with λ. These consistent correlations are indicative of increased polymer chain orientation in the tensile direction, as discussed in later sections of this chapter. Maximum values of the mechanical characteristics of the drawn films produced in this study, compared to those of the as-cast polymers, are presented in Table 5.3.

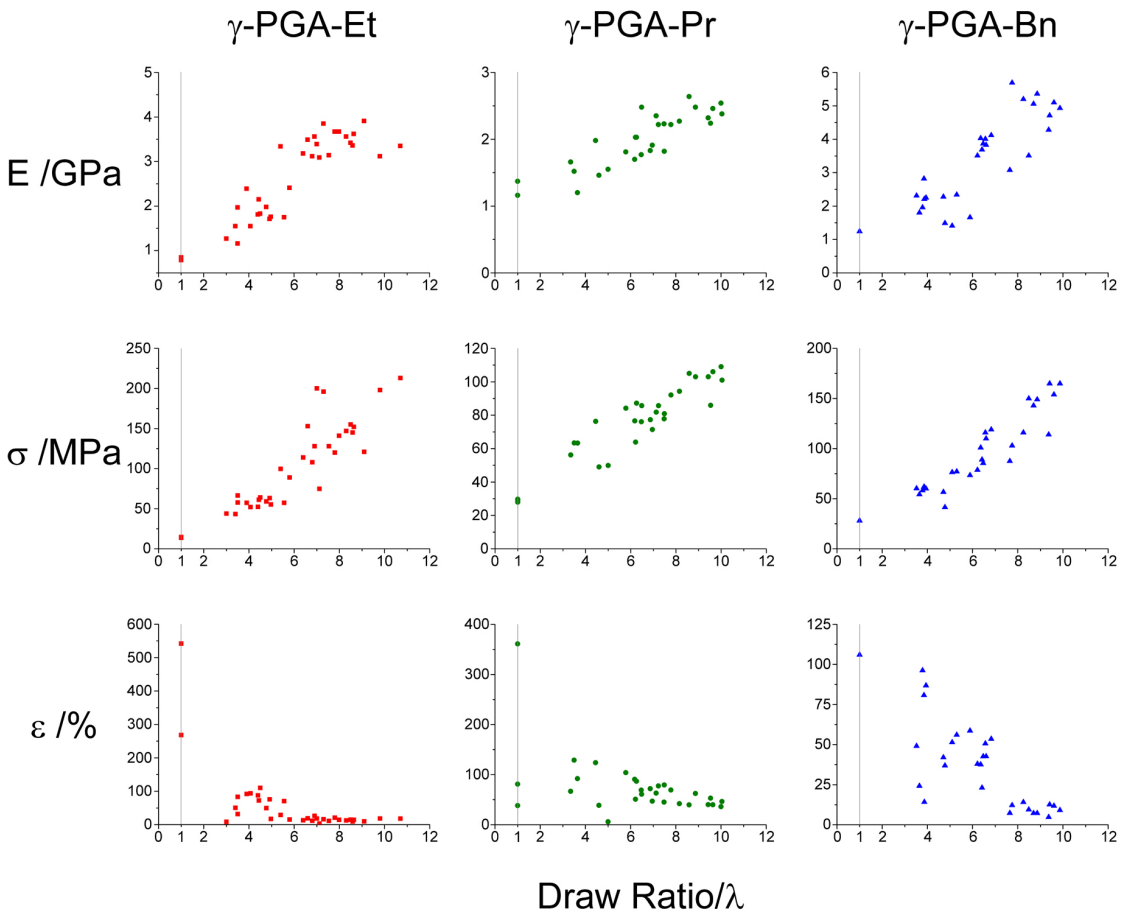


Figure 5.7: Influence of tensile deformation on Young's modulus, E, tensile strength, σ, and strain at break, ϵ, at RT for all polymers studied.

From this data presented it can be concluded that by drawing to λ = 10, the modulus of γ-PGA-Et increased by a factor of about 4.5 and the tensile strength improved by over a factor of 13. Benzyl esterified γ-PGA offered the highest modulus, with a 4.3 fold increase to 5.36 GPa. The maximum tensile strength achieved with γ-PGA-Bn was found to be 149 MPa, a dramatic increase of more than 5-fold, but still inferior to that of γ-PGA-Et. Drawing γ-PGA-Pr resulted in a nearly double value of its modulus and tripled the tensile strength, with only a 10-fold decrease in strain at break.

Table 5.3: Mechanical properties of esterified γ-PGA films as-cast and maximum properties achieved by drawing to λ = 10.

Polymer	Film	E/ GPa	σ/ MPa	ϵ/ %
γ-PGA-Et	As-cast	0.85	14.7	542
	Drawn	3.85	196	16.1
γ-PGA-Pr	As-cast	1.37	29.2	360
	Drawn	2.54	109	36
γ-PGA-Bn	As-cast	1.24	28.1	106
	Drawn	5.36	149	7.3

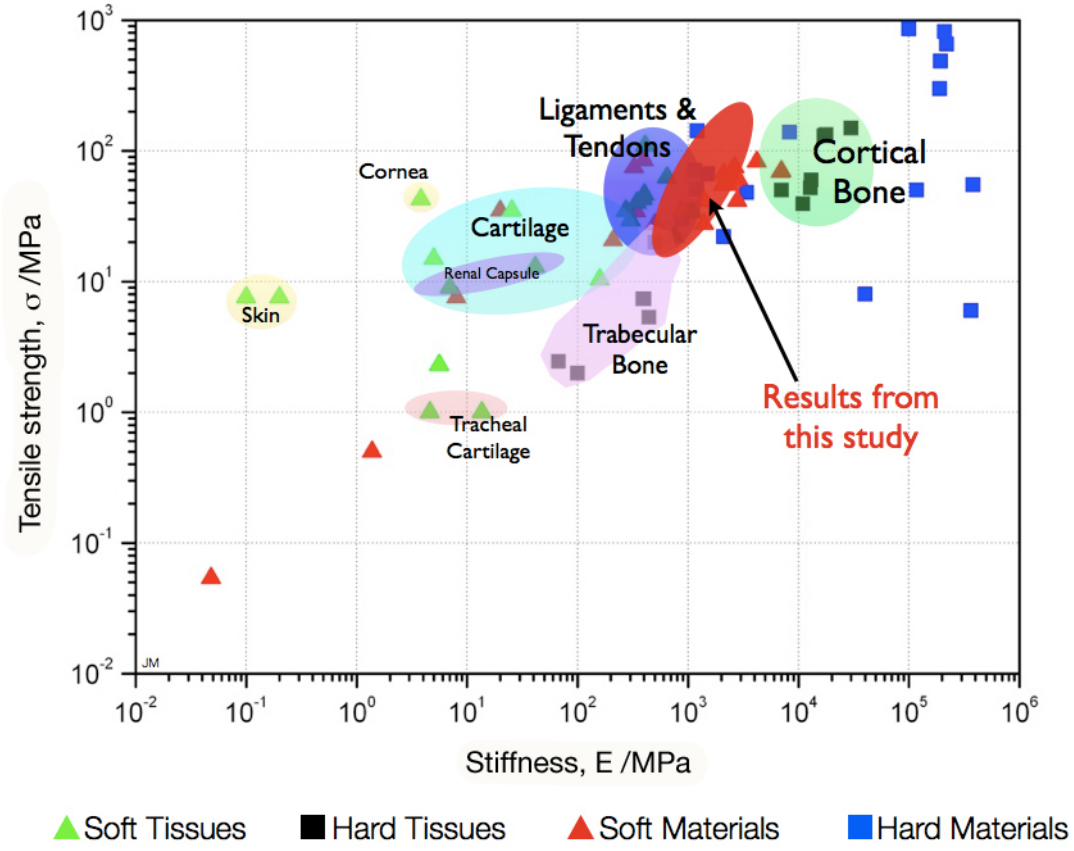


Figure 5.8: Tensile strength vs. stiffness of the present polymer series compared with human tissues in the Ashby style plot presented earlier (Section 1.2.2).

In accord with results obtained with common polymers by using tensile deformation, the above results clearly indicate that the mechanical properties were greatly enhanced for all γ-PGA films. Most importantly, properties achieved approached similar values to those of soft human tissues (cf. Figure 5.8); yet their strain at break remained at or above a physiologically relevant 7%.

An interesting phenomenon was discovered upon retesting drawn polymer samples again at room temperature. At draw ratios approximately λ > 5, a double yield point in the stress-strain curves was observed upon retest for all three polymer species. This

double yield point could be indicative of an α-helix conformation of the macromolecules, as will be discussed in the section on wide-angle X-ray scattering analysis.

5.4.4 Estimated theoretical chain stiffness

As previously reported, it is possible to estimate the theoretical maximum stiffness of a single chain, or perfectly ordered, uniaxially arranged crystal, from the development of the Young's modulus with draw ratio of flexible chain molecules.[183] That maximum value of E, can be estimated according to the following relation, in its simplified form (Equation 5.1[183]) for $\lambda \geq 5$ reads:

$$E = [E_h^{-1} + (E_u^{-1} - E_h^{-1})(\frac{3\pi}{4})\lambda^{-3/2}]^{-1} \tag{5.1}$$

where E_h is the theoretical maximum Young's modulus and E_u that of perfectly isotropic material - in the theory denoted as referring to those of "helix" and "coil" segments. Employing the data present in Figure 5.7, the following estimates for E_h were obtained (Table 5.4). Also indicated in this table are the standard error and correlation of the calculations.

Table 5.4: Calculated theoretical moduli for esterified γ-PGA films using Equation 5.1.

Modulus	**γ-PGA-Et**	**R^2**	**γ-PGA-Pr**	**R^2**	**γ-PGA-Bn**	**R^2**
E_u /GPa	0.85	-	1.37	-	1.24	-
E_h /GPa	4.64 ± 0.46	0.766	2.52 ± 0.29	-0.175	5.26 ± 0.61	0.624
E_{uc} /GPa	0.5 ± 0.09	0.869	0.51 ± 0.19	0.137	0.4 ± 0.06	0.692
E_{hc} /GPa	7.2 ± 1.74	0.869	3.5 ± 0.79	0.137	12.56 ± 4.52	0.692

In the approach of Irvine and Smith,[183] a uniform distribution of stress in the helix and coil elements was assumed. In the table above, the measured "unoriented" modulus, E_u, and a calculated, perfectly unoriented modulus E_{uc} with the corresponding E_{hc} are also presented. Unfortunately, due to the nature of solution casting, γ-PGA films may have some orientation in the direction of tension, and the experimental value of E_u could introduce error in the calculations. Accordingly, all calculations for E_h were performed also employing E_{uc}, as determined by fitting both E_{uc} and E_h. Furthermore, inclusions of impurities from the chemical synthesis and purification steps in the films resulted in scatter of the data as shown in Figure 5.7. Thus, justifiably, only the maximum values achieved at the various draw ratios were used, as these are closest to the true values achievable for an optimal material.

Reviewing the above results, it is not surprising that the ethyl-modification featured a higher value of E_h than its propyl counterpart. Somewhat surprising, however, the most bulky substituent, benzyl, appears to be the highest value for the γ-PGA.

5.4.5 Structural characteristics

Polarised optical microscopy

Polarised optical microscopy was employed to investigate the increase in macromolecular orientation in the drawn polymer samples. Figure 5.9 shows two tapes overlaid at ~90° of all esterified polymers, oriented to $\lambda \geq 10$, under cross-polarised light. Orientation was observed with a maximum light intensity at ±45° to the polarisers, while no light was observed through the samples at 0° and 90°, indeed indicative of a high degree of uniaxial macromolecular order in the various tapes. The addition of a quarter wavelength retardation plate, displays both a subtractive (yellow) and additive (blue) effect through the oriented samples.

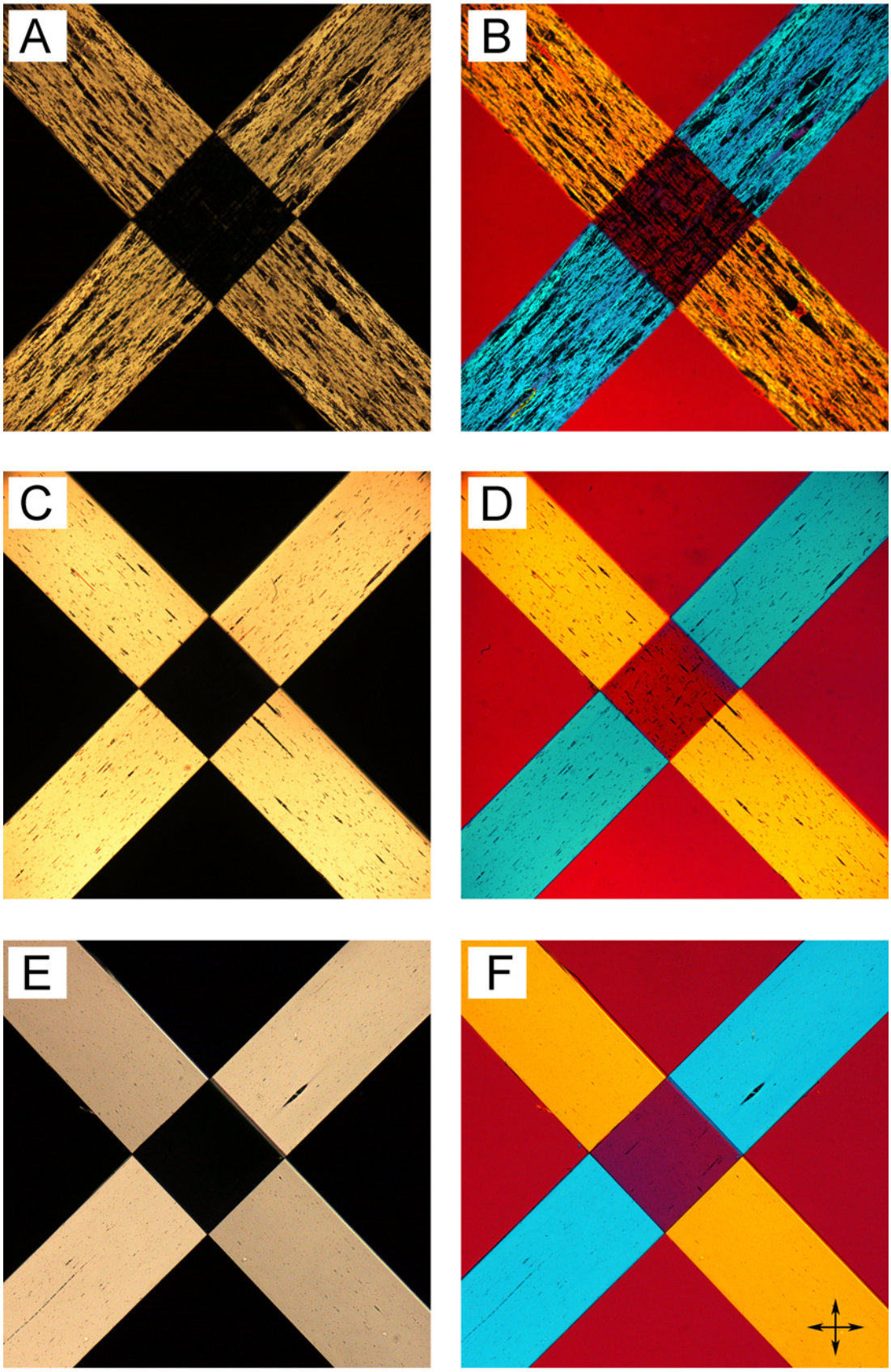


Figure 5.9: Polarised optical microscopy images of overlayed, 10 times drawn polymer films γ-PGA-Et (A,B) γ-PGA-Pr (C,D), and γ-PGA-Bn (E,F). Orientation is seen using both normal polarized light (A,C,E) and with the use of a quarter wavelength retardation plate (B,D,F).

Wide-angle x-ray scattering

Structural features of the drawn films, and in particular the macromolecular orientation therein were also investigated by means of wide-angle x-ray scattering (WAXS). A typical diffraction pattern of a γ-PGA Et film drawn at 115°C to λ = 9, and annealed at 145°C for 5 min to further promote molecular order, is presented in Figure 5.10. Clearly, the pattern is indicative of a high degree of uniaxial orientation of the polymer in the direction of deformation.

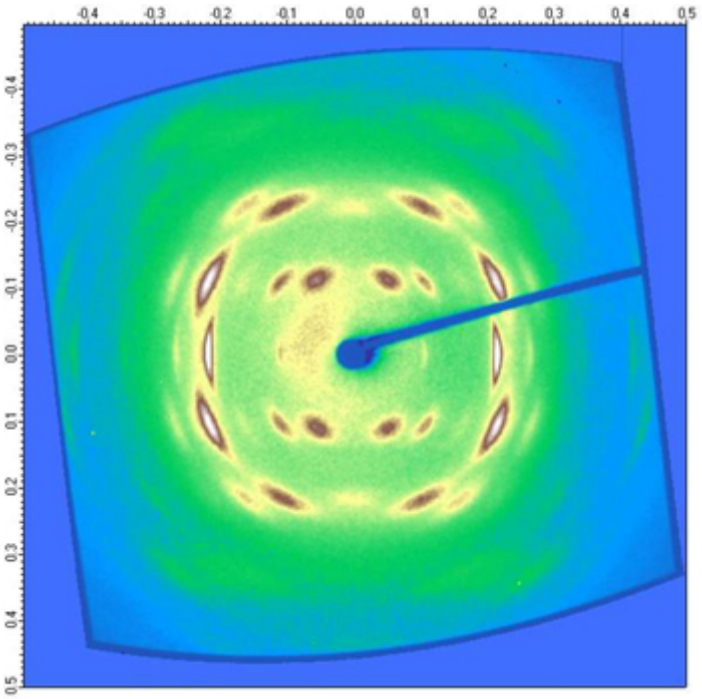


Figure 5.10: Wide-angle x-ray scattering of γ-PGA-Et film, λ = 9, drawn at 115°C and annealed at 145°C for 5 min, drawing direction vertical.

The WAXS data were employed to determine the crystal lattice parameters of γ-PGA-Et, which was found to be orthorhombic (see Table 5.5). The crystal density was calculated to be ρ_{cal} = 1.36 g cm^{-3}, which is in modest agreement with the density of 1.25 g cm^{-3} measured in KI water solution.

Table 5.5: Calculated WAXS lattice parameters from Figure 5.10 for γ-PGA-Et, oriented to λ = 9.

Layer line	**hkl**	**d_{exp}/ Å**	**d_{calc}/ Å**	**Intensity**
l=0	200	9.24	9.2	w
	010/400	4.61	4.55	vs
	210	3.76	4.08	w
	600/510	2.89	3.07	vw
	800	2.38	2.28	w
l=1	101	8.1	8.18	s
	201	6.59	6.48	s
	301	5.1	5.09	w
	011/401	4.17	4.07	vs
	311/501	3.49	3.39	w
	801	2.22	2.23	vw
l=2	002	4.55	4.57	w
	202	4.12	4.09	s
	302	3.67	3.66	w
	412	2.7	2.64	vw
l=3	303	2.72	2.73	vw
	403	2.58	2.54	vw
	503	2.37	2.35	vw
Lattice parameters				
Orthorhombic; $P2_122_1$; for (h00) and (00l) h,l=2n				
a=18.40 Å, b=4.55 Å, c=9.13 Å				

The WAXS pattern of γ-PGA-Pr was found to be similar to that of γ-PGA-Et, except that it featured better resolved diffraction peaks, which is attributed to the higher draw ration of the films (Figure 5.11). Also, in the of γ-PGA-Et pattern the (010) and (400) peaks overlap. Hence, the diffraction diagram of γ-PGA-Pr, where these peaks can be distinguished, was examined first (Table 5.6).

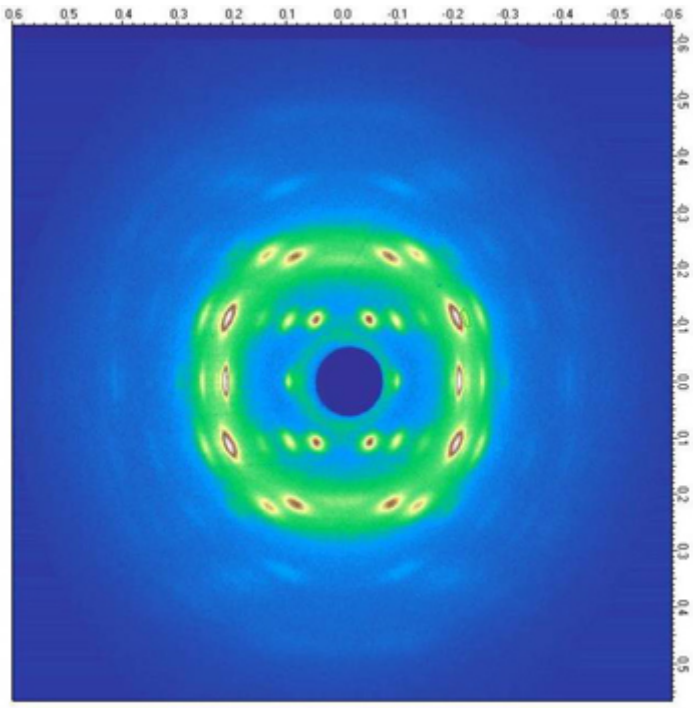


Figure 5.11: Wide-angle x-ray scattering of γ-PGA-Pr film, λ = 13, drawn at 120°C and annealed at 145°C for 5 min, drawing direction vertical.

The meridional peak appears on the second layer line, which could indicate a 2/1 helical conformation with a subunit parameter of 4.66 Å, or the *c*-parameter of 9.23 Å. The observed peak is relatively weak. To examine the possible meridional peaks of higher order, the fiber was tilted by 20°. In this case, only the second order of 002 reflection, or 004 peak were observed.

The *a*-parameter was calculated from the smallest equatorial projection of the reflection on the 1st layer line ($a \sim 20$ Å). The obtained value is bigger than 14.5 Å, corresponding to the fully extended lateral ester groups pointed in opposite directions. This means that there is more than one chain in the *a*-direction. The *b*-parameter was computed from the position of the first strong equatorial peak, which is not an order of (100). If one assumes that the orthorhombic unit cell of the compound consists of 4 monomer units, the calculated crystal density is ρ_{cal}=1.29 g cm^{-3}. This is in reasonable agreement with the observed density of 1.23 g cm^{-3}, determined for a semicrystalline sample in an aqueous KI solution.

As far as the molecular conformation within the unit cell is concerned, it is tentatively concluded that it consists of layers stabilised by intermolecular hydrogen bonds.

Table 5.6: Calculated WAXS lattice parameters from Figure 5.11 for γ-PGA-Pr, oriented to λ = 13.

Layer line	**hkl**	**d_{exp}/ Å**	**d_{calc}/ Å**	**Intensity**
l=0	200	10.04	10.04	s
	400	4.99	5.02	w
	010	4.69	4.76	vs
	210	4.36	4.3	w
	310	3.89	3.88	s
	600	3.34	3.35	w
	020	2.4	2.38	vw
l=1	101	8.36	8.39	s
	201	6.88	6.79	s
	301	5.43	5.42	m
	011	4.22	4.23	vs
	311	3.61	3.68	m
	701	2.73	2.74	vw
l=2	002	4.66	4.62	m
	202	4.23	4.19	s
	302	3.79	3.8	s
	012	3.35	3.31	w
	412	2.76	2.76	vw
	612	2.36	2.35	vw
l=3	303	2.8	2.8	w
	403	2.6	2.62	vw
	503	2.45	2.44	vw
l=4	004	2.12	2.31	vw
Lattice parameters				
Orthorhombic; $P2_122_1$; for (h00) and (00l) h,l=2n				
a=20.07 Å, b=4.76 Å, c=9.23 Å				

The corresponding WAXS pattern and calculated lattice parameters for γ-PGA-Bn, oriented to λ = 13.5 are presented in Figure 5.12 and Table 5.7, respectively.

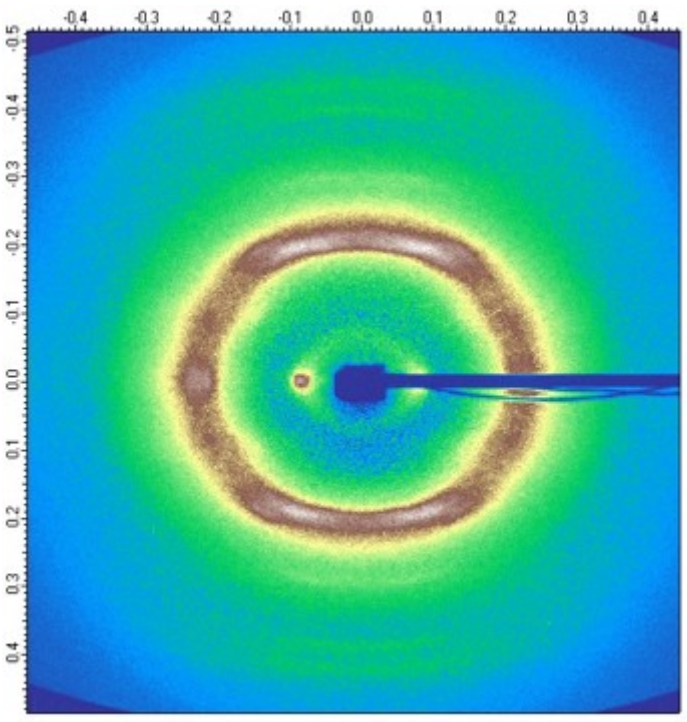


Figure 5.12: Wide-angle x-ray scattering of γ-PGA-Bn film, λ = 13.5, drawn at 115°C .

Table 5.7: Calculated WAXS lattice parameters from Figure 5.12 for γ-PGA-Bn, oriented to λ = 13.5.

Layer line	**hkl**	**d_{exp}/ Å**	**d_{calc}/ Å**	**Intensity**
l=0	200	12.17	12.04	s
	010	4.63	4.58	w
	210	4.21	4.28	w
l=1	401	5.77	6.26	vw
	501	4.38	4.34	vw
l=2	202	4.73	4.57	s
	302	4.3	4.26	w
l=3	203	3.32	3.22	w
l=4	004	2.54	2.51	vw
	204	2.36	2.32	vw
Lattice parameters				
Orthorhombic; $P2_122_1$; for (h00) and (00l) h,l=2n				
a=24.06 Å, b=4.58 Å, c=10.05 Å				

The 2D WAXS pattern of γ-PGA-Bn was found to feature only a few diffraction peaks. The model used to analyze the above ethyl- and propyl-substitued samples was applied, but slightly modified due to the presence of the aromatic ring. The data recorded indicated that this polymer is also of an orthorhombic crystalline nature. The calculated crystal density is ρ_{cal}=1.25 g cm^{-3}, which is well below the measured density of 1.40 g cm^{-3},

determined by pycnometry, for reasons yet unclear. The lattice parameters obtained for γ-PGA-Bn are similar to those previously published[184], which was reported to indicate a 5/2 α-helical confirmation.

Polarised Raman spectroscopy

Polarized Raman spectra recorded in the region 1000-3600 cm^{-1} of unoriented and oriented polymer films are presented in Figures 5.13 A-C. The notation X|X represents spectra recorded parallel to the direction of film orientation, while Y|Y spectra were perpendicular to the direction of film orientation. Almost no signal was observed in the cross polarised geometries, i.e. X|Y, Y|X. Characteristic Raman peaks are observed at 3295 cm^{-1} (Amide A, ν ν N-H), 1642 cm^{-1} (Amide I, ν ν C=O), 1607 cm^{-1} (Amide II, ν ν C-N + δ N-H), 1294 cm^{-1} (Amide III, δ N-H).

The Y|Y spectra show higher intensity for N-H and C=O stretching vibration bands at 3295 cm^{-1} and 1642 cm^{-1} in comparison with X|X spectra for the samples with shorter alkyl lateral chains (Figure 5.13 A, B). This difference was not observed for the the benzyl-substituted material.

The amide II band was not observed for alkyl-esterified γ-PGA polymers, which may be due to an α-helical structure. Janko *et. al* reported on anisotropic Raman scattering in collagen bundles, which showed that typical amide Raman peaks of the protein backbone change depending on alignment.[185] They found the stabilisation of the triple helical structure in collagen, formed by interchain H-bonds between N-H and C=O bonds (in collagen, bonds of glycines and prolines, respectively), are represented by the amide I and amide III bands.[185]

Table 5.8: Common Raman shift values for secondary protein structures, as reproduced from[28].

Structure	**Amide I / cm^{-1}**	**Amide III / cm^{-1}**	**Skeletal C-C / cm^{-1}**
α-Helix	1660-1645	1310-1260	950-885
β-Pleated sheet	1680-1665	1240-1225	1010-1000
Random coil	1680-1665	1260-1240	960-950

However, the amide II peak for the γ-PGA-Bn film shows dichroism, which corresponds to the conventional orientation of the macromolecule in a fibre. Also, the observed dichroic ratios for γ-PGA-Et and γ-PGA-Pr samples are expected for a structure with C=O and N-H bonds oriented normal to the chain axis[184]. Thus the Raman data generally confirm the proposed structural model.

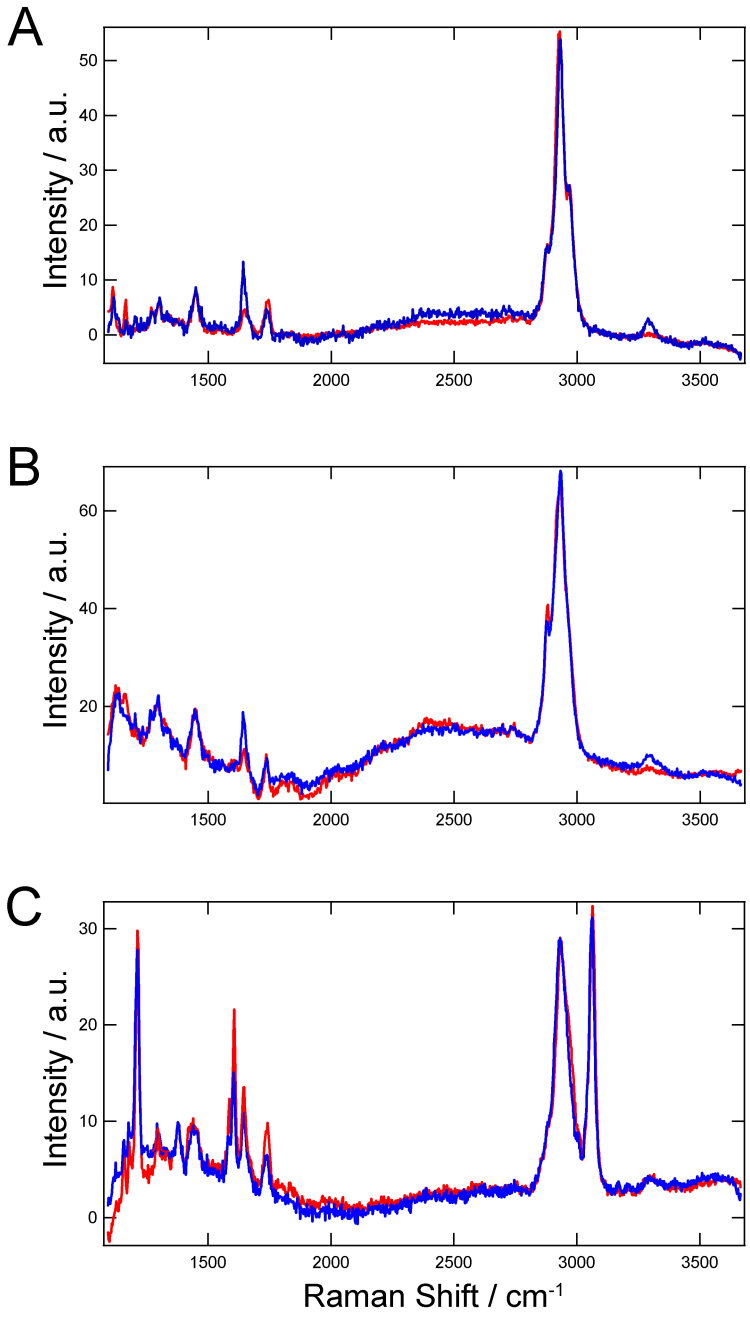


Figure 5.13: Raman spectra recorded in X|X (red) and Y|Y(blue) orientations for oriented A) γ-PGA-Et, B) γ-PGA-Pr, and C) γ-PGA-Bn polymer films.

Thermal analysis

Higher draw ratios were found to thermally display an increase in degree of crystallinity. In lieu of exact calculations for the material's crystalline percentage, which are reliant on knowing the exotherm of a perfect polymer crystal, the ratio of normalised exothermic and endothermic heat flows are presented in Table 5.9. As draw ratio increases, the exotherm associated with crystallisation decreases in area while melting remains unchanged. This is true for all modified γ-PGA polymer species, and is shown graphically

from the first heating DSC traces in Figures 5.14, 5.15, and 5.16 for γ-PGA-Et, γ-PGA-Pr, and γ-PGA-Bn, respectively. All polymers were then melt-crystallised and did not display any crystallisation in second heating traces.

Samples of the various esterified PGAs, both as-cast and oriented, were also analysed by differential scanning calorimetry (DSC), in order to explore their thermal properties. Typical DSC-thermograms of the various materials are presented in Figures 5.14-5.16. Interestingly, as-cast, dried films (λ = 1) of all modified polymers featured a well-defined glass transition temperature and a pronounced crystallisation endotherm. The latter rapidly diminished with increasing draw ratio in all cases, indicative of orientation-induced crystallisation of the macromolecules.

Unfortunately, the relatively poor quality of the DSC-traces did not permit a reliable determination of the various values of the melting enthalpy. Furthermore, it would not be possible to extract degrees of crystallinity as their values for 100% crystalline material are not known. Thus, the ratio of the melting endotherm and the exothermic enthalpy of crystallisation recorded in the first heating cycle was chosen to represent the development of crystalline order with draw ratio. These data are presented in Table 5.9. The latter reveal that all as-cast, dried films were essentially amorphous (ratio ~1). Notably, crystallinity typically developed at λ > 4, most pronounced for for γ-PGA-Et for reasons which are not yet clear.

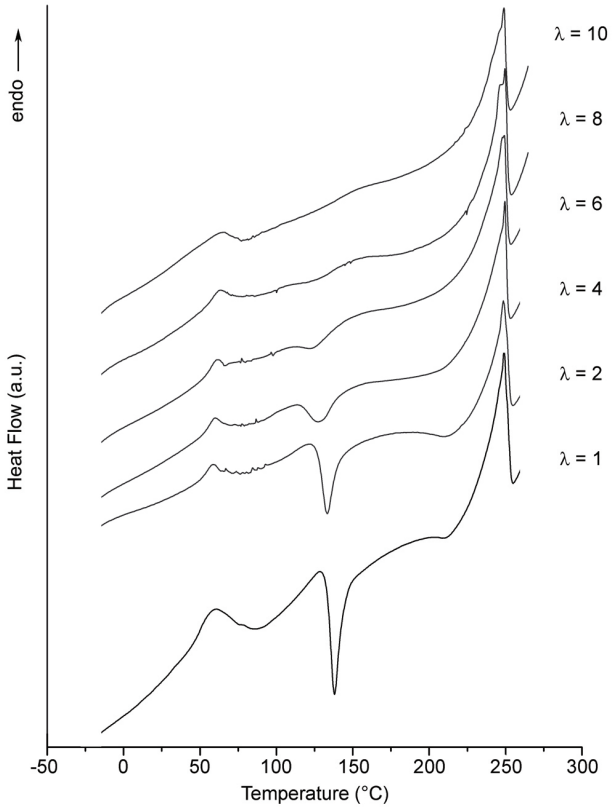


Figure 5.14: First-heating DSC thermograms of γ-PGA-Et films drawn to λ = 10.

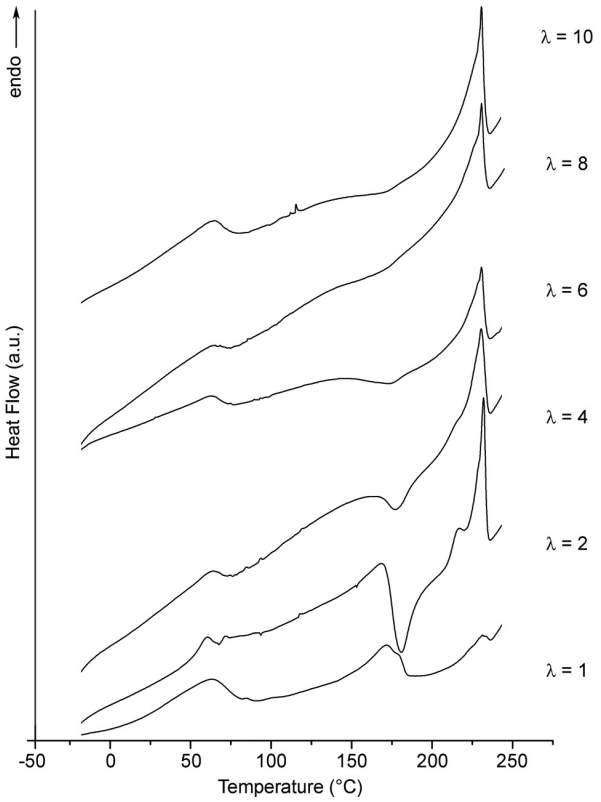


Figure 5.15: First-heating DSC thermograms of γ-PGA-Pr films drawn to λ = 10.

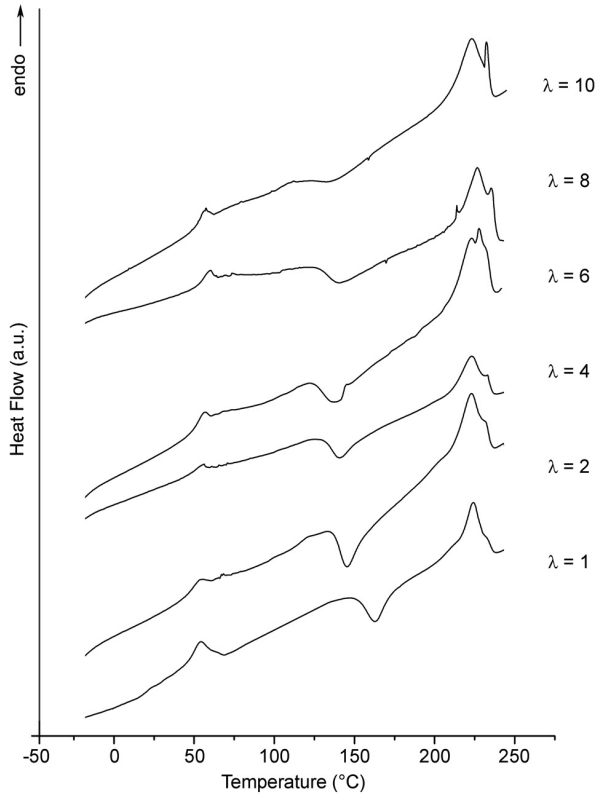


Figure 5.16: First-heating DSC thermograms of γ-PGA-Bn films drawn to λ = 10.

Table 5.9: Normalised endotherm/exotherm ratios for γ-PGA films drawn to λ = 10.

Draw ratio / λ	**γ-PGA-Et**	**γ-PGA-Pr**	**γ-PGA-Bn**
1 (as-cast)	1.53	1.63	1.35
2	1.81	1.58	1.44
4	3.65	1.69	1.58
6	6.54	1.95	1.85
8	14.10	2.38	2.26
10	28.68	3.11	2.80

5.5 Conclusions

In this chapter, solution-cast films of native and esterified γ-PGA were subject to tensile testing at room temperature to explore their mechanical properties. Due to hydrogen bonding between chains, the unmodified γ-PGA-H film was found to be brittle at room temperature with a Young's modulus of ~5 GPa, tensile strength of 94 MPa and 2% strain at break. By contrast, all modified γ-PGA polymers were found to be very ductile at room temperature, displaying an inverse relationship between side group size and strain at break of 542%, 361%, and 106% for γ-PGA-Et, γ-PGA-Pr, and γ-PGA-Bn films, respectively. Unoriented γ-PGA-Et films concomitantly displayed the lowest values of E = 0.85 GPa, σ_y = 14.7 MPa.

Subsequently, solution-cast films of the esterified γ-PGA were oriented by tensile deformation between their glass transition temperature T_g and peak crystallisation temperature T_c to increase their (uniaxial) macromolecular order and, accordingly, their mechanical properties. An increase in stiffness was achieved for γ-PGA-Bn, reaching a value of the Young's modulus of over 5 GPa, tensile strength of nearly 150 MPa, and a strain at break of 7.25%. It was been demonstrated that the mechanical characteristics of these polymers can be tailored over a wide range for desired bioapplications.

It was shown by WAXS that γ-PGA-Et, γ-PGA-Pr, and γ-PGA-Bn polymers form α-helical structures, whereas the main chain conformation remains close to planar. The proposed orientation of hydrogen bonds was confirmed by polarised Raman spectroscopy. The unit cells of all three esterified polymers are orthorhombic, containing 4 monomers. The *a*-parameter was found to be affected by the lateral chain size, which indicates that the changes in the chemical structure are accommodated within the sheet planes by increasing the inter-chain distance.

Finally, esterification of γ-PGA polymers expectedly shielded of the H-bonds present in the unmodified form. This allowed tailoring of their mechanical properties over an exceptional range by tensile deformation. Taken together, these results may hold promise for use in tissue engineering applications, where mechanically appropriate, biodegradable scaffolds are required.

Chapter 6

Scaling up γ-PGA-Bn synthesis

6.1 Introduction

The next stage of this thesis was to scale up esterified γ-PGA synthesis. Following the synthesis described in Chapter 2, the total amount of material produced was roughly 1.5-1.7 g, with a 60-70% yield. Furthermore, batch-to-batch variation in degree of esterification had a prominent effect on thermal properties as well as the weight average molecular weight (M_w) of the polymers.

Previously discussed in Chapter 5, this variability in M_w would result in different mechanical properties. As a result, tensile deformation studies were limited by the mass of material from a single batch and would benefit from increasing produced quantities.

Similarly, in order to perform quantitative cellular studies, it is vital to increase the synthesis to produce an abundance of material. This will enable fabrication of several scaffolds with sufficient size and similar mechanical properties. Furthermore, more material is required to perform cellular studies which investigate any effect from varying the degree of γ-PGA-Bn polymer orientation.

In theory, as the esterification procedure is performed on a molar-ratio basis, the reaction should be easily scalable. In practice, however, this requires new equipment, handling of large volumes for purification, and safely disposing of waste quantities. This chapter reports chemical, thermal and structural characterisation of scaled γ-PGA-Bn syntheses.

6.2 Experimental

6.2.1 Chemical synthesis

General

All starting polymer (γ-D,L-PGA Na^+ salt, produced by *Bacillus subtilis*) was purchased from Natto Biosciences (Shanghai, China). All reagents and solvents were purchased from Aldrich and used as received, unless otherwise specified.

Free acid form of γ-PGA

Similar to synthesis in Section 2.2.1, γ-PGA Na^+ salt (40 g) was dissolved in 1 L of distilled water. The solution was acidified with HCl 6M to pH 1.5, distributed in 75 ml volumes, frozen at -80°C and lyophilised for at least 96 h. The freeze-dried solid resulted soft and porous.

γ-PGA esterification

Batches of 3, 4, or 5-times the quantity of polymers detailed in Section 2.2.1 were synthesised using a SC162 temperature regulated stirrer hot plate (complete with SCT1 temperature controller; Bibby Scientific Limited; Stone, U.K.) with an oil bath for even, controlled heating of the solutions. γ-PGA free acid (+ NaCl) (7.2, 9.6, or 12 g, for 3x, 4x and 5x, respectively; all 0.01 M) was introduced into a 1000 mL round bottom flask equipped with a temperature regulated stirrer hot plate, and suspended in 540, 720, or 900 mL of anhydrous NMP. The suspension was heated by oil bath to 80°C and stirred for 24 h to dissolve the γ-PGA-H. After that time, the mixture was cooled to 60°C and $NaHCO_3$ (12.9, 17.2, or 21.5 g as 0.85 M, 1.14 M, or 1.42 M, respectively) was added. After 2 h, the benzyl bromide was added dropwise (22.8, 30.4, or 38 mL, respectively) to the mixture for a 5x molar excess over 5 min. The mixture was stirred at 60°C for a period of time ranging from 36 to 40 h. The reaction was quenched by removing the round bottom flask from the oil bath, cooling to room temperature and stirring stopped. The withdrawal for ^{1}H-NMR was precipitated and degree of esterification calculation was calculated as in Section 2.2.1. If the degree of esterification was below 100%, the NMP solution was re-heated to 60°C, stirring, and 1 molar equivalent of bromide was added. The reaction continued for 24 h, after which another NMR sample was withdrawn as before.

Following confirmation of reaction esterification by ^{1}H-NMR, the reacted γ-PGA /NMP supernatant was decanted at a ratio of 1:10 NMP:cold HCl (pH 1.5) into 5 L beakers (final volume per beaker up to 4.25 L), and left to precipitate overnight at 4°C. The remaining salts ($NaHCO_3$ and NaBr) were discarded. The sticky precipitate was filtered on a glass filter (1 L, Por 3), washed with cold diH_2O (1.5-3 L), followed by an equal volume of diethyl ether, soaked in 500 mL diethyl ether for 1-3 h, filtered again, and finally dried on the filter at RT overnight in the fume cupboard.

Purification

The esterified γ-PGA was dissolved in dried DMSO (0.2-0.5% final solution; SeccoSolv®, Merck; chemical provided by VWR) by mild heating (40°C) and stirring. The solution was then precipitated 1:10 in diH_2O for at least 6 h after which 3 drops of 6M HCl were added to clarify the solution and encourage precipitation. The solid was filtered on a glass filter (as before), repeatedly washed with H_2O and Et_2O, and then dried at RT overnight in the fume cupboard.

6.2.2 Characterisation

All polymers produced were characterised as previously stated in Chapter 2 using ^{1}H-NMR, SEC, TGA, and DSC.

^{1}H-NMR

All polymer batches were characterised using ^{1}H-NMR as in Chapter 2 and found to be fully esterified.

6.3 Results

6.3.1 Synthesis

All batches produced in this chapter were found to have a yield of 90-95%, a large improvement on those produced in Chapter 2 (60-70%). This increase is most likely attributed to the new hotplate/stirrer setup with a temperature regulated feedback system, which ensured reactions were maintained at 60°C using oil baths. The previous setup used and discussed in Chapter 2 was set to 60°C, yet was still liable to environmental temperature variations. This may have had an effect on a steady oil bath temperature, but was no longer a concern with the new feedback controlled system.

6.3.2 ^{1}H-NMR

All polymer batches (γ-PGA-Bn-3 - γ-PGA-Bn-8) were fully esterified as calculated by ^{1}H-NMR integration.

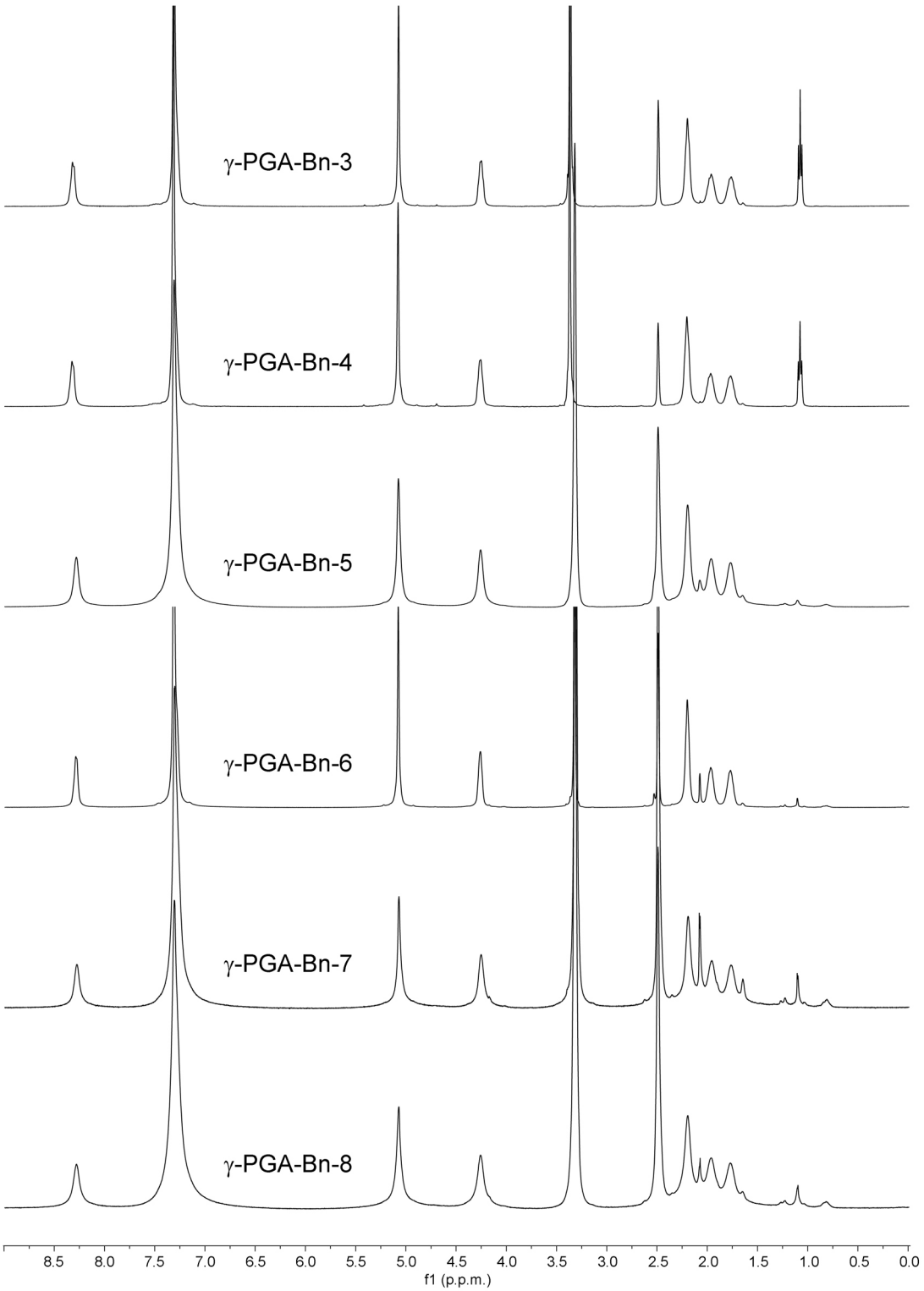


Figure 6.1: ^{1}H-NMR for γ-PGA-Bn scaled up batches (DMSO-d6, 25°C).

6.3.3 Size exclusion chromatography

The molecular weight distributions of the γ-PGA-Bn batches were determined using SEC as reported in Section 2.3.4. All esterified γ-PGA polymer results are relative to PMMA standards (in DMF with 1g/L LiBr). As discussed in Chapter 2, the starting, bacterially produced γ-PGA-H polymer has a high weight average molecular weight M_w of γ-PGA-H is 2.83 x 10^5, with a fairly broad distribution as shown in its' polydispersity index (PDI, 2.40).

Scaling up of synthesis appeared to have a small effect on the weight average molecular weight and a larger effect on its distribution. Measured M_w varied from 9.20 x 10^4 to 2.48 x 10^5 with polydispersities within the range of 3.08-3.56. The γ-PGA-Bn polymers presented in Section 2.3.4 had similar values of M_w (ranging 8.67 x 10^4 to 1.46 x 10^5), but with less polydispersity amongst the batches than scaled batches. This increased P.D.I. in scaled up batches may also have an effect on mechanical properties.

Therefore, in the future, it would be advantageous to run the polymer through a preparative SEC column and collect fractions to reduce the variation in M_w. This would especially be useful in future mechanical studies, including tensile deformation. The selection of column would need to take into account both the polymer's limited solubility in organic solvents, and the toxicity of LiBr, which is used with this SEC.

Table 6.1: SEC results for scaled up γ-PGA-Bn series polymers.

Polymer	**Synthesis**	**M_n/g mol^{-1}**	**M_w/g mol^{-1}**	**P.D.I.**
γ-PGA-Bn	3	2.94 x 10^4	9.20 x 10^4	3.12
	4	3.71 x 10^4	1.25 x 10^5	3.36
	5	4.78 x 10^4	1.70 x 10^5	3.56
	6	3.36 x 10^4	1.03 x 10^5	3.08
	7	7.43 x 10^4	2.48 x 10^5	3.33
	8	4.80 x 10^4	1.69 x 10^5	3.54

6.3.4 Thermal characterisation

Thermal characterisation was performed on the produced polymer powders. Both TGA and DSC analysis are tabulated in Table 6.2, along with the two γ-PGA-Bn batches produced in Chapter 2 (γ-PGA-Bn-1 and γ-PGA-Bn-2). These results demonstrate there is little thermal variation between the scaled up batches, unlike those produced in Chapter 2.

Table 6.2: Thermal characterisation of all γ-PGA-Bn batches, where T_c represents crystallisation upon cooling.

Synthesis	T_g /°C	T_c /°C	T_m 1 /°C	T_m 2 /°C	5% T_d /°C
1	55	163	224	217	244
2	50	156	221	212	236
3	64	168	225	223	256
4	66	168	225	223	258
5	62	169	227	224	254
6	66	169	227	224	257
7	64	170	225	224	258
8	64	169	225	222	254

Thermogravimetric analysis

Thermogravimetric analyses (TGA) were performed on all γ-PGA-Bn polymers to determine any variation in temperatures of thermal degradation. The values at which polymers experienced 5% decomposition are presented in Table 6.2 with DSC thermal characterisation results. All scaled up batches had a 5% T_d of 256°C ± 1.8°C. This shows an overall increase in 5% T_d and decrease in variability when compared to that of the measured values for γ-PGA-Bn-1 and γ-PGA-Bn-2 produced in Chapter 2 (244°C and 236°C, respectively). This change is reasonably due to the increased degree of esterification of scaled γ-PGA-Bn batches (100% by ^{1}H-NMR integration). Recalling the degree of esterification achieved in Chapter 2 (γ-PGA-Bn-1 = 99% while γ-PGA-Bn-2 = 96%), it may be concluded that an increase in degree of conversion also results in more resistance to depolymerisation of the main chain. Taken together, these results support the experimentally observed increase in the onset of 5% thermal degradation.

Differential scanning calorimetry

Differential scanning calorimetry (DSC) was employed to determine the transition temperatures of the scaled γ-PGA-Bn polymers. DSC was performed on purified powders and the heating/cooling rates were kept at 10°C min^{-1}. All heating traces of esterified polymers are presented in Figure 6.2 and the results tabulated in Table 6.2.

All the T_g values of scaled batches increased to 62-66°C with little variability. This was also found to be the case with other thermal transition temperatures, namely recrystallisation (T_{rc}) and T_m. As seen in Table 6.2 the 5% T_d is higher for scaled up polymers, indicating they experience less degradation at the melting temperature. The increased range between T_m and 5% T_d explains the decrease in magnitude of T_m shift seen in the second heating runs. All of these results obtained from DSC are expected with an increase in level of esterification, as well as more regularity of the polymer main chain. The repeatability of synthesis characteristics, regardless of reaction size, presents a very encouraging outcome when compared with the variability seen in Chapter 2.

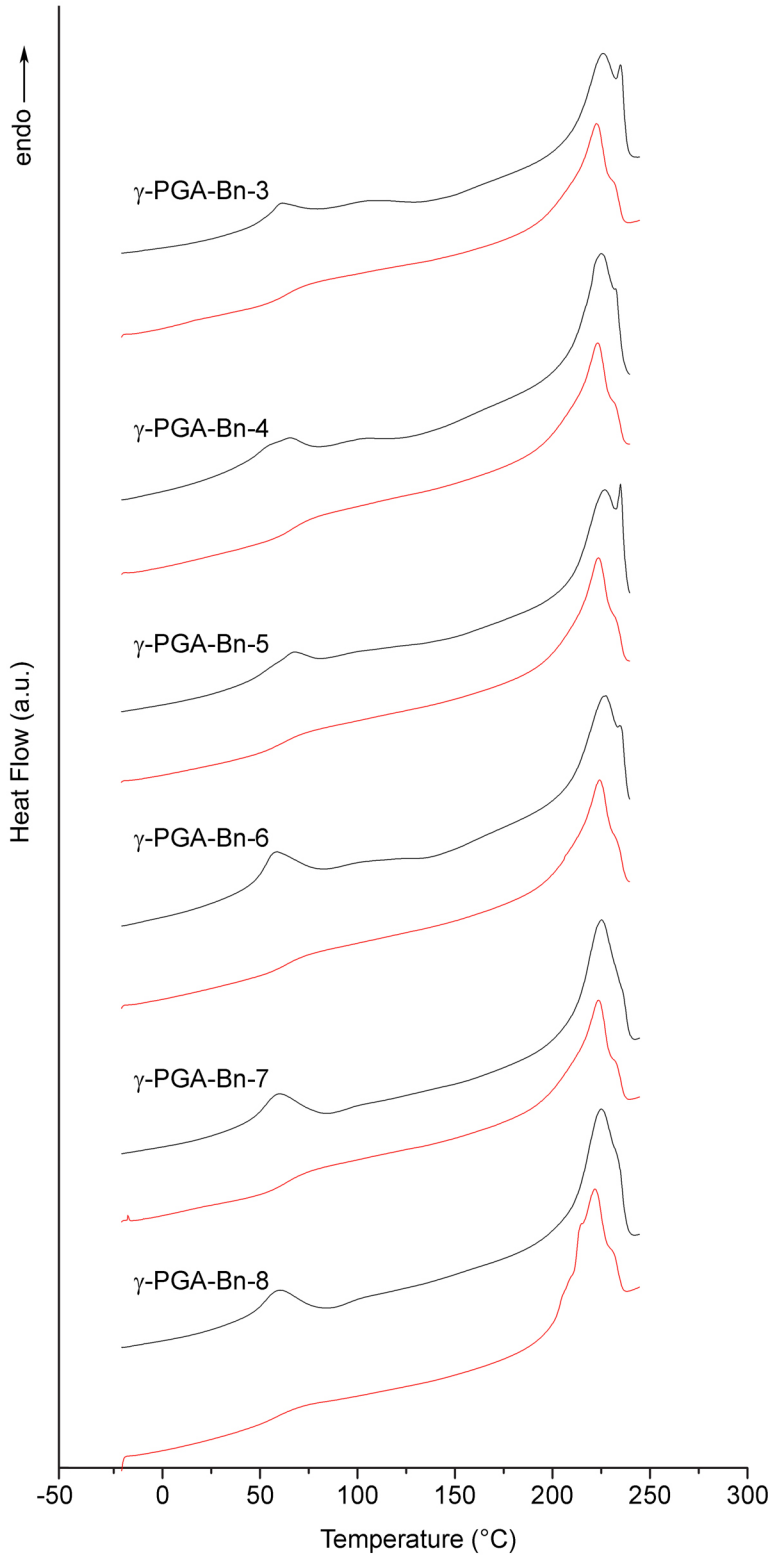


Figure 6.2: DSC heating traces for γ-PGA-Bn scaled up batches where black indicates first heating and red is the second.

6.3.5 Density measurements

Finally, the densities of scaled γ-PGA-Bn polymers were calculated using gas pycnometry. The values measured are listed in Table 6.3 and the density of γ-PGA-Bn (scaled) was found to be 1.400 ± 0.011 g cc^{-1}. This may be related to the degree of modification as chain regularity is known to affect polymer crystal packing. Thus, repeatable, full modification of scaled γ-PGA-Bn batches also allows increased reproducible polymer densities. Chain regularity and degree of crystallinity have a direct effect on mechanical properties, as discussed in Chapter 5, thus consistent batches are more ideal for mechanical testing.

Table 6.3: Density of all γ-PGA-Bn scaled-up batches.

Synthesis	Batch size	Density /g cc^{-1}
3	4x	1.398
4	3x	1.400
5	5x	1.399
6	5x	1.388
7	5x	1.420
8	5x	1.393

Overall, by changing the experimental equipment, the syntheses now reproducibly yields more product with very little variability between batches. Using a temperature-regulated feedback hotplate stirrer in this chapter substantially improved the synthesis. Thus it is thought that this esterification is particularly sensitive to temperature changes. The work shown here also demonstrates that laboratory synthesis may be scaled, but is limited to equipment size within a laboratory setting. Therefore, this synthesis may potentially be performed on a small industrial scale, with limiting factors being solvent waste removal and polymer purification on a larger scale.

6.4 Conclusions

This chapter presented six successful syntheses of γ-PGA-Bn in larger quantities than those in Chapter 2. Reactions of 3, 4, and 5 times the quantity in Chapter 2 displayed both a high yield and repeatability, independent of overall starting volume. Polymer M_w were maintained above 90,000 Da with a slight increase in polydispersity, and thus would benefit from fraction collection for a more narrow M_w range prior to processing. Batches produced here had a higher level of esterification, resulting in an increase in thermal properties, namely T_g and 5% T_d. Similarly, less degradation occurred with melting and polymer density had little variability between all batches. These improvements in batch consistency seen in this chapter are due to changing the experimental setup, indicating this reaction is enhanced with maintaining a continual reaction temperature. Though limited to a laboratory setting, this work demonstrates the ability to increase yield and total product, implying it may be scaled to an industrial size if waste removal can be optimised.

Chapter 7

Conclusions and outlook

Tissue engineering has the potential to change modern medicine as we know it. Research in regenerative medicine focuses highly on biomaterials which have the ability to guide the body to repair itself, providing a degradable scaffold that encourages ingrowth. The aim of the work presented in this thesis was to address four ideal qualities of engineered constructs: biodegradability, biocompatibility, appropriate mechanical properties, and tailorability. To do this, a naturally-produced polyamino acid, poly(gamma-D,L-glutamic acid; γ-PGA) was utilised as it is non-toxic, enzymatically degraded, and relatively unexplored in tissue engineering applications.

Initially, to limit the high water solubility of γ-PGA, the side chain was esterified using either an alkyl or aryl group as previously reported.[146] Following acidification to yield a reactive, free -COOH side group, over 90% modification of γ-PGA was achieved using ethyl, propyl, or benzyl bromide, yielding γ-PGA-Et, γ-PGA-Pr, or γ-PGA-Bn, respectively. A high weight average molecular weight ($\geq 10^5$ Da) was maintained throughout the synthesis. Attributed to a reduction in H-bonds between chains, esterification introduced more macromolecular order and caused a drop in the glass transition temperature (T_g) of all modified polymers when compared with the native acid form (γ-PGA-H). Modifying the side chain also led to a large increase in the onset of 5% thermal degradation (T_d), opening a wider range for thermal processing of the polymers. Contact angle increased with increasing side chain hydrophobicity and values for γ-PGA-Bn were found to be similar to that of FDA approved poly(L-lactic acid; PLLA).

Unfortunately, the discovery of degradation upon melting eliminated the possibility of using traditional polymer melt-processing techniques. Furthermore, limited quantities of material were produced per synthesis, at a yield of 60-70%. Variability in degree of esterification between batches, attributed to the experimental equipment used for the reaction, inhibited combining multiple syntheses for other studies.

Next, in an alternative approach to γ-PGA modification, the native γ-PGA-H polymer was altered by using a carbodiimide to couple L-phenylalanine-NH_2 (generating γ-PGA-Phe) to the free -COOH side group. A one-step synthesis only yielded γ-PGA-Phe with

roughly 30% degree of coupling. Therefore, a two-step synthesis was employed: firstly reacted in a mixture of aqueous/organic solvent and purified, followed by a reaction in only organic solvent. Fully coupled, the γ-PGA-Phe had several impurities from the reaction, most notably the poorly soluble byproduct dicyclohexylurea (DCU). As DCU is very difficult to remove from the γ-PGA-Phe, the synthesis will likely benefit from using a different carbodiimide which yields an easily removable urea.

Addition of the L-phenylalanine-NH_2 caused an increase in T_g to 156 °C, due to the introduction of more hydrogen bonding. Similar then to the γ-PGA-H, this polymer is expected to be very brittle at RT and anticipated to have a Young's modulus over 5 GPa. Further synthesis, in larger quantities, is necessary to produce enough material for mechanical testing to test this hypothesis.

To date, this is first time γ-PGA-H has been fully modified using phenylalanine. Though the Akashi group have published several papers on amphiphilic nanoparticles made of 53% coupled γ-PGA, they use an ethyl ester-modified L-phenylalanine.[162–170] Therefore, this two-step synthesis opens the possibility for full functionalisation of γ-PGA with other amino acids or even short peptide sequences to better mimic the extracellular matrix of a target replacement tissue.

Biocompatibility of esterified γ-PGA films (as-cast) was tested and all polymer films passed the ISO 10993:5 cytotoxicity test, often used by industry as a prelude to *in vivo* studies. This indicated the films do not release any toxic byproducts. Furthermore, all films supported human fibroblast attachment and proliferation, with cells viable up to seven days.

As found in chapter 2, the contact angle of γ-PGA-Bn, 88.1° ± 1.2, was also similar to that of a polymer studied recently by Joy *et* al.[172], whose quantitative cell studies indicated this polymer had improved cell attachment and proliferation when compared with polymers having similar contact angles to γ-PGA-Et and γ-PGA-Pr. Therefore, γ-PGA-Bn was chosen to subsequently focus on for further cell and dissolution studies. Human foreskin fibroblasts formed well defined actin stress fibres colocalised with focal adhesions when cultured on γ-PGA-Bn films, indicating the cells were well adhered to the substrates.

After 28 days incubation at 37°C, γ-PGA-Bn films soaked in H_2O, phosphate buffered saline (PBS) or simulated body fluid (SBF) all lost ~4% of their starting weight. Regardless of soaking media, films became opaque at seven days while submicron holes were detected in the film surfaces using scanning electron microscopy. By day 28, an increased amount of surface dissolution was visible on films soaked in salt-containing media (PBS and SBF). As most mass was maintained, the γ-PGA-Bn should mainly be degraded by enzymes. Thus, *in vivo* testing of γ-PGA-Bn is required to assess this polymer's implantation lifetime.

Following chemical synthesis and biological characterisation, mechanical properties

of solution-cast, esterified γ-PGA polymer films were determined used tensile testing at RT. The native γ-PGA-H was found to be brittle, with a Young's modulus of ~5 GPa, 94 MPa tensile strength, and only 2% strain at break due to interchain hydrogen bonding. Esterification introduced ductility to all three polymer types, with an inverse relationship between strain at break and side group size, i.e. 542%, 361%, and 106% for γ-PGA-Et, γ-PGA-Pr, and γ-PGA-Bn films, respectively.

To maximise their mechanical properties by increasing overall macromolecular order, these as-cast, modified γ-PGA films were subsequently subjected to uniaxial tensile deformation at temperatures between T_g and peak crystallisation temperature T_c. Able to be drawn over 10 times, all polymers experienced an increase in stiffness and tensile strength while strain at break was maintained at or above a physiologically relevant 7.25%. γ-PGA-Bn had the highest Young's modulus of over 5 GPa, with a tensile strength of nearly 150 MPa.

Depending on choice of side group or degree of induced orientation, mechanical characteristics of these polymers can be tailored over a wide range for desired bioapplications. This ability could potentially be expanded by also tailoring the weight-average molecular weight of synthesised batches, opening more options of tissues to target for regeneration.

A similar issue arose with both mechanical and biocompatibility testing: limited material quantity with synthesis batch variability. Thus, this work finally focused upon scaling up the synthesis in an approach to further product development towards industry. Additionally, a temperature-regulated feedback stirrer hotplate was employed to reduce batch-to-batch synthesis variation. Using the new setup regularly produced over 12 g of fully-esterified γ-PGA-Bn with an increased yield (up to 94%). This work demonstrated the reaction may be scaled, though this was the size limit of the reaction setup. The synthesis may benefit further from using sealed, pressurised filtration for ease of waste disposal and removal of impurities.

The work performed in this thesis centres around modifying γ-PGA for use in regenerative medicine applications. As shown in this work, by varying side-group chemistry or molecular alignment, properties of modified γ-PGA polymers may be designed to suit specific applications, thus addressing four important tissue engineering requirements: tailorability, appropriate mechanical properties, biocompatibility, and biodegradability.

If more time were available, it would have been optimal to produce larger, aligned γ-PGA-Bn scaffolds for further testing. More in-depth cell studies (cell interaction studies, including cell proliferation, extracellular matrix protein characterisation, genetic expression, and imaging on oriented polymer samples using both primary and stem cells for successful implant growth) would be performed to determine the abilities of the different polymers to support cell growth and structuring. This would also ascertain which tissues would be best to target so that the scaffolds may be carried forward towards commercialisation. Optimisation of polymer purification, including fraction collection to reduce

polydispersity, would be highly pertinent for making reproducible scaffolds in a prelude to manufacturing medical products.

Different cell types would provide information about the abilities of the scaffold to support growth of various tissues for different biological sites and organs. As the modified γ-PGA polymers are enzymatically degraded, an ideal outcome would include optimisation of material properties to be subsequently tested *in vivo* for determining the implanted scaffold's lifetime, as well as assess performance and tissue ingrowth.

Finally, it would also have been advantageous to produce larger quantities of the fully-modified γ-PGA-Phe in order to test the mechanical properties and biocompatibility of this material. Equally as interesting, conjugating short peptide sequences to the γ-PGA and seeing their effect on cell growth would have opened the possibility for wider tissue engineering applications. As this material has such high potential in tissue engineering, with numerous possibilities to functionalise, an abundance of related future work possibilities exist.

Bibliography

[1] J.H. George. E-poster. *UK Society for Biomaterials Conference*, 2006.

[2] S. Mwenifumbo, M.S. Shaffer, and M.M. Stevens. Exploring cellular behaviour with multi-walled carbon nanotube constructs. *J Mat Chem*, 17(19):1894–1902, 2007.

[3] P.J. Yang and J.S. Temenoff. Engineering orthopedic tissue interfaces. *Tissue Eng Pt B-Rev*, 15(2):127–41, 2009.

[4] D.L. Bartel, D.T. Davy, and T.M. Keaveny. *Orthopaedic Biomechanics: Mechanics and Design in Musculoskeletal Systems*. Pearson/Prentice Hall, Upper Saddle River, 2006.

[5] J. Black and G. Hastings, editors. *Handbook of Biomaterials Properties*. Chapman and Hall, London, 1st edition, 1998.

[6] C.R. Ethier and C.A Simmons. *Introductory Biomechanics: From Cells to Organisms*. Cambridge University Press, Cambridge, 1st edition, 2007.

[7] G.E. Kempson, H. Muir, C. Pollard, and M. Tuke. The tensile properties of the cartilage of human femoral condyles related to the content of collagen and glycosaminoglycans. *Biochim Biophys Acta*, 297(2):456–72, 1973.

[8] Y-C. Kuo and Y-R. Hsu. Tissue-engineered polyethylene oxide/chitosan scaffolds as potential substitutes for articular cartilage. *J Biomed Mater Res A*, 91(1):277–87, 2009.

[9] W-J. Li, R.L. Mauck, J.A. Cooper, X. Yuan, and R.S. Tuan. Engineering controllable anisotropy in electrospun biodegradable nanofibrous scaffolds for musculoskeletal tissue engineering. *J Biomech*, 40(8):1686–93, 2007.

[10] T. Majima, T. Funakosi, N. Iwasaki, S-T. Yamane, K. Harada, S. Nonaka, A. Minami, and S-I. Nishimura. Alginate and chitosan polyion complex hybrid fibers for scaffolds in ligament and tendon tissue engineering. *J Orthop Sci*, 10(3):302–7, 2005.

[11] F.T. Moutos, L.E. Freed, and F. Guilak. A biomimetic three-dimensional woven composite scaffold for functional tissue engineering of cartilage. *Nat Mater*, 6(2): 162–7, 2007.

[12] P. Neumann, T.S. Keller, L. Ekström, L. Perry, T.H. Hansson, and D.M. Spengler. Mechanical properties of the human lumbar anterior longitudinal ligament. *J Biomech*, 25(10):1185–94, 1992.

[13] C.L.E. Nijst, J.P. Bruggeman, J.M. Karp, L. Ferreira, A. Zumbuehl, C.J. Bettinger, and R. Langer. Synthesis and characterization of photocurable elastomers from poly(glycerol-co-sebacate). *Biomacromolecules*, 8(10):3067–73, 2007.

[14] K.M. Quapp and J.A. Weiss. Material characterization of human medial collateral ligament. *J Biomech Eng*, 120(6):757–63, 1998.

[15] A. Race, K.A. Mann, and A.A. Edidin. Mechanics of bone/poly(methyl methacrylate) composite structures: an in vitro study of human vertebrae. *J Biomech*, 40(5): 1002–10, 2007.

[16] S. Ramakrishna, J. Mayer, E. Wintermantel, and K.W. Leong. Biomedical applications of polymer-composite materials: a review. *Compos Sci Technol*, 61(9): 1189–1224, 2001.

[17] R.L. Reis and J. San Román. *Biodegradable Systems in Tissue Engineering and Regenerative Medicine*. CRC Press, Boca Raton, 2005.

[18] C.R. Roberts, J.K. Rains, P.D. Pare, D.C. Walker, B. Wiggs, and J.L. Bert. Ultrastructure and tensile properties of human tracheal cartilage. *J Biomech*, 31(1): 81–6, 1998.

[19] P. Sevilla, C. Aparicio, J.A. Planell, and F.J. Gil. Comparison of the mechanical properties between tantalum and nickel-titanium foams implant materials for bone ingrowth applications. *J Alloy Compd*, 439(1-2):67–73, 2007.

[20] J.G. Snedeker, P. Niederer, F.R. Schmidlin, M. Farshad, C.K. Demetropoulos, J.B. Lee, and K.H. Yang. Strain-rate dependent material properties of the porcine and human kidney capsule. *J Biomech*, 38(5):1011–21, 2005.

[21] R. Sodian, J.S. Sperling, D.P. Martin, A. Egozy, U. Stock, J.E. Mayer, Jr, and J.P. Vacanti. Fabrication of a trileaflet heart valve scaffold from a polyhydroxyalkanoate biopolyester for use in tissue engineering. *Tissue Eng*, 6(2):183–8, 2000.

[22] Y. Wang, G.A. Ameer, B.J. Sheppard, and R. Langer. A tough biodegradable elastomer. *Nat Biotechnol*, 20(6):602–6, 2002.

[23] T.J. Webster, editor. *Nanotechnology for the Regeneration of Hard and Soft Tissues*. World Scientific Publishing Co. Pte. Ltd, Singapore, 1st edition, 2007.

[24] Y. Zeng, J. Yang, K. Huang, Z. Lee, and X. Lee. A comparison of biomechanical properties between human and porcine cornea. *J Biomech*, 34(4):533–7, 2001.

[25] F.W. Küster, A. Thiel, and A. Ruland. *Rechentafeln für die Chemische Analytik*. de Gruyter, Berlin, 104. auflage edition, 1993.

[26] M. Hesse, H. Meier, and B. Zeeh. *Spektroskopische Methoden in der Organischen Chemie*. Thieme Verlag, Stuttgart, Germany, 6 edition, 2002.

[27] W. Martienssen and H. Warlimont. *Springer Handbook of Condensed Matter and Materials Data*. Springer, Heidelberg, 2005.

[28] H.-U. Gremlich and B. Yan. *Infrared and Raman Spectroscopy of Biological Materials*. M. Dekker, New York, 2001.

[29] United States Bone and Joint Decade. *The Burden of Musculoskeletal Diseases in the United States*. American Academy of Orthopaedic Surgeons, Rosemont, IL, 2008.

[30] D. Butler, M. Dressler, H. Awad, and F. Guilak (ed.). *Functional Tissue Engineering: Assessment of Function in Tendon and Ligament Repair*. Springer, New York, 2003.

[31] D.M. Doroski, K.S. Brink, and J.S. Temenoff. Techniques for biological characterization of tissue-engineered tendon and ligament. *Biomaterials*, 28(2):187–202, 2007.

[32] J.M. Clark and D.T. Harryman, 2nd. Tendons, ligaments, and capsule of the rotator cuff. gross and microscopic anatomy. *J Bone Joint Surg Am*, 74(5):713–25, 1992.

[33] H. Yadav, S. Nho, A. Romeo, and J.D. MacGillivray. Rotator cuff tears: pathology and repair. *Knee Surg Sport Tr A*, 17(4):409–21, 2009.

[34] J.M. Hootman and C.G. Helmick. Projections of united states prevalence of arthritis and associated activity limitations. *Arthritis Rheum*, 54(1):226–9, 2006.

[35] T. Aigner and J. Stove. Collagens - major component of the physiological cartilage matrix, major target of cartilage degeneration, major tool in cartilage repair. *Adv Drug Deliver Rev*, 55(12):1569–93, 2003.

[36] C.K. Kuo, W.J. Li, R.L. Mauck, and R.S. Tuan. Cartilage tissue engineering: its potential and uses. *Curr Opin Rheumatol*, 18(1):64–73, 2006.

[37] E.H. Lee and J.H.P. Hui. The potential of stem cells in orthopaedic surgery. *J Bone Joint Surg Br*, 88-B(7):841–51, 2006.

[38] M.M. Stevens and J.H. George. Exploring and engineering the cell surface interface. *Science*, 310(5751):1135–8, 2005.

[39] N.D. Evans, E. Gentleman, and J.M. Polak. Scaffolds for stem cells. *Mater Today*, 9(12):26–33, 2006.

[40] L.G. Griffith and G. Naughton. Tissue engineering - current challenges and expanding opportunities. *Science*, 295(5557):1009–14, 2002.

[41] R. Murugan and S. Ramakrishna. Design strategies of tissue engineering scaffolds with controlled fiber orientation. *Tissue Eng*, 13(8):1845–66, 2007.

[42] W. Fodor. Tissue engineering and cell based therapies, from the bench to the clinic: The potential to replace, repair and regenerate. *Reprod Biol Endocrin*, 1(1):102–8, 2003.

[43] F. Bronner, M.C. Farach-Carson, and A.G. Mikos. *Engineering of Functional Skeletal Tissues*, volume 3 of *Topics in Bone Biology*. Springer, London, 2007.

[44] L.T. de Jonge, S.C.G. Leeuwenburgh, J.G.C. Wolke, and J.A. Jansen. Organic-inorganic surface modifications for titanium implant surfaces. *Pharm Res*, 25(10): 2357–69, 2008.

[45] L.F. Bonewald and M.L. Johnson. Osteocytes, mechanosensing and wnt signaling. *Bone*, 42(4):606–15, 2008.

[46] C. Galli, G. Passeri, and G.M. Macaluso. Osteocytes and wnt: the mechanical control of bone formation. *J Dent Res*, 89(4):331–43, 2010.

[47] C.H. Turner, S.J. Warden, T. Bellido, L.I. Plotkin, N. Kumar, I. Jasiuk, J. Danzig, and A.G. Robling. Mechanobiology of the skeleton. *Science Signaling*, 2(68):pt3, 1–4, 2009.

[48] L.L. Hench and J.R. Jones. *Biomaterials, Artificial Organs and Tissue Engineering*. CRC Press, Boca Raton, 2005.

[49] M. Brittberg, A. Lindahl, G. Homminga, A. Nilsson, O. Isaksson, and L. Peterson. A critical analysis of cartilage repair. *Acta Orthop Scand*, 68(2):186–9, 1997.

[50] L. Peterson, T. Minas, M. Brittberg, A. Nilsson, E. Sjogren-Jansson, and A. Lindahl. Two- to 9-year outcome after autologous chondrocyte transplantation of the knee. *Clin Orthop Relat R*, 374:212–34, 2000.

[51] W. Richter. Cell-based cartilage repair: illusion or solution for osteoarthritis. *Curr Opin Rheumatol*, 19(5):451–6, 2007.

[52] A.R. Poole, T. Kojima, T. Yasuda, F. Mwale, M. Kobayashi, and S. Laverty. Composition and structure of articular cartilage - a template for tissue repair. *Clin Orthop Relat R*, 391:S26–S33, 2001.

[53] M.B. Goldring. Update on the biology of the chondrocyte and new approaches to treating cartilage diseases. *Best Pract Res Cl Rh*, 20(5):1003–25, 2006.

[54] R.B. Martin, D.B. Burr, and N.A. Sharkey. *Skeletal Tissue Mechanics*. Springer, New York, 1998.

[55] S.C. Cowin and S.B. Doty. *Tissue Mechanics*. Springer, New York, 2007.

[56] R.M. Alexander and H.C. Bennet-Clark. Storage of elastic strain energy in muscle and other tissues. *Nature*, 265(5590):114–7, 1977.

[57] D. Amiel, C. Frank, F. Harwood, J. Fronek, and W. Akeson. Tendons and ligaments: a morphological and biochemical comparison. *J Orthop Res*, 1(3):257–65, 1984.

[58] J.H-C. Wang. Mechanobiology of tendon. *J Biomech*, 39(9):1563–82, 2006.

[59] K.L. Moffat, W-H.S. Sun, P.E. Pena, N.O. Chahine, S.B. Doty, G.A. Ateshian, C.T. Hung, and H.H. Lu. Characterization of the structure-function relationship at the ligament-to-bone interface. *P Natl Acad Sci USA*, 105(23):7947–52, 2008.

[60] L.L. Hench and J. Wilson, editors. *Clinical Performance of Skeletal Prostheses*. Chapman and Hall, Cambridge, 1996.

[61] M.F. Ashby, L.J. Gibson, U. Wegst, and R. Olive. The mechanical properties of natual materials. i. material property charts. *Proc R Soc Lon Ser-A*, 450(1938): 123–40, 1995.

[62] L. Akard, J. Lane, M. Wiemann, K. Lynn, M. Swinney, K. Hood, S. Hanks, R. Ash, J. Thompson, D. English, and J. Jansen. Hematopoietic reconstitution following peripheral stem-cell (pbsc) transplant. *Blood*, 82(10):A428, 1993.

[63] J. Jansen, S. Hanks, J.M. Thompson, M.J. Dugan, and L.P. Akard. Transplantation of hematopoietic stem cells from the peripheral blood. *J Cell Mol Med*, 9(1):37–50, 2005.

[64] J.A. Thomson, J. Itskovitz-Eldor, S.S. Shapiro, M.A. Waknitz, J.J. Swiergiel, V.S. Marshall, and J.M. Jones. Embryonic stem cell lines derived from human blastocysts. *Science*, 282(5391):1145–7, 1998.

[65] C. De Bari, F. Dell'Accio, J. Vanlauwe, J. Eyckmans, I.M. Khan, C.W. Archer, E.A. Jones, D. McGonagle, T.A. Mitsiadis, C. Pitzalis, and F.P. Luyten. Mesenchymal multipotency of adult human periosteal cells demonstrated by single-cell lineage analysis. *Arthritis Rheum*, 54(4):1209–21, 2006.

[66] C. De Bari, F. Dell'Accio, and F.P. Luyten. Human periosteum-derived cells maintain phenotypic stability and chondrogenic potential throughout expansion regardless of donor age. *Arthritis Rheum*, 44(1):85–95, 2001.

[67] P.J. Emans, D.A.M. Surtel, E.J.J. Frings, S.K. Bulstra, and R. Kuijer. In vivo generation of cartilage from periosteum. *Tissue Eng*, 11(3-4):369–77, 2005.

[68] H. Nakahara, S.P. Bruder, V.M. Goldberg, and A.I. Caplan. In vivo osteochondrogenic potential of cultured-cells derived from the periosteum. *Clin Orthop Relat R*, 259:223–32, 1990.

[69] H. Nakahara, V.M. Goldberg, and A.I. Caplan. Culture-expanded human periosteal-derived cells exhibit osteochondral potential in vivo. *J Orthop Res*, 9 (4):465–76, 1991.

[70] H. Nakahara, V.M. Goldberg, and A.I. Caplan. Culture-expanded periosteal-derived cells exhibit osteochondrogenic potential in porous calcium-phosphate ceramics in vivo. *Clin Orthop Relat R*, 276:291–8, 1992.

[71] M.M. Stevens, R.P. Marini, D. Schaefer, J. Aronson, R. Langer, and V.P. Shastri. In vivo engineering of organs: The bone bioreactor. *P Natl Acad Sci USA*, 102(32): 11450–5, 2005.

[72] M.M. Stevens, R.P. Marini, I. Martin, R. Langer, and V.P. Shastri. Fgf-2 enhances tgf-beta 1-induced periosteal chondrogenesis. *J Orthop Res*, 22(5):1114–9, 2004.

[73] S.C. Manolagas. Birth and death of bone cells: basic regulatory mechanisms and implications for the pathogenesis and treatment of osteoporosis. *Endocr Rev*, 21 (2):115–37, 2000.

[74] S.L. Dallas and L.F. Bonewald. Dynamics of the transition from osteoblast to osteocyte. *Ann NY Acad Sci*, 1192:437–43, 2010.

[75] J.H.P. Hui, F. Chen, A. Thambyah, and E.H. Lee. Treatment of chondral lesions in advanced osteochondritis dissecans - a comparative study of the efficacy of chondrocytes, mesenchymal stem cells, periosteal graft, and mosaicplasty (osteochondral autograft) in animal models. *J Pediatr Orthoped*, 24(4):427–33, 2004.

[76] H.A. Benhardt and E.M. Cosgriff-Hernandez. The role of mechanical loading in ligament tissue engineering. *Tissue Eng Pt B-Rev*, 15(4):467–75, 2009.

[77] C.H. Lee, H.J. Shin, I.H. Cho, Y-M. Kang, I.A. Kim, K-D. Park, and J-W. Shin. Nanofiber alignment and direction of mechanical strain affect the ecm production of human acl fibroblast. *Biomaterials*, 26(11):1261–70, 2005.

[78] S. Liao, B.J. Li, Z.W. Ma, H. Wei, C. Chan, and S. Ramakrishna. Biomimetic electrospun nanofibers for tissue regeneration. *Biomed Mater*, 1(3):R45–R53, 2006.

[79] U. Hersel, C. Dahmen, and H. Kessler. Rgd modified polymers: biomaterials for stimulated cell adhesion and beyond. *Biomaterials*, 24(24):4385–415, 2003.

[80] C.K. Miranti and J.S. Brugge. Sensing the environment: a historical perspective on integrin signal transduction. *Nat Cell Biol*, 4(4):E83–90, 2002.

[81] R.O. Hynes. Integrins: bidirectional, allosteric signaling machines. *Cell*, 110(6): 673–87, 2002.

[82] F.G. Giancotti and E. Ruoslahti. Transduction - integrin signaling. *Science*, 285 (5430):1028–32, 1999.

[83] M.D. Pierschbacher and E. Ruoslahti. Cell attachment activity of fibronectin can be duplicated by small synthetic fragments of the molecule. *Nature*, 309(5963): 30–3, 1984.

[84] D. Choquet, D.P. Felsenfeld, and M.P. Sheetz. Extracellular matrix rigidity causes strengthening of integrin-cytoskeleton linkages. *Cell*, 88(1):39–48, 1997.

[85] B.Z. Katz, E. Zamir, A. Bershadsky, Z. Kam, K.M. Yamada, and B. Geiger. Physical state of the extracellular matrix regulates the structure and molecular composition of cell-matrix adhesions. *Mol Biol Cell*, 11(3):1047–60, 2000.

[86] L.Y. Koo, D.J. Irvine, A.M. Mayes, D.A. Lauffenburger, and L.G. Griffith. Co-regulation of cell adhesion by nanoscale rgd organization and mechanical stimulus. *J Cell Sci*, 115(7):1423–33, 2002.

[87] R.J. Pelham and Y.L. Wang. Cell locomotion and focal adhesions are regulated by the mechanical properties of the substrate. *Biol Bull*, 194(3):348–9, 1998.

[88] J.M. Anderson, M. Kushwaha, A. Tambralli, S.L. Bellis, R.P. Camata, and H.-W. Jun. Osteogenic differentiation of human mesenchymal stem cells directed by extracellular matrix-mimicking ligands in a biomimetic self-assembled peptide amphiphile nanomatrix. *Biomacromolecules*, 10(10):2935–44, 2009.

[89] W.D. Staatz, K.F. Fok, M.M. Zutter, S.P. Adams, B.A. Rodriguez, and S.A. Santoro. Identification of a tetrapeptide recognition sequence for the alpha 2 beta 1 integrin in collagen. *J Biol Chem*, 266(12):7363–7, 1991.

[90] G.M. Harbers and K.E. Healy. The effect of ligand type and density on osteoblast adhesion, proliferation, and matrix mineralization. *J Biomed Mater Res A*, 75(4): 855–69, 2005.

[91] K.M. Hennessy, B.E. Pollot, W.C. Clem, M.C. Phipps, A.A. Sawyer, B.K. Culpepper, and S.L. Bellis. The effect of collagen i mimetic peptides on mesenchymal stem cell adhesion and differentiation, and on bone formation at hydroxyapatite surfaces. *Biomaterials*, 30(10):1898–1909, 2009.

[92] J.M. Anderson, J.B. Vines, J.L. Patterson, H. Chen, A. Javed, and H.-W. Jun. Osteogenic differentiation of human mesenchymal stem cells synergistically enhanced by biomimetic peptide amphiphiles combined with conditioned medium. *Acta Biomater*, 7(2):675–82, 2011.

[93] J.J. Qian and R.S. Bhatnagar. Enhanced cell attachment to anorganic bone mineral in the presence of a synthetic peptide related to collagen. *J Biomed Mater Res*, 31 (4):545–54, 1996.

[94] C.G. Knight, L.F. Morton, A.R. Peachey, D.S. Tuckwell, R.W. Farndale, and M.J. Barnes. The collagen-binding a-domains of integrins alpha(1)beta(1) and alpha(2)beta(1) recognize the same specific amino acid sequence, gfoger, in native (triple-helical) collagens. *J Biol Chem*, 275(1):35–40, 2000.

[95] M. Thorwarth, S. Schultze-Mosgau, F. Wehrhan, P. Kessler, S. Srour, J. Wiltfang, and K.A. Schlegel. Bioactivation of an anorganic bone matrix by p-15 peptide for the promotion of early bone formation. *Biomaterials*, 26(28):5648–57, 2005.

[96] C.D. Reyes, T.A. Petrie, K.L. Burns, Z. Schwartz, and A.J. Garcia. Biomolecular surface coating to enhance orthopaedic tissue healing and integration. *Biomaterials*, 28(21):3228–35, 2007.

[97] A.M Wojtowicz, A. Shekaran, M.E. Oest, K.M. Dupont, K.L. Templeman, D.W. Hutmacher, R.E. Guldberg, and A.J. García. Coating of biomaterial scaffolds with the collagen-mimetic peptide gfoger for bone defect repair. *Biomaterials*, 31(9): 2574–82, 2010.

[98] I.C. Bonzani, J.H. George, and M.M. Stevens. Novel materials for bone and cartilage regeneration. *Curr Opin Chem Biol*, 10(6):568–75, 2006.

[99] W.E. Teo, W. He, and S. Ramakrishna. Electrospun scaffold tailored for tissue-specific extracellular matrix. *Biotechnol J*, 1(9):918–29, 2006.

[100] J.C. Middleton and A.J. Tipton. Synthetic biodegradable polymers as orthopedic devices. *Biomaterials*, 21(23):2335–46, 2000.

[101] W.J. Li, R. Tuli, X.X. Huang, P. Laquerriere, and R.S. Tuan. Multilineage differentiation of human mesenchymal stem cells in a three-dimensional nanofibrous scaffold. *Biomaterials*, 26(25):5158–66, 2005.

[102] R.J. Young and P.A. Lovell. *Introduction to polymers*. Chapman and Hall, London, 2nd edition, 1991.

[103] F.M. Veronese and G. Pasut. Pegylation, successful approach to drug delivery. *Drug Discov Today*, 10(21-24):1451–8, 2005.

[104] O. Bostman and H. Pihlajamaki. Clinical biocompatibility of biodegradable orthopaedic implants for internal fixation: a review. *Biomaterials*, 21(24):2615–21, 2000.

[105] G.E. Wnek, M.E. Carr, D.G. Simpson, and G.L. Bowlin. Electrospinning of nanofiber fibrinogen structures. *Nano Lett*, 3(2):213–6, 2003.

[106] M.C. McManus, E.D. Boland, H.P. Koo, C.P. Barnes, K.J. Pawlowski, G.E. Wnek, D.G. Simpson, and G.L. Bowlin. Mechanical properties of electrospun fibrinogen structures. *Acta Biomater*, 2(1):19–28, 2006.

[107] I.C. Um, D.F. Fang, B.S. Hsiao, A. Okamoto, and B. Chu. Electro-spinning and electro-blowing of hyaluronic acid. *Biomacromolecules*, 5(4):1428–36, 2004.

[108] X.F. Wang, I.C. Um, D.F. Fang, A. Okamoto, B.S. Hsiao, and B. Chu. Formation of water-resistant hyaluronic acid nanofibers by blowing-assisted electro-spinning and non-toxic post treatments. *Polymer*, 46(13):4853–67, 2005.

[109] X.Y. Geng, O.H. Kwon, and J.H. Jang. Electrospinning of chitosan dissolved in concentrated acetic acid solution. *Biomaterials*, 26(27):5427–32, 2005.

[110] Y.R.V. Shih, C.N. Chen, S.W. Tsai, Y.J. Wang, and O.K. Lee. Growth of mesenchymal stem cells on electrospun type i collagen nanofibers. *Stem Cells*, 24(11): 2391–7, 2006.

[111] S.P. Zhong, W.E. Teo, X. Zhu, R.W. Beuerman, S. Ramakrishna, and L.Y.L. Yung. An aligned nanofibrous collagen scaffold by electrospinning and its effects on in vitro fibroblast culture. *J Biomed Mater Res A*, 79A(3):456–63, 2006.

[112] S.P. Zhong, W.E. Teo, X. Zhu, R. Beuertnan, S. Ramakrishna, and L.Y.L. Yung. Development of a novel collagen-gag nanofibrous scaffold via electrospinning. *Mater Sci Eng C-Bio*, 27(2):262–6, 2007.

[113] J.A. Matthews, G.E. Wnek, D.G. Simpson, and G.L. Bowlin. Electrospinning of collagen nanofibers. *Biomacromolecules*, 3(2):232–8, 2002.

[114] J.A. Matthews, E.D. Boland, G.E. Wnek, D.G. Simpson, and G.L. Bowlin. Electrospinning of collagen type ii: A feasibility study. *J Bioact Compat Pol*, 18(2): 125–34, 2003.

[115] K.J. Shields, M.J. Beckman, G.L. Bowlin, and J.S. Wayne. Mechanical properties and cellular proliferation of electrospun collagen type ii. *Tissue Eng*, 10(9-10): 1510–7, 2004.

[116] X. Fang and D.H. Reneker. Dna fibers by electrospinning. *J Macromol Sci Phys*, B36(2):169–73, 1997.

[117] Y.Z. Zhang, J. Venugopal, Z.M. Huang, C.T. Lim, and S. Ramakrishna. Crosslinking of the electrospun gelatin nanofibers. *Polymer*, 47(8):2911–7, 2006.

[118] Z.M. Huang, Y.Z. Zhang, S. Ramakrishna, and C.T. Lim. Electrospinning and mechanical characterization of gelatin nanofibers. *Polymer*, 45(15):5361–8, 2004.

[119] B.M. Min, G. Lee, S.H. Kim, Y.S. Nam, T.S. Lee, and W.H. Park. Electrospinning of silk fibroin nanofibers and its effect on the adhesion and spreading of normal human keratinocytes and fibroblasts in vitro. *Biomaterials*, 25(7-8):1289–97, 2004.

[120] C.S. Ki, J.W. Kim, J.H. Hyun, K.H. Lee, M. Hattori, D.K. Rah, and Y.H. Park. Electrospun three-dimensional silk fibroin nanofibrous scaffold. *J Appl Polym Sci*, 106(6):3922–8, 2007.

[121] K. Ohgo, C.H. Zhao, M. Kobayashi, and T. Asakura. Preparation of non-woven nanofibers of bombyx mori silk, samia cynthia ricini silk and recombinant hybrid silk with electrospinning method. *Polymer*, 44(3):841–6, 2003.

[122] S.H. Kim, Y.S. Nam, T.S. Lee, and W.H. Park. Silk fibroin nanofiber. electrospinning, properties, and structure. *Polym J*, 35(2):185–90, 2003.

[123] E.J.F. Prodhomme, A.L. Tutt, M.J. Glennie, and T.D.H. Bugg. Multivalent conjugates of poly-gamma-d-glutamic acid from bacillus licheniformis with antibody f(ab ') and glycopeptide ligands. *Bioconjugate Chem*, 14(6):1148–55, 2003.

[124] M.H. Sung, C. Park, C.J. Kim, H. Poo, K. Soda, and M. Ashiuchi. Natural and edible biopolymer poly-gamma-glutamic acid: Synthesis, production, and applications. *Chem Rec*, 5(6):352–66, 2005.

[125] J.M. Buescher and A. Margaritis. Microbial biosynthesis of polyglutamic acid biopolymer and applications in the biopharmaceutical, biomedical and food industries. *Crit Rev Biotechnol*, 27(1):1–19, 2007.

[126] B. Edde, J. Rossier, J.P. Lecaer, E. Desbruyeres, F. Gros, and P. Denoulet. Post-translational glutamylation of alpha-tubulin. *Science*, 247(4938):83–5, 1990.

[127] C. Janke, K. Rogowski, D. Wloga, C. Regnard, A.V. Kajava, J.M. Strub, N. Temurak, J. van Dijk, D. Boucher, A. van Dorsselaer, S. Suryavanshi, J. Gaertig, and B. Edde. Tubulin polyglutamylase enzymes are members of the ttl domain protein family. *Science*, 308(5729):1758–62, 2005.

[128] J. van Dijk, K. Rogowski, J. Miro, B. Lacroix, B. Edde, and C. Janke. A targeted multienzyme mechanism for selective microtubule polyglutamylation. *Mol Cell*, 26(3):437–48, 2007.

[129] K. Rogowski, J. van Dijk, M.M. Magiera, C. Bosc, J-C. Deloulme, A. Bosson, L. Peris, N.D. Gold, B. Lacroix, M.B. Grau, N. Bec, C. Larroque, S. Desagher, M. Holzer, A. Andrieux, M-J. Moutin, and C. Janke. A family of protein-deglutamylating enzymes associated with neurodegeneration. *Cell*, 143(4):564–78, 2010.

[130] G-H. Ho, T-I. Ho, K-H. Hsieh, Y-C. Su, P-Y. Lin, J. Yang, K-H. Yang, and S-C. Yang. gamma-polyglutamic acid produced by bacillus subtilis (natto): Structural characteristics, chemical properties and biological functionalities. *J Chin Chem Soc-Taip*, 53(6):1363–84, 2006.

[131] H. Poo, C. Park, M-S. Kwak, D-Y. Choi, S-P. Hong, I-H. Lee, Y.T. Lim, Y.K. Choi, S-R. Bae, H. Uyama, C-J. Kim, and M-H. Sung. New biological functions and applications of high-molecular-mass poly-gamma-glutamic acid. *Chem Biodivers*, 7(6):1555–62, 2010.

[132] G. Ivanovics and V. Bruckner. Uber die chemische natur der immunspezifischen kapselsubstanz der milzbrandbazillen. *Naturwissenschaften*, 16:205, 1937.

[133] S. Makino, C. Sasakawa, I. Uchida, N. Terakado, and M. Yoshikawa. Cloning and co2-dependent expression of the genetic region for encapsulation from bacillus anthracis. *Mol Microbiol*, 2(3):371–6, 1988.

[134] J. Kream, B.A. Borek, C.J. Digrado, and M. Bovarnick. Enzymatic hydrolysis of gamma-glutamyl polypeptide and its derivatives. *Arch Biochem Biophys*, 53(2): 333–40, 1954.

[135] B.E. Volcani and P. Margalith. A new species (flavobacterium-polyglutamicum) which hydrolyzes the gamma-l-glutamyl bond in polypeptides. *J Bacteriol*, 74(5): 646–55, 1957.

[136] K. Kimura, L.S.P. Tran, I. Uchida, and Y. Itoh. Characterization of bacillus subtilis gamma-glutamyltransferase and its involvement in the degradation of capsule poly-gamma-glutamate. *Microbiology*, 150:4115–23, 2004.

[137] G.P. Chen, T. Ushida, and T. Tateishi. Scaffold design for tissue engineering. *Macromol Biosci*, 2(2):67–77, 2002.

[138] Y. Ikada. *Tissue Engineering: Fundamentals and Applications*, volume v. 8. Academic Press/Elsevier, Amsterdam, 1st ed edition, 2006.

[139] D.J. Mooney, D.F. Baldwin, N.P. Suh, L.P. Vacanti, and R. Langer. Novel approach to fabricate porous sponges of poly(d,l-lactic-co-glycolic acid) without the use of organic solvents. *Biomaterials*, 17(14):1417–22, 1996.

[140] A.G. Mikos, Y. Bao, L.G. Cima, D.E. Ingber, JP Vacanti, J.P., and R. Langer. Preparation of poly(glycolic acid) bonded fiber structures for cell attachment and transplantation. *J Biomed Mater Res*, 27(2):183–9, 1993.

[141] C. Schugens, V. Maquet, C. Grandfils, R. Jerome, and P. Teyssie. Biodegradable and macroporous polylactide implants for cell transplantation .1. preparation of macroporous polylactide supports by solid-liquid phase separation. *Polymer*, 37 (6):1027–38, 1996.

[142] A.G. Mikos, A.J. Thorsen, L.A. Czerwonka, Y. Bao, R. Langer, D.N. Winslow, and J.P. Vacanti. Preparation and characterization of poly(l-lactic acid) foams. *Polymer*, 35(5):1068–77, 1994.

[143] E. Sachs, M. Cima, P. Williams, D. Brancazio, and J. Cornie. Three dimensional printing: Rapid tooling and prototypes directly from a cad model. *J Eng Ind-T Asme*, 114(4):481–8, 1992.

[144] N. Dagalakis, J. Flink, P. Stasikelis, J.F. Burke, and I.V. Yannas. Design of an artificial skin. part iii. control of pore structure. *J Biomed Mater Res*, 14(4):511–28, 1980.

[145] S. Ramakrishna. *An Introduction to Electrospinning and Nanofibers*. World Scientific, Hackensack, NJ, 2005.

[146] H. Kubota, Y. Nambu, and T. Endo. Convenient and quantitative esterification of poly (gamma-glutamic acid) produced by microorganism. *J Polym Sci Part A-Polym Chem*, 31(11):2877–8, 1993.

[147] H.J. Johnson, S.J. Northup, P.A. Seagraves, P.J. Garvin, and R.F. Wallin. Biocompatibility test procedures for materials evaluation in vitro. i. comparative test system sensitivity. *J Biomed Mater Res*, 17(4):571–86, 1983.

[148] P. Smith and P.J. Lemstra. Ultra-high-strength polyethylene filaments by solution spinning/drawing. *J Mater Sci*, 15(2):505–14, 1980.

[149] H.N. Rydon. 260. polypeptides. part x. the optical rotatory dispersion of poly-gamma-d-glutamic acid. *J Chem Soc*, pages 1328–33, 1964.

[150] C.G. Pitt, F.I. Chasalow, Y.M. Hibionada, D.M. Klimas, and A. Schindler. Aliphatic polyesters. i. the degradation of poly(epsilon-caprolactone) in vivo. *J Appl Polym Sci*, 46(11):3779–87, 1981.

[151] H. Nishida, M. Yamashita, M. Nagashima, N. Hattori, T. Endo, and Y. Tokiwa. Theoretical prediction of molecular weight on autocatalytic random hydrolysis of aliphatic polyesters. *Macromolecules*, 33(17):6595–601, 2000.

[152] G.L. Siparsky, K.J. Voorhees, and F.D. Miao. Hydrolysis of polylactic acid (pla) and polycaprolactone (pcl) in aqueous acetonitrile solutions: Autocatalysis. *J Environ Polym Degr*, 6(1):31–41, 1998.

[153] H. Kubota, Y. Nambu, and T. Endo. Convenient esterification of poly(gamma-glutamic acid) produced by microorganism with alkyl-halides and their thermal-properties. *J Polym Sci Part A-Polym Chem*, 33(1):85–8, 1995.

[154] H.G. Bray, J.E. Gregory, and M. Stacey. Chemistry of tissues: I. chondroitin from cartilage. *Biochem J*, 38(2):142–6, 1944.

[155] K.H. Meyer, M.E. Odier, and A.E. Siegrist. Constitution de l'acide chondroitine-sulfurique. *Helv Chim Acta*, 31:1400–19, 1948.

[156] K.H. Meyer, J. Fellig, and E.H. Fischer. La constitution de l'acide hyaluronique. sur les polysaccharides amines iii. *Helv Chim Acta*, 34(3):939–51, 1951.

[157] R.W. Jeanloz. The methyl ester of methylated hyaluronic acid. *J Biol Chem*, 197 (1):141–50, 1952.

[158] L. Benedetti, R. Cortivo, T. Berti, A. Berti, F. Pea, M. Mazzo, M. Moras, and G. Abatangelo. Biocompatibility and biodegradation of different hyaluronan derivatives (hyaff) implanted in rats. *Biomaterials*, 14(15):1154–60, 1993.

[159] J. Melis, M. Morillo, A.M. de Ilarduya, and S. Munoz-Guerra. Poly(alpha-alkyl gamma-glutamate)s of microbial origin: I. ester derivatization of poly(gamma-glutamic acid) and thermal degradation. *Polymer*, 42(23):9319–27, 2001.

[160] I. Arvanitoyannis, E. Nikolaou, and N. Yamamoto. Novel biodegradable copolyamides based on adipic acid, bis(p-aminocyclohexyl)methane and several alpha-amino acids: synthesis, characterization and study of their degradability for food packaging applications. 4. *Polymer*, 35(21):4678–89, 1994.

[161] H.G. Weyland, P.J. Hoftyzer, and D.W. Van Krevelen. Prediction of the glass transition temperature of polymers. *Polymer*, 17:79–87, 1970.

[162] M. Matalsaki, K. Hiwatari, M. Higashi, T. Kaneko, and M. Akashi. Stably-dispersed and surface-functional bionanoparticles prepared by self-assembling amphipathic polymers of hydrophilic poly(gamma-glutamic acid) bearing hydrophobic amino acids. *Chem Lett*, 33(4):398–9, 2004.

[163] S. Yamaguchi, T. Tatsumi, T. Takehara, A. Sasakawa, M. Yamamoto, K. Kohga, T. Miyagi, T. Kanto, N. Hiramastu, T. Akagi, M. Akashi, and N. Hayashi. Epha2-derived peptide vaccine with amphiphilic poly(gamma-glutamic acid) nanoparticles elicits an anti-tumor effect against mouse liver tumor. *Cancer Immunol Immun*, 59(5):759–67, 2010.

[164] T. Akagi, M. Higashi, T. Kaneko, T. Kida, and M. Akashi. Hydrolytic and enzymatic degradation of nanoparticles based on amphiphilic poly(gamma-glutamic acid)-graft-l-phenylalanine copolymers. *Biomacromolecules*, 7(1):297–303, 2006.

[165] T. Akagi, M. Higashi, T. Kaneko, T. Kida, and M. Akashi. In vitro enzymatic degradation of nanoparticles prepared from hydrophobically-modified poly(gamma-glutamic acid). *Macromol Biosci*, 5(7):598–602, 2005.

[166] T. Akagi, T. Kaneko, T. Kida, and M. Akashi. Multifunctional conjugation of proteins on/into bio-nanoparticles prepared by amphiphilic poly(gamma-glutamic acid). *J Biomater Sci Polym Ed*, 17(8):875–92, 2006.

[167] T. Akagi, T. Kaneko, T. Kida, and M. Akashi. Preparation and characterization of biodegradable nanoparticles based on poly(gamma-glutamic acid) with l-phenylalanine as a protein carrier. *J Control Release*, 108(2-3):226–36, 2005.

[168] S. Okamoto, H. Yoshii, T. Akagi, M. Akashi, T. Ishikawa, Y. Okuno, M. Takahashi, K. Yamanishi, and Y. Mori. Influenza hemagglutinin vaccine with poly(gamma-glutamic acid) nanoparticles enhances the protection against influenza virus infection through both humoral and cell-mediated immunity. *Vaccine*, 25(49):8270–8, 2007.

[169] T. Akagi, K. Watanabe, H. Kim, and M. Akashi. Stabilization of polyion complex nanoparticles composed of poly(amino acid) using hydrophobic interactions. *Langmuir*, 26(4):2406–13, 2010.

[170] M. Ryu, T. Nakazawa, T. Akagi, T. Tanaka, R. Watanabe, M. Yasuda, N. Himori, K. Maruyama, T. Yamashita, T. Abe, M. Akashi, and K. Nishida. Suppression of phagocytic cells in retinal disorders using amphiphilic poly(gamma-glutamic acid) nanoparticles containing dexamethasone. *J Control Release*, 151(1):65–73, 2010.

[171] T. Kokubo and H. Takadama. How useful is sbf in predicting in vivo bone bioactivity? *Biomaterials*, 27(15):2907–15, 2006.

[172] A. Joy, D.M. Cohen, A. Luk, E. Anim-Danso, C. Chen, and J. Kohn. Control of surface chemistry, substrate stiffness, and cell function in a novel terpolymer methacrylate library. *Langmuir*, 27(5):1891–9, 2011.

[173] A.J. Ridley and A. Hall. The small gtp-binding protein rho regulates the assembly of focal adhesions and actin stress fibers in response to growth factors. *Cell*, 70(3): 389–99, 1992.

[174] Y.L. Wang. Reorganization of actin filament bundles in living fibroblasts. *J Cell Biol*, 99(4-Pt.1):1478–85, 1984.

[175] J.P. Heath and G.A. Dunn. Cell to substratum contacts of chick fibroblasts and their relation to the microfilament system. a correlated interference-reflexion and high-voltage electron-microscope study. *J Cell Sci*, 29:197–212, 1978.

[176] W.H. Carothers and J.W. Hill. Studies on polymerization and ring formation xv. artificial fibers from synthetic linear condensation superpolymers. *J Amer Chem Soc*, 54:1579–87, 1932.

[177] H.M. de Oca, D.F. Farrar, and I.M. Ward. Degradation studies on highly oriented poly(glycolic acid) fibres with different lamellar structures. *Acta Biomater*, 7(4): 1535–41, 2011.

[178] J. Rose. Patent; high strength bioresorbables containing poly-glycolic acid. *WO/2003/064531*, 2003.

[179] J. Rose. Patent; high strength bioreabsorbable co-polymers. *WO/2005/014718*, 2005.

[180] I.M. Ward. *Mechanical properties of solid polymers*. Wiley, Chichester, 2nd edition, 1983.

[181] P. Smith, P.J. Lemstra, and J.P.L. Pijpers. Tensile strength of highly oriented polyethylene. 2. effect of molecular weight distribution. *J Polym Sci Part B-Polym Phys*, 20(12):2229–41, 1982.

[182] G. Capaccio, T.A. Crompton, and I.M. Ward. Drawing behavior of linear polyethylene. ii. effect of draw temperature and molecular weight on draw ratio and modulus. *J Polym Sci Part B-Polym Phys*, 18(2):301–9, 1980.

[183] P.A. Irvine and P. Smith. Development of the axial young modulus with draw ratio of flexible-chain polymers. *Macromolecules*, 19(1):240–2, 1986.

[184] J. Melis, D. Zanuy, C. Aleman, M. Garcia-Alvarez, and S. Munoz-Guerra. On the crystal structure of poly(alpha-benzyl gamma,dl-glutamate) of microbial origin. *Macromolecules*, 35(23):8774–80, 2002.

[185] M. Janko, P. Davydovskaya, M. Bauer, A. Zink, and R.W. Stark. Anisotropic raman scattering in collagen bundles. *Opt Lett*, 35(16):2765–7, 2010.

Publications

Patent

M. M. Stevens, C. Gentilini, J. R. May, *Process for preparation of polymer films*, **UK patent based on provisional number GB1011542.6**, filed by Imperial Innovations, Ltd. on July 9, 2010.

Conference contributions

J. R. May, C. Gentilini, M. M. Stevens. *Highly-aligned Poly-DL-γ-Glutamic Acid Scaffolds for Ligament Tissue Engineering*. Poster presentation, **Second Symposium of the Musculoskeletal Technology Network**, Imperial College London, U.K. February 2011.

J. R. May, C. Gentilini, M. M. Stevens. *Highly-aligned Poly-DL-γ-Glutamic Acid Scaffolds for Ligament Tissue Engineering*. Poster presentation, **Orthopaedic Research Society annual meeting**, Long Beach, California, U.S.A. January 2011.

J. R. May, C. Gentilini, M. M. Stevens. *Highly-aligned Poly-γ-Glutamic Acid Scaffolds for Musculoskeletal Tissue Engineering Applications*. Poster presentation, **MACRO 2010, IUPAC annual conference**, Glasgow, U.K. July 2010.

J. R. May, C. Gentilini, Y. Dong, D. E. Clarke, M. M. Stevens. *Engineering polymer-based scaffolds for tissue engineering*. Invited oral presentation, **Polymer Fibres 2010**, Edinburgh, Scotland, July 2010.

J. R. May, C. Gentilini, D. E. Clarke, M. M. Stevens. *Highly-aligned Poly-γ-Glutamic Acid Scaffolds for Musculoskeletal Tissue Engineering Applications*. Oral presentation, **Imperial College Department of Materials Postgraduate Research Day**, London, UK, March 2010.

C. Gentilini, Y. Dong, J. R. May, M. M. Stevens. *Water Resistant Poly-γ-Glutamic Acid Electrospun Scaffolds for Tissue Engineering Applications*. Poster presentation, **European Society of Biomaterials annual conference**, Lausanne, Switzerland. September 2009.

J. R. May, M. M. Stevens. *Biofunctionalisation of Electrospun Scaffolds.* Poster presentation, **Imperial College Department of Materials Postgraduate Research Day**, London, UK, March 2008.

Articles in preparation

J. R. May, C. Gentilini, D. E. Clarke, P. Smith, M. M. Stevens. *Highly-aligned Poly-γ-Glutamic Acid Scaffolds for Musculoskeletal Tissue Engineering Applications*. In preparation, August 2011.

C. Gentilini, Y. Dong, J. R. May, E.T. Pashuck, S. Goldoni, D.E. Clarke, L. T. De Jonge, M. M. Stevens. *Modified Poly (γ-Glutamic Acid) Fibrous Scaffolds for Tissue Engineering*. In preparation, June 2011.